PREDIS

Deliverable 4.11
Aluminium and steel reactivity in magnesium phosphate cement

28/06/2024 Version Final

Dissemination Level PUBLIC

Lead authors

Crina Bucur (RATEN) and María Cruz Alonso (CSIC)
RATEN
Campului no. 1, 115400 Mioveni, Romania

crina.bucur@nuclear.ro
+40 741464552

Project acronym PREDIS	Project title PRE-DISposal management of radioactive waste		Grant agreement No. 945098
Deliverable No. D4.11	Deliverable title Aluminium and steel reactivity in magnesium phosphate cement		Version Final
Type Report	Dissemination level PUBLIC		**Due date** M46
Lead beneficiary RATEN			WP No. 4
Main authors Crina Bucur (RATEN), María Cruz Alonso (CSIC)	Reviewed by Abdesselam Abdelouas (IMT), WP4 Leader	Accepted by Maria Oksa (VTT), Coordinator	
Contributing author(s) Carla Fernández-García (CSIC), Céline CANNES (CNRS/IJCLab), Thi Kim Khanh LE (CNRS/IJCLab), José Luis Leganés (ENRESA), Aurel David (RATEN), Valentin Lautaru (RATEN), Manuela Fulger (RATEN)			Pages *85*

Abstract

This report summarizes the main results obtained in the Subtasks T4.6.5 "Al corrosion in magnesium phosphate cements" and T4.6.6 "Steel corrosion in contact with magnesium phosphate cements".

The partners involved in these subtasks (CNRS/IJCLab, CSIC, ENRESA and RATEN) investigated the behaviour of Aluminium (and its alloys) and steel in contact with magnesium phosphate cements (MPC) with the aim of providing experimental data on Al corrosion in MPC, including the volume of hydrogen generated and evaluate the reactivity of the steel envelop of the primary package in contact with MPC. For comparison, the tests were also performed for ordinary Portland cement (OPC) matrix.

For aluminium and its alloys embedded in MPC, the corrosion rates measured by all partners are significantly lower (around 2 orders of magnitude) than in OPC and consequently, the hydrogen generated in chemical conditions relevant for MPC is much lower than in OPC.

The reactivity of C-steel in MPC is similar to that in OPC, with the difference that in the MPC initially the corrosion rate is higher and it decreases towards the end of the test, while in OPC it is initially lower and it increases towards the end of the test. C-steel is significantly corroded in low cost MPC compared to the reference MPC. However, the overall impedance of LC-MPC formulations increases with prolonged exposure, suggesting a potential enhancement in corrosion resistance.

Coordinator contact
Maria Oksa
VTT Technical Research Centre of Finland Ltd
Kivimiehentie 3, Espoo / P.O. Box 1000, 02044 VTT, Finland
E-mail: maria.oksa. @vtt.fi
Tel: +358 50 5365 844

TABLE OF CONTENTS

1   Introduction

Nuclear power plants, fuel reprocessing and other industrial activities have produced some radioactive wastes containing aluminium and categorized as low to intermediate level (LIL) radioactive metallic waste [1]. Before their final disposal in a near-surface repository, the Al radioactive metal and its alloys need to be stabilised and solidified using waste matrices that allow producing stable waste forms that accomplish the waste acceptance criteria for disposal. The high alkaline ordinary Portland cement (OPC) (pH > 12.6) is commonly used as cementitious material for the LIL waste immobilisation.

The Pourbaix diagram, also known as E_H–pH diagram, is a plot of the thermodynamically stable phases of the metals in aqueous electrochemical systems at different pH. In the case of aluminium, the E_H–pH diagram is that as shown in Figure 1 [2]. This diagram illustrates the amphoteric nature of Al which is attacked both in acidic and alkaline media. At pH < 4, Al is corroded by an oxidation to Al^{3+} cations. The Al corrosion also occurs in a high alkaline aqueous media with pH values > 9 generating the formation of AlO_2^- anions. In addition, the passivation of the Al metal occurs in the intermediate pH domain between 4 and 9, where an alumina oxide (Al_2O_3) layer is formed. However, these conditions in the Al Pourbaix diagram are limited by the stability region of water, which are marked between the two dashed lines in Figure 1-a. Under highly reducing conditions, water is reduced to H_2 gas, according to Equations (1) in acidic conditions and (2) in alkaline aqueous media. The H_2 risk evolution is detrimental for the safety aluminium radioactive immobilisation.

$$2H^+ + 2e^- \rightarrow H_{2(g)} \tag{1}$$

$$2H_2O + 2e^- \rightarrow H_{2(g)} + 2OH^- \tag{2}$$

$$2Al + 6H_2O \rightarrow Al_2O_3 \cdot 3H_2O + 3H_2 \tag{3}$$
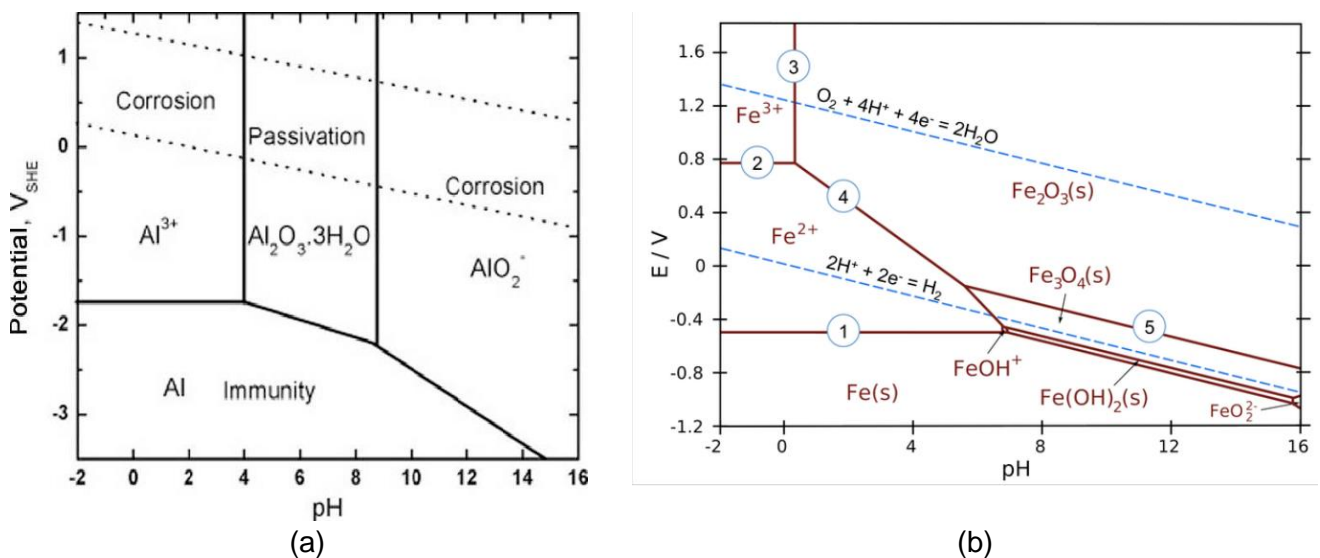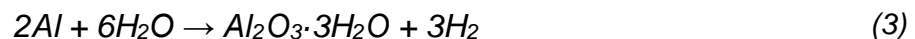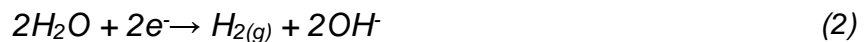
Figure 1. E_H-pH Pourbaix diagram for aluminium (a) [2] and for iron-water system at 25°C [3]

According to the Pourbaix diagram in Figure 1-a, Al would not be stable in a highly alkaline environment such as that exhibited by the OPC matrices (pH > 12.6), commonly used in LIL radioactive waste. The interaction of Al with these alkaline matrices can lead to a higher corrosion risk and H_2 gas formation, as observed in the Al overall reaction in an aqueous media in Equation (3). The volume of H_2 accumulated could rise to volumetric changes and deformations in the wasteform that could compromise its structural integrity, resulting in a high risk of explosion and compromising the efficacy of the wasteform [4].

For this reason, the development of cementitious matrices that guarantee the stability of aluminium and control the H_2 formation is a fundamental issue. Reducing the pore pH of the cementitious material by controlling the major ions in the pore water that reduce the alkalinity of Portland cements is one possible route to be explored [5], and more recently the search for alternative binders with neutral pore pH, such as magnesium potassium phosphate cement (MPC), has gained considerable importance [6].

Reducing the pore pH of the cementitious material, may in turn affect the material used as the primary waste package, that is usually Carbon steel (C-steel). When C-steel container is in contact with the cement pore water, aqueous corrosion might occur and produce both steel oxidation and hydrogen gas, which can lead to the damage of the package and so the loss of the radioactivity confinement. In addition, galvanic corrosion between C-steel and metallic waste such as aluminium can also release hydrogen.

The corrosion products developed on carbon steel- water systems at low temperatures (Figure 1-b) consist of ferrous hydroxides $Fe(OH)_2$ and hydrated ferrous species (α-FeOOH and γ-FeOOH) [3]. Hydroxides and other hydrated ferrous species can be transformed into hematite magnetite or maghemite as the temperature increases.

The balance between Fe and the various oxidation species Fe^{+2}, Fe^{+3}, Fe_2O_3, $Fe(OH)_2$, Fe_3O_4, is indicated in the Pourbaix diagram for iron (Figure 1-b) by the lines drawn on the diagram, while the surfaces delimited by the lines indicate the regimes of immunity, passivity of corrosion.

The pH generated by the conditioning matrix is an important parameter in determining corrosion rates of steel; for all ferrous systems the optimal pH for minimizing the generation of corrosion products is around 9 .5 and even higher.

The process to prepare MPC is based on a reaction between MgO, potassium dihydrogen phosphate (KH_2PO4) and water leading to the precipitation of the main reaction product, which is K-struvite: $MgKPO_4.6H_2O$. A reference formulation, optimized by the CEA for the Al encapsulation, has been proposed at the beginning of the studies performed in Task 6. In this formulation, the mortar is composed of an equimolar of MgO and KH_2PO_4 mixture, the ratio water/cement is equal to 0.51 and boric acid H_3BO_3 is used as retarder [7]. As most of the raw materials proposed to be used are either of high purity or from few providers, "Low-Cost" MPC formulations (LC-MPC) for the encapsulation of reactive metals at industrial scale were investigated in PREDIS WP4 and these LC-MPC formulations were considered in the studies performed to assess the steel reactivity (T4.6.6).

2   Main Goals

This document outlines the main experimental results obtained regarding the reactivity of aluminium alloys (T4.6.5) and steel (T4.6.6) in cementitious matrices such as Portland cements (OPC) and magnesium phosphate cements (MPC), including low-cost formulations.

The study was structured to address several relevant aspects of Al immobilisation:

1. Influence of the Portland based and MPC pore ion composition on Al and AlMg alloy corrosion and passivation mechanism. Individual and combined effect of main pore ion composition.

2. Al alloy corrosion response in contact with MPC and OPC blended cements. Understanding of the metal/matrix interface.

3. Effect of magnesium-to-phosphate ratio (M/P) and curing moisture content on Al alloy corrosion and H_2 gas evolution in order to optimize the MPC formulation.

4. Influence of MgO characteristics and retarders on Al corrosion.

5. Reactivation of corrosion process and H_2 evolution of Al alloy due to alkalisation of the MPC matrix. Interaction between MPC and OPC matrices.

6. Steel reactivity in OPC and MPC, with different formulations.

3 Al reactivity in magnesium phosphate cement (MPC)

3.1 Summary of experimental conditions

Table 1 summarises the main parameters investigated, the system used, the type of method for assessing hydrogen evolution and the partners involved in the experimental studies dedicated to assess the Al behaviour in cementitious environments (OPC and MPC).

Table 1. Aim and main parameters covered for Al reactivity in the different conditions of the study

Aim	Main parameter	System	H_2 assessment	Partner
MPC &OPC ionic composition	passivation, corrosion rate, vol. H_2	simulated pore solution	electrochemical	CSIC
	vol. of H_2	simulated pore solution&paste	electrochemical/ chemical	RATEN
	mass loss	simulated pore solution	gravimetry test	ENRESA
MgO /KH$_2$PO$_4$	corrosion rate, vol. H_2	mortar	electrochemical	CSIC
Moisture content	corrosion rate, vol. H_2	mortar	electrochemical	CSIC
MgO and retarder type	passivation, corrosion rate, vol. H_2	solution &mortar	electrochemical	CSIC,CNRS
MPC & OPC blend binders	corrosion rate, matrix interaction, vol. H_2	mortar	electrochemical	CSIC
	corrosion mechanism	mortar	electrochemical	ENRESA
Alkalisation of MPC matrix	corrosion rate, vol. H_2	mortar	electrochemical	CSIC

3.2 Work carried out

Table 2 describes the tests conditions, systems and different test methods carried out in the present study for the reactivity of Al alloys in cementitious systems.

Table 2. Description of the different variables studied for Al reactivity in cementitious systems

System			Design	Curing	Days	H_2 method	pH	Al alloy		Partner
MPC	Solution	MPC 1M M/P 7d hydr	Filtered suspen-sion	Isolated	150	LPR (R$_p$)	≈ 7.5	Al 99.5%		CSIC
								3.5%Mg		
					≈100	Chemical	7.1	3%Mg		RATEN
		Borate	500 to 200 ppm		25 to 150	LPR (R$_p$) EIS	≈ 8.5	Al 99.5%	3.5%Mg	CSIC
		Phosph-ate	10000 to 500 ppm				≈ 4			

System			Design	Curing	Days	H$_2$ method	pH	Al alloy		Partner
		Borate + Phosph.	6500 Ph + 200 Bo (ppm)		150	LPR (R$_p$)	5.34			
		1M M/P low-cost	0.18M H$_3$BO$_3$ + 0.18M Na$_2$S$_2$O$_3$		25	EIS	≈ 8.5	Al 99.5%		CSIC CNRS
	Matrix	Paste		W. imm	153	Chemical / LPR (R$_p$)	7.1	3%Mg		RATEN
		Mortar	1M M/P	W. imm	230	Gravimetry LPR (R$_p$) BSE/EDS	≈ 8	Al 99.5%		ENRESA
				W. imm + alk	300 + 250	LPR (R$_p$) SEM/EDX	10.5	Al 99.5%	3.5%Mg	CSIC
				Isolated	90	LPR (R$_p$)	7.5			
							8.5			
			2M M/P	100% RH			10			
			3M M/P				10.5			
			1M M/P low-cost	Isolated	140	EIS LPR (R$_p$)	8.5	Al 99.55		CSIC CNRS
OPC blended cements	Solution	OPC/ SPS	NaOH	Isolated	10, 30	Gravimetry LPR (R$_p$) BSE/EDS	13	Al 99.5%		ENRESA
			Synthetic water				12.6			
			Ca(OH)$_2$ sat				7-13			
					100	LPR (R$_p$)	≈ 12.5	Al 99.5% / 3.5%Mg		CSIC
						Chemical	12.6	3%Mg		RATEN
	Matrix	Paste	CEM I	W. imm	153	Chemical / LPR (R$_p$)	12.6	3%Mg		RATEN
		Mortar	CEM I	W. imm	230	Gravimetry LPR (R$_p$) BSE/EDS	12.6	Al 99.5%		ENRESA
			CEM II							
			CEM I	W. imm + alk	300 + 250	LPR (R$_p$) SEM/EDX	12.5	Al 99.5%	3.5%Mg	CSIC
			CEM IV				12			
			CEM I + SF				10.5			

3.2.1 Materials used and samples description

3.2.1.1 CSIC

The materials and samples used for the investigation carried out by CSIC were:

- Raw materials

Two commercial aluminium alloys were employed, identified as A1050 (as pure Al) and AA5754 (Al alloy containing 3.5% in Mg). The chemical compositions are included in Table 3.

Table 3. Chemical elemental composition of A1050, pure Al, and AA5754, AlMg alloy (in % wt.)

Material	Al	Mg	Fe	Cu	Si	Mn	Cr	Zn	Ti
A1050	99.5	0.1	0.2	0.001	0.1	0.1	-	0.1	0.1
AA5754	94.5	3.5	0.4	0.3	0.4	0.3	0.3	0.2	0.2

For the preparation of OPC blended matrices, different binders were used: one ordinary Portland cement (CEM I 42.5R/SR) and two Portland blended cements with mineral additions to reduce the pH by the pozzolanic reaction: one commercial CEM IV/B 32.5N-SR blended with fly ash type F (FA) and blast furnace slag (BFS) (36% to 55% content), and one CEM I blended with 50% of silica fume (SF). The chemical composition of the binders, determined by XRF technique, is shown in Table 4.

For the preparation of MPC matrices, two different types of magnesia were employed: a hard-burnt MgO (97%, 1000 -1500° C) and a low-cost MgO (97%, < 750° C) to optimise the economic cost of the MPC reference formulation. Chemical analysis in Table 4 revealed no significant differences between both MgO, as confirmed by X-ray diffraction patterns (XRD) shown in Figure 2-left. A well-defined crystalline structure with periclase (MgO) as main mineral phase is detected. H_3BO_3 and $Na_2O_3S_2 \cdot 5H_2O$ were also introduced as effective chemical retarders. In addition, the low-cost fertilizer KH_2PO_4 and the FA type F as a filler material were added. XRD pattern of the FA in Figure 2-right shows a vitreous structure with mullite and quartz as main mineral phases, along with ferric secondary phases as hematite.

Table 4. MPC and OPC blended cements chemical composition: binders and raw materials (in % wt.)

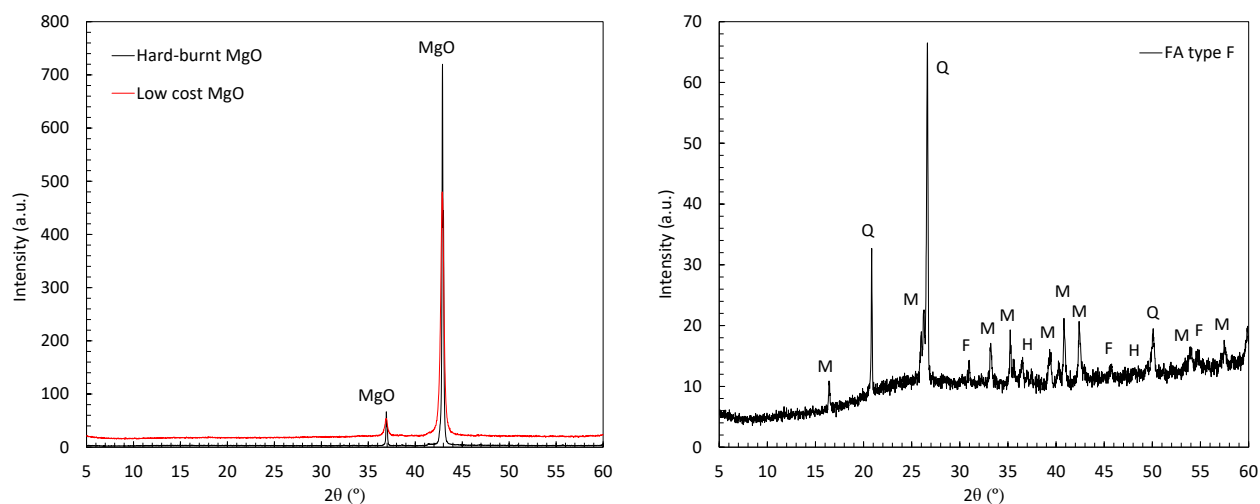| Material	Na_2O	K_2O	CaO	SiO_2	Al_2O_3	Fe_2O_3	MgO	SO_3	CaO_{free}	CO_2	NiO
CEM I	0.2	0.3	60.3	17.4	4.7	5.1	1.8	3.2	1.8	-	-
CEM IV	0.6	1.4	41.5	32.6	12.9	4.5	1.6	3.5	-	-	-
SF	0.1	0.7	0.6	97.6	0.3	0.1	0.2	0.2	-	-	-
FA	0.4	1.7	4.6	46.8	24.7	20.2	1.1	0.5	-	-	-
LC-MgO	-	-	1.9	0.4	0.03	0.1	97.5	0.02	-	0.03	0.02
HB-MgO	-	-	1.1	1.0	0.4	0.2	96.6	0.01	-	0.7	0.01

Figure 2. XRD patterns of both hard-burnt and low cost MgO (left) and FA type F (right). Legend: MgO: Periclase; M: Mullite; Q: Quartz; F: Fe$_3$O$_4$; H: Hematite

For the preparation of MPC simulated solutions, mainly constituted of phosphate ions from the chemical characterisation preformed and described in D4.8, KH$_2$PO$_4$ salt (98% purity) was used. The other alternative ions present in the MPC pore solution depend on the type of additive used as setting retarder, so when considering boric acid as a retarder, K$_2$B$_4$O$_7$-4H$_2$O salt (99% purity) or boric acid (H$_3$BO$_3$> 96% purity) were used. In addition, sodium thiosulphate pentahydrate (Na$_2$O$_3$S$_2$ - 5H$_2$O, 99.5% purity) was used. Ca(OH)$_2$ was employed to prepare a simulated pore solution of an OPC matrix.

- <u>Samples preparation</u>:

As noted in Table 2, CSIC considers the preparation of simulated pore solution systems to study the Al corrosion process in MPC matrices. MPC simulated pore solution (SPS) was prepared due to a filtered suspension of a 7-day hydrated 1M M/P ratio MPC paste [8]. In addition, Ca(OH)$_2$ saturated solution was considered as reference pore media of an OPC paste. As outlined in D4.8, the progression of the acid-base reaction in MPC 1M M/P ratio gives a decreasing evolution of the main phosphate and borate ions in the pore solution over time [9]. As a result, the individual and combined effects of both ions at different concentrations were evaluated on the Al passivation mechanism. Solutions of K$_2$B$_4$O$_7$·4H$_2$O and KH$_2$PO$_4$ salts were prepared accordingly.

Table 5 summarizes all the chemical products, concentrations, and pH values of the different prepared solution systems.

In addition, the effect of the chemical retarder in the Al passivation in MPC was investigated by CSIC in collaboration with CNRS in solution systems. Aqueous solutions by combining boric acid or thiosulfate with deionized free-CO_2 water were prepared and mixed at a concentration listed in

Table 5.The pH was maintained at approximately 8.5 through the addition of small amounts of a NaOH solution to simulate the neutral pore pH of the MPC matrices.

For the corrosion studies in solutions, a three-electrode cell configuration was designed using one or two coupons of A1050 and AA5754 as working electrode (WE), a 5 mm diameter graphite bare as counter electrode (CE), and an external Ag/AgCl as reference electrode (RE). An exposure surface area of 9 to 4 cm^2 was delimited using an electrochemical isolated tape. Continuous monitoring of the corrosion potential (E_{corr}), linear polarisation resistance (LPR) and electrochemical impedance spectroscopy (EIS) were carried out to determine the kinetic processes of Al. All the solutions were kept in plastic containers of about 200 - 250 mL volume guaranteeing the isolation and any contact with the laboratory atmosphere, as shown in Figure 3-a. The tests were carried out thermostatically at 22$\pm$ 2 ºC, and at 25 ºC.

Table 5. Concentrations and chemical products for solution systems preparation

Pore Solution	Chemical products	Concentration (units)	pH
MPC	7d-Hy MPC paste	Filtered suspension	≈ 7.5
	$K_2B_4O_7 \cdot 4H_2O$	500 (ppm)	8.70
		300 (ppm)	8.50
		200 (ppm)	8.40
	KH_2PO_4	10000 (ppm)	4.28
		6500 (ppm)	4.31
		3000 (ppm)	4.57
		500 (ppm)	5.48
	$K_2B_4O_7 \cdot 4H_2O + KH_2PO_4$	200 + 6500 (ppm)	5.34
	H_3BO_3	0.18 (molar)	8.50
	$Na_2O_3S_2\text{-}5H_2O$		
OPC	$Ca(OH)_2$	Saturated	12.50

As noted in Table 2, CSIC also contributes to the study of Al reactivity in cementitious matrices. OPC blended mortar samples (CEM I, CEM IV and CEM I + 50%SF) were prepared using the mix dosages included in Table 6. In addition, MPC mortars with different MgO/KH_2PO_4 (M/P) ratios of 1, 2, and 3M were prepared based on the MPC reference formulation [10]. Additionally, low-cost MPC mortars were prepared in collaboration with the CNRS by varying the proportion of chemical retarders (boric acid and thiosulfate) and the type of MgO, as shown in Table 6. Standardized graded sand with 99% silica content was incorporated in all mortar samples following the sand/solid mass ratio included in Table 6. Specimens were cured at a room temperature of 22 ± 2 ºC under different curing conditions depending on the type of test: (1) in a chamber at 100% RH, (2) immersed in water or alkaline solution and (3) isolated (named as endogenous curing). Prismatic mortar samples were prepared for the 100% RH and immersion curing condition (see Figure 3-b). For the endogenous curing, cylindrical mortar samples were prepared in sealed plastic containers as shown in Figure 3-c. In addition, cylindrical MPC mortars with an M/P ratio of 1 M were embedded with a prismatic CEM I mortar for the alkalisation test, following the cell configuration shown in Figure 3-d.

Table 6. Mix proportions for MPC, low cost MPC and OPC blended mortars

	M/P	H_2O/solid	FA/solid	Sand/solid	H_3BO_3/solid	$Na_2O_3S_2$/solid
Unit	Molar	Mass				
OPC blended	-	0.51	-	3.00	-	-
MPC (with HB-MgO)	1	0.50	1.00	1.00	0.02	-
	2					-
	3					-
MPC low cost (with LC-MgO)	1	0.50	1.00	1.00	0.02	0.03
					-	0.05

In all cases, a three-electrode cell was designed for corrosion studies with one or two coupons embedded of A1050 or AA5754 (WE), graphite bare (CE) and an external Ag/AgCl electrode or platinum wire embedded in the case of low cost MPC mortars (RE). An exposure surface area of 9 to 4 cm^2 was delimited using an electrochemical isolated tape. LPR and EIS techniques were carried out. For the mortar specimens under water or alkaline water immersion condition, the matrix microstructure

was characterized by mercury intrusion porosimetry (MIP) and X-ray diffraction (XRD) at the end of the test. In addition, pore pH [11] and pore solution were analysed by ICP-OES. Furthermore, to study the metal/matrix interface, scanning electron microscopy (SEM) coupled with energy-dispersive X-ray spectroscopy (EDX) was employed at the end of the experiment to characterise the microstructure of MPC and OPC blended matrices at the Al/mortar interface.
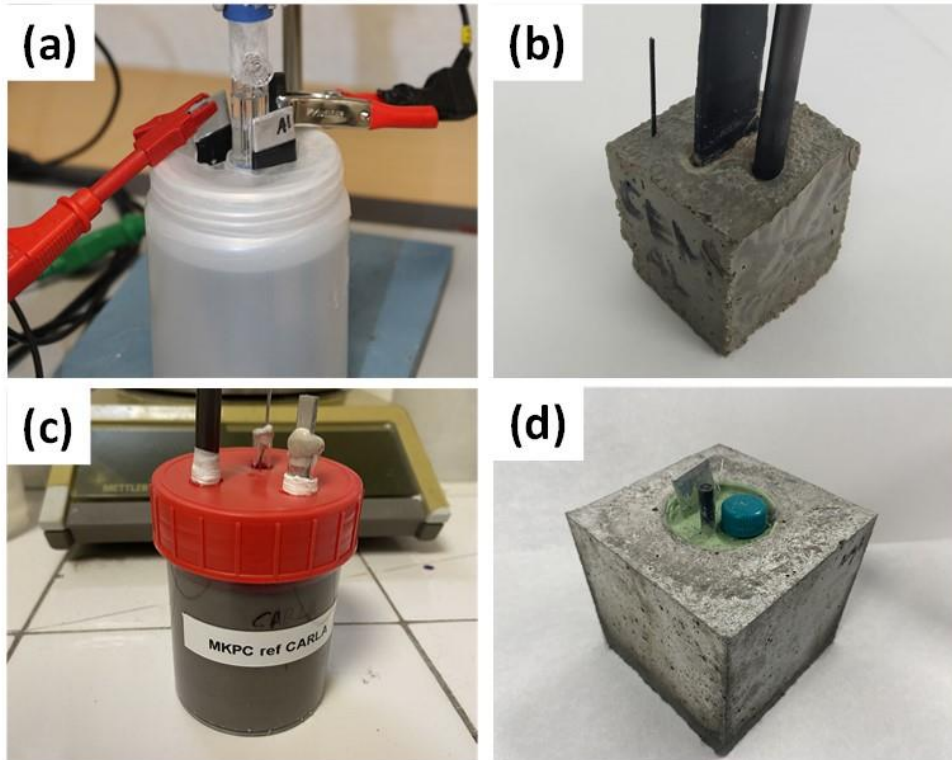

Figure 3. Cell configuration performed by CSIC for: a) solution, b) mortar under isolated condition, c) mortar under 100%RH and water immersion condition, and d) mortar with CEM I coat for alkalinisation test

To quantify the EIS experimental data in mortar and solution systems, an appropriate equivalent electrical circuit (EEC) model was selected to fit the data based on the Randles model [12]. The EIS fitting results provided the charge transfer resistance parameter (R_t) which was used to study the Al corrosion kinetic. From LPR technique, R_p is obtained, equivalent to R_t from EIS, after removing the ohmic drop (R) of the mortar to obtain the real R_p, by calculating the corrosion current density (i_{corr}) in $\mu A/cm^2$ as given in Equation (4) according to [13]. The corrosion rate (V_{corr}) has been expressed in μm/year, calculated according to the procedure described in [14] in Equation (5):

$$i_{corr} \ (\mu A/cm^2) \ = (B/R_{t/p})/S \qquad (4)$$
$$V_{corr} \ (\mu m/year) \ = 3.27 \ \ x \ \ i_{corr}/\rho \ \ x \ \ EW \qquad (5)$$

where i_{corr} is the current density ($\mu A/cm^2$), S is the Al exposure surface (4 to 9 cm^2), B is the Stern-Geary constant (26 mV based on [7]), V_{corr} is the corrosion rate (μm/year), ρ is the density of aluminium (2.7 g/cm^3) and EW is the equivalent weight (9 g for Al).

The corrosion rates obtained using the R_t from the EIS fitting results or R_p from LPR allow quantification of the volume of H_2 released from the Al alloy in the different mortar or aqueous solution systems. The calculation based on the Faradays´ law was performed using the Equations (6) and (7) described in [6,7]:

$$W_{Loss}(Al) = (Q_{acum} \; x \; Mass \; (Al))/(n \; x \; F) \qquad (6)$$
$$V \; (L) = [(3/2) \; x \; (W_{Loss} \; (Al)/Mass \; (Al)) \; x \; ((R \; x \; T)/P)] \, / \, S \qquad (7)$$

where W_{Loss} is the weight loss of Al (g), Q_{acum} is the accumulated charge (C), Mass is the molecular weight of Al (26.98u), n is the number of moles in the reaction, F is the Faraday's constant (96485 C/mol), R is the gas constant (0.082 atm L/K·mol), T is the absolute temperature (298 K), and P is the pressure (1 atm).

3.2.1.2   ENRESA

Table 7 summarises the tests carried out by ENRESA. Aluminium was employed for the studies.
For the corrosion studies in solutions, alkaline water was prepared incorporating NaOH in distillate water, with the aim of reaching the different pH studied: 7, 9, 11, 12 and 13. Another alkaline water by adding $Ca(OH)_2$ was also prepared (pH 12 to 13). In addition, synthetic water of the CABRIL (CEM I) and HORMISEC (CEM II) mortars were formulated following the results of lixiviation tests by additions of KOH and NaOH in the proportions depicted in Table 7. These solutions were prepared under oxic (or atmospheric) conditions as well as under anoxic (or reducing) conditions with $O_2 < 50$ ppb. In this case, gravimetry measurements were carried out to assess the Al corrosion in solution systems. In addition, analysis by backscattered electron micrograph combined with energy dispersive spectroscopy (BES/EDS) was performed to identify the passive layer at the Al surface.

For mortar preparation, MPC, CABRIL (CEM I) and HORMISEC (CEM II) type binders were used. Corrosion test on aluminium specimens embedded in the mortars were carried out using LPR and gravimetry techniques. The architecture of the mortar samples is depicted in Figure 4. Water immersion curing condition was used under anoxic or oxic conditions. To understand the Al reactivity at the metal/matrix interface level, BES/EDS analysis were also conducted.

Table 7. Test and additional information performed by ENRESA for Al corrosion studies

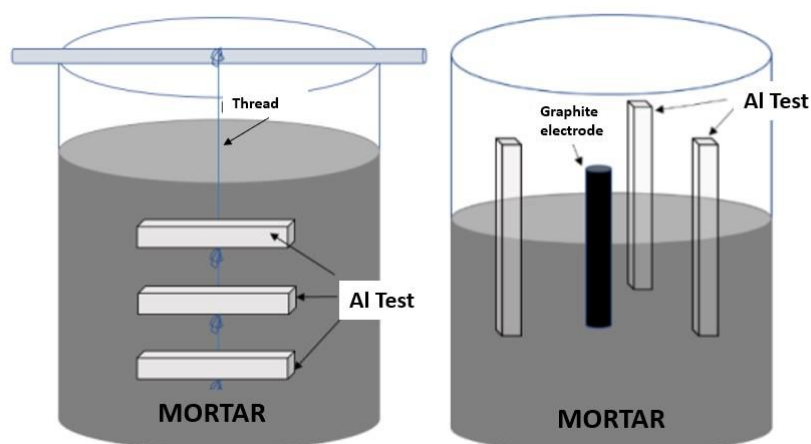| Test system	Type	Composition	Condition		pH	Test time (days)
Solution	Alkaline water	H_2O + NaOH	Oxic	Anoxic	7	30
					9	30
					11	30
					12	24
					13	≈ 4
		H_2O + $Ca(OH)_2$			11	30
					12	
					12.6	
					13	
	CABRIL synthetic water	0.60g KOH + 0.08g NaOH			12.6	10 and 30
	HORMISTIC synthetic water	0.18g KOH + 0.05g NaOH			12.6	10 and 30
Mortar	CABRIL	CEM I	Oxic	Anoxic	12.6	≈ to 227
	HORMISEC	CEM II				
	MPC	1M M/P ratio			≈ 8	228

Figure 4. Architecture of the mortar specimens prepared for pure Al corrosion studies

3.2.1.3 RATEN

- Alloy composition and matrices /solutions composition:

Material used was AlMg3 alloy with the following standard composition and actual values from the samples (accordingly to batch bulletin) (Table 8).

Table 8. Chemical composition of the 5754 AlMg alloy (%)

Composition	Si	Fe	Cu	Mn	Mg	Cr	Zn	Al
Min	0.07	0.13	0.01	0.05	2.65	0.16	0.02	97
Max	0.08	0.24	0.01	0.09	2.8	0.19	0.02	96
Actual	0.07	0.2	0.01	0.06	2.75	0.17	0.02	96.72

The following tests were performed in simulated pore solutions:

1) Long-term chemical test in which total hydrogen volume developed was measured and an average corrosion rate was calculated based on the hydrogen volume experimentally measured.
2) Electrochemical tests, using linear polarization resistance at different periods corresponding with the chemical measurements, in which electrochemical parameters were recorded (corrosion current, polarization resistance, corrosion rate and open circuit potential) and based on these parameters the hydrogen volume developed was calculated.

To simulate the pore solution of Portland cement, a saturated $Ca(OH)_2$ solution was prepared (pH 12.6), while the MPC pore solution (pH 7.1) was prepared based on CSIC analysis (Table 9), using the following chemical reagents: $NaOH$, SiO_2, CaO, KH_2PO_4, H_3BO_3, K_2SO_4, KOH, MgO, Al from ICP standard solution.

Table 9. Reference for the MPC pore solution

MgO/KH₂PO₄	pH	ppm								
		P	K	Mg	B	S	Ca	Na	Si	Al
1M	7.25	3363	8161	76	258	432	17	29	20	0.2

The samples with embedded AlMg3 coupons were carried out using two types of matrices (OPC and MPC) and the recipes of the matrices prepared are presented in Table 10 (OPC) and Table 11 (MPC).

Table 10. Portland cement-based paste recipe

Matrix	Water/Solid	Cement	H_2O(g)	Total (g)
PC1	0.4	125	50	175

Table 11. MPC-based paste recipe

Matrix	Water/Solid	MgO (light burned)	KH_2PO_4	H_2O	Ash	H_2BO_3	Total
	(-)	(g)	(g)	(g)	(g)	(g)	(g)
MPC1	0.5556	30	110	100	40	6	286

Both the chemical and electrochemical tests performed in simulated pore solutions were performed in isolated conditions, under argon atmosphere. For the AlMg3 coupons embedded in the two matrixes, the chemical tests were performed in argon atmosphere while the electrochemical tests were performed in open top conditions (free contact with atmosphere).

- Experimental methods and assumptions:

Chemical tests were based on the idea of collecting and measuring the developed gases from the reaction of the aluminium alloy with the testing environment. The assumption made was that in simulated pore solution the only gas developed is hydrogen. For the embedded samples the assumption was that some gases (air) are still present in the matrix thus we used 2 samples one with AlMg3 coupon completely embedded and a reference sample without AlMg3 coupon. The difference between the gas volumes measured for these two samples represents the hydrogen volume developed.

The hydrogen volumes measured (in ml), were normalized using the perfect gas model (Equation 8) and divided by initial active surface area of the AlMg3 coupon to determine the specific hydrogen volume (mL/cm^2). Since measurements were performed at different time intervals, evaluation was based on pure stoichiometric reaction of aluminium with water (Equation 9). The mass loss was estimated (Equation 10) and based on this the corrosion rate was calculated (Equation 11). The reported corrosion rate values represent an average on the period between two measurements not the one at the specific time (number of hours elapsed).

$$pv/T = (p_0 \ x \ v_0)/(T_0) \qquad (8)$$

where p is the measured pressure (mm Hg); v is the volume of the hydrogen developed (mL); T is the absolute temperature at the time of the measurement (K); p_0 has the value of 1atm (760 mm Hg); T_0 has the value of 273.15K (0 °C); and v_0 is the normal volume of perfect gas.

$$Al + 3H_2O \rightarrow Al(OH)_3 + 3/2H_2 \qquad (9)$$

The mass loss is calculated using the following equation:

$$m_{loss} = M_{Al} \ x \ (V_{measured}/(V_0 \ x \ 3/2)) \qquad (10)$$

In addition, the corrosion rate (V_{corr}) in μm/year was calculated with the following formula:

$$V_{corr} = (K \; x \; W)/(A \; x \; t \; x \; D) \qquad\qquad (11)$$

where K is a constant of 8.76×10^4; t is the exposure time (h); A is the sample surface area (cm^2); W is the mass loss (m$_{loss}$) (g); and D the alloy density (g/cm^3).

Electrochemical tests - were performed using linear polarization resistance technique with AUTOLAB 302N potentiostat/ galvanostat interface with a computer (OS Windows XP) using the NOVA 11.1 software for testing control and data acquisition and recording. Electrochemical parameters measured or calculated with Tafel slope method were the corrosion current (i$_{corr}$), polarization resistance (R$_p$), corrosion rate (V$_{corr}$) and corrosion potential/open circuit potential (OCP).

For the testing, the potential was varied ± 100mV vs OCP determined with SCE (standard calomel electrode) and scanning speed of 0.5mV/s. In addition, experimental polyethylene electrochemical cells were used and adapted for the control atmosphere, in the case of solution testing, and open top, in the case of embedded coupons. Using electrochemical parameter (corrosion current), the mass loss (Equation 12) was estimated and then the normalized hydrogen volume (Equation 13) was calculated.

$$m_{loss} = (I_{corr} \; x \; t \; x \; M)/(z \; x \; F) \qquad\qquad (12)$$

$$V \; = 3/2 \; x \; (m_{loss}/M) x \; ((R \; x \; T)/P) \qquad\qquad (13)$$

where I$_{corr}$ is the corrosion current (A); t is the exposure time (h); M is the molar mass (g/mol); Z is the number participant electrons (in the reaction); F is the Faraday's constant (96485.33 C/mol); m$_{loss}$ is the mass loss during the chemical reactions (corrosion); R is the universal gas constant (0.082 L·atm/mol·K); T is the testing temperature (K); and P is the testing pressure (mm Hg).

For both types of tests (in simulated pore solutions and with AlMg3 embedded in OPC and MPC), the chemical tests were performed using the experimental set-up composed of (Figure 5):

1) Test cell;
2) Digital barometer for measuring absolute pressure, with a measurement range of 0-1.3 bar with a precision of 0.1%;
3) Two thermometers, one for measuring the ambient temperature and another for the solution temperature;
4) Gradated glass columns, screens with shut-off valves, used for collecting hydrogen;
5) METTLER TOLEDO Seven Excellence TM multiparametric analyser, for pH, conductivity of aqueous solutions measurements.
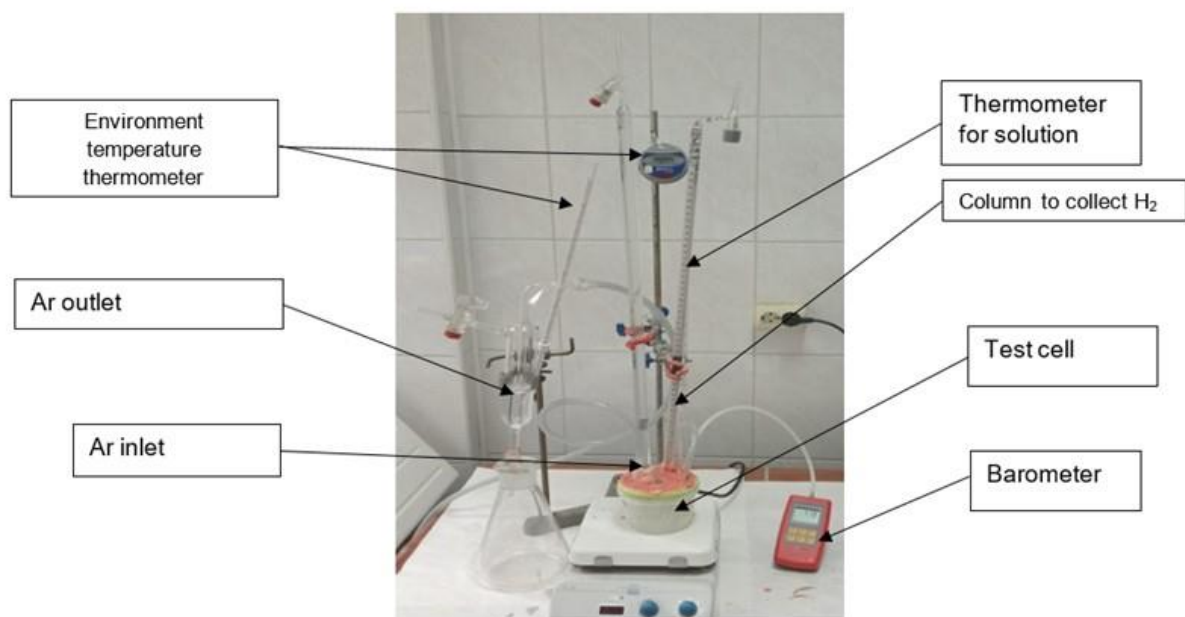
Figure 5. Chemical testing assembly carried out by RATEN

The test cells used in the electrochemical tests are presented in Figure 6, for simulated pore solutions and Figure 7, for AlMg3 coupons embedded in the two matrices investigated.
The tests were performed out at atmospheric pressure, a parameter that was also monitored.

Figure 6. Electrochemical test cell assembly (in solution systems)

The electrochemical cell contains three electrodes: the working electrode, which is the tested sample, a counter electrode (Pt), and a reference electrode (Ag/AgCl).
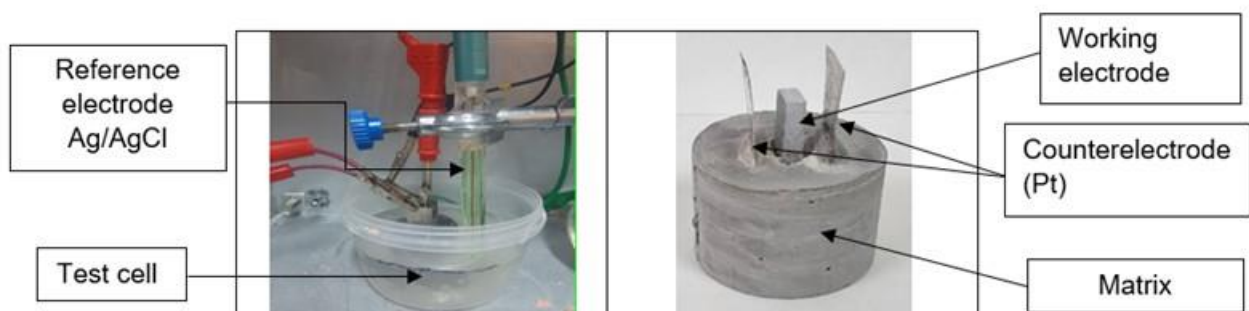
Figure 7. Electrochemical cell assembly used for AlMg3 embedded in the two matrices

3.3 Main findings: Aluminium corrosion and H_2 evolution

3.3.1 Effect of MPC&OPC pore ion composition

- <u>CSIC</u>:

To evaluate the influence of the pore ion composition on Al corrosion response and H_2 evolution, CSIC prepared the different solutions with different pH values mentioned in

Table 5. An MPC/SPS (pH 7.5) was compared against a $Ca(OH)_2$ saturated solution representing the pore pH of an OPC paste (pH 12.6). In the highly alkaline $Ca(OH)_2$ sat. solution, higher corrosion rates are observed for both Al and AlMg alloys, which remain constant after 6 months of testing as shown in Figure 8-left. As the pH is outside the Al passivation domain (pH 4-9), passivation is not achieved in the $Ca(OH)_2$ sat. solution for both metal alloys, with corrosion rate values of about ≈54.24µm/year leading higher volumes of H_2 release in Figure 8-right (116 L/m^2). In contrast, during the initial stage of interaction, both Al and AlMg alloys show a V_{corr} decreasing evolution when exposed to an MPC-SPS. As observed in Figure 8-left, the corrosion rate displays values of V_{corr} between 3-2 µm/year after one week. As a result, lower volumes of H_2 release for MPC/SPS than $Ca(OH)_2$ saturated solution are identified in Figure 8-right (4.97 L/m^2).

Since the MPC pore solution mainly consists of borate (named as Bo) and phosphate (named as Pht) ions (D4.8), CSIC also analysed the individual and combined effect of both in aqueous solutions with Bo at 200 ppm (pH 8.4), Pht at 6500 ppm (pH 4.31) or both combined (Bo + Pht) (pH 5.3).
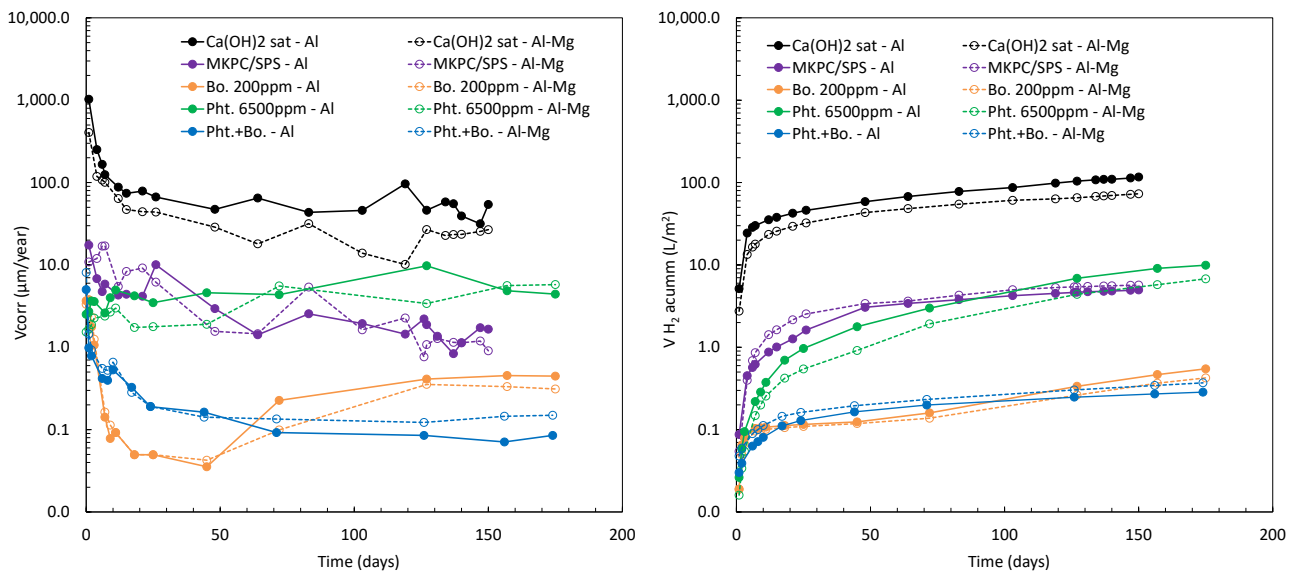
Figure 8. Corrosion rate (V_{corr}) (left) and accumulated H_2 release (right) versus time for MPC/SPS, $Ca(OH)_2$ sat., 200ppm of Bo, 6500ppm of Pht or both combined solutions

Figure 8-left shows that Pht solution exhibits some higher V_{corr} compared to Bo solution (4.4 µm/year at day 170), similar to the MPC/SPS (pH 7.5). However, higher volumes of H_2 gas over time are detected in Figure 8-right for Pht solution than MKCP/SPS (≈10 L/m^2 for Al and AlMg alloys). Although Bo ions initially induce higher V_{corr} (3 µm/year) in Bo and Bo + Pht solutions, Al alloys rapidly evolve to a lower corrosion risk with final V_{corr} values of 0.3 to 0.1 µm/year and H_2 volumes of about 0.3 L/m^2. This test indicates that borate ions, in the presence or absence of phosphate ions, make a positive contribution to Al passivation over time than phosphate alone, probably due to the differences in the pH which are affecting the passivation kinetic.

The effect of the concentration of the phosphate and borate ions in the MPC pore solution was also analysed by the CSIC on the Al passivation mechanism in a short period interaction (26 days). Aqueous solutions at different concentrations of borates (Bo) (200 to 500ppm, pH ≈8.5) and phosphates (Pht) (500 to 10000ppm, pH ≈4) solutions were prepared. Figure 9-left shows a higher V_{corr} from electrochemical measurements at higher Bo content (from 0.5 to 2 µm/year for 200 to 500 ppm, respectively). However, for all Bo concentrations there is a decrease in the early stages of interaction, which stabilised after 15 days of exposure. For Pht ions, Figure 9-left shows that higher concentrations lead to a reduction in Al corrosion risk (2.3 to 1.24 µm/year, from 500 to 10000 ppm); however, no significant changes are detected.

This effect of the different Pht and Bo ion concentrations were also analysed by estimating the amount of H_2 gas released using Equations (6) and (7). Figure 9-right shows the accumulated H_2 gas over time in all Pht and Bo solutions. As noted above, high Bo content results in higher H_2 gas release (from 0.3 to 1.03 L/m^2 at 200 to 500 ppm). In contrast, high Pht content results in less H_2 evolution (from 0.85 to 0.45 L/m^2 at 500 to 10000 ppm). Borates do not show a negative effect, although the effect becomes less positive at low concentrations. On the other hand, phosphate has a positive effect and contributes to the Al passivation process: the higher the phosphate content in the pore media, the lower corrosion kinetic and faster the Al passivation process.
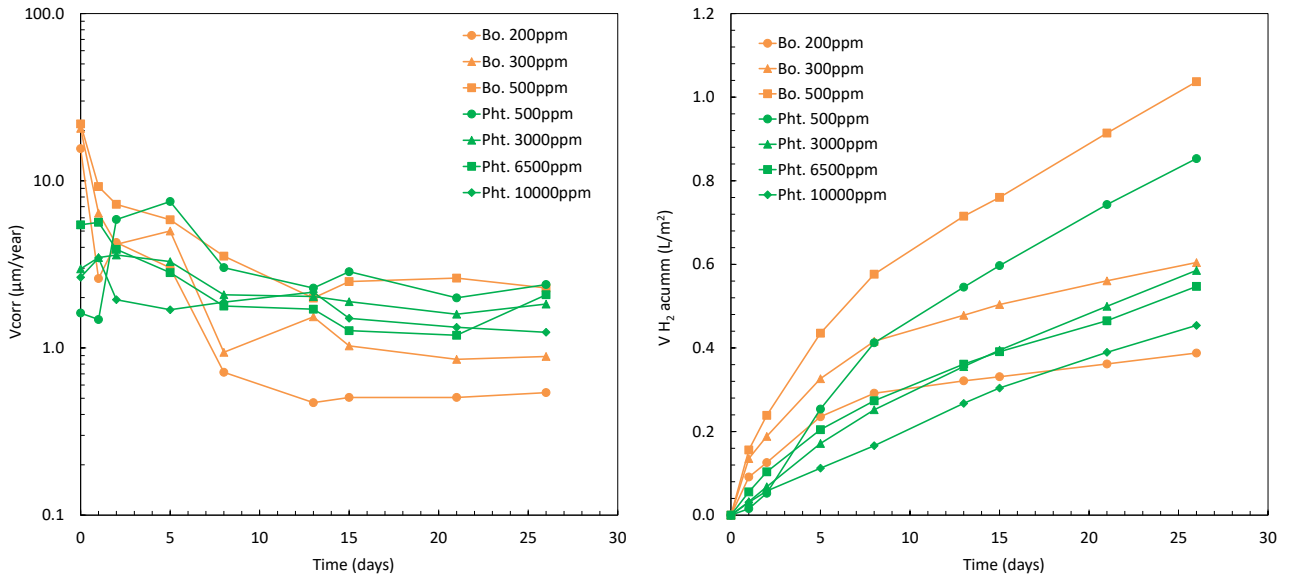
Figure 9. Corrosion rate (V_{corr}) (left) and accumulated H_2 release (right) versus time for Bo (200 to 500 ppm) and Pht(10000 to 500 ppm) aqueous solutions

To understand the effect of both ions on the mechanism of Al alloy passivation, Figure 10 shows Nyquist spectrums obtained from EIS measurements for the highest and lowest concentrations of Bo and Pht solutions. At the lower Bo concentration (200 ppm, Figure 10-a), an increase in the diameter of the capacitive semicircles is observed over time, indicating a lower corrosion risk in the early stages of interaction with the media. After 13 days, the diameter of the semicircles appears to decrease, showing no further evolution. In addition, tails are detected, indicating an adsorption phenomenon of Bo ions on the metal surface, more evident at higher concentrations (see Figure 10-b). This could be explained by the fact that the borate ions would interact with the Al_2O_3 layer on the Al surface, limiting in this way the generation of the passive film more evident at higher borate concentrations. In contrast, for Pht ions at different concentrations, these tails in the Nyquist semicircles are less pronounced as shown in Figure 10-c, d. This could be explained by the fact that the phosphate ions form a new protective film on the Al surface or are slightly absorbed into the Al_2O_3 passive layer. The diameter of the capacitive semicircles is much larger than for Bo ions, which effectively reduces the corrosion risk at higher Pht concentrations due to its lower pH from 4 to 5 (see Figure 10-d). The phosphates in the MPC matrices are contributing to the Al passivation.
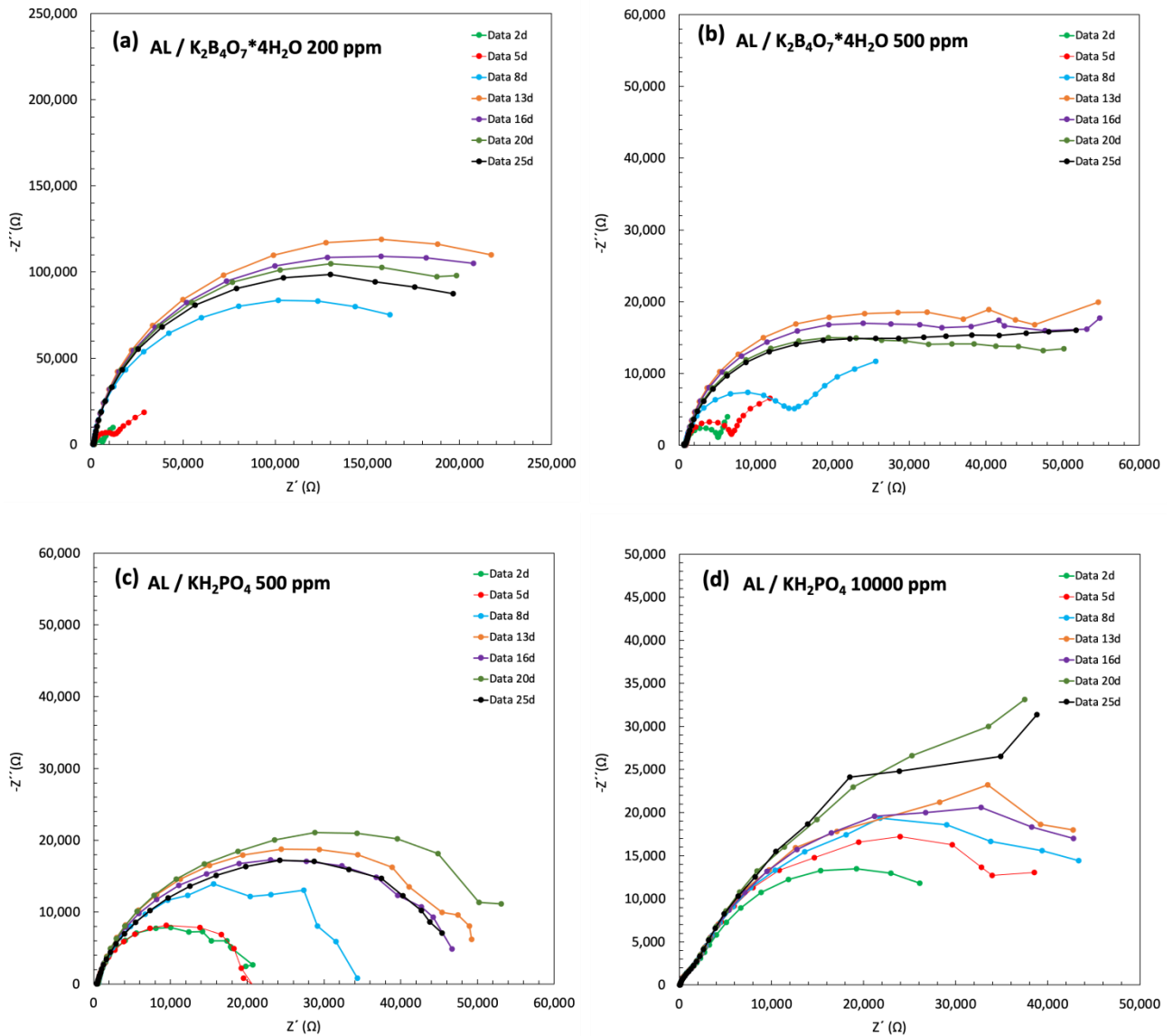
Figure 10. Nyquist diagrams from EIS measurements of: a) Bo solution at 200 ppm, b) Bo solution at 500 ppm, c) Pht solution at 500 ppm, and d) Pht solution at 10000 ppm

The effect of the chemical retarders in MPC formulation such as boric acid and thiosulphate was also analysed by CSIC and CNRS on the Al passivation mechanism. Three different aqueous solution were prepared: 2% of boric acid, 5% of thiosulfate and 2% boric acid + 3% thiosulfate. The solutions were studied for over 25 days in isolated hermetic plastic containers.

A significant effect is detected in the corrosion rate evolution depending on the chemical retarder used as observed in Figure 11-left. A decreased tendency over time is identified in the three solutions with a similar behaviour over the first 10 days with lower V_{corr} with thiosulfate in the first stage of interaction. After that time, the presence of only boric acid shows the lowest V_{corr} values (0.157 µm/year) followed by only thiosulfate (0.337 µm/year) at the end of the test. Both chemical retarders have a positive effect on the Al corrosion response, higher with boric acid as detected in previous borate solutions. However, when both retarders act at the same time, a negative behaviour is detected with final V_{corr} values of about 0.896 µm/year. This could be related that the thiosulfate inhibits the positive effect of the boric acid on the Al passivation mechanism.

To understand in depth the effect of both retarders on the Al corrosion response, the accumulated volume of H_2 gas release was calculated using Equations (6) and (7) and it is observed in Figure 11-

right. No significant differences on the volume release are detected in the three systems, slightly lower in the presence of only boric acid followed by thiosulfate solution (≈0.6 L/m² at day 30).
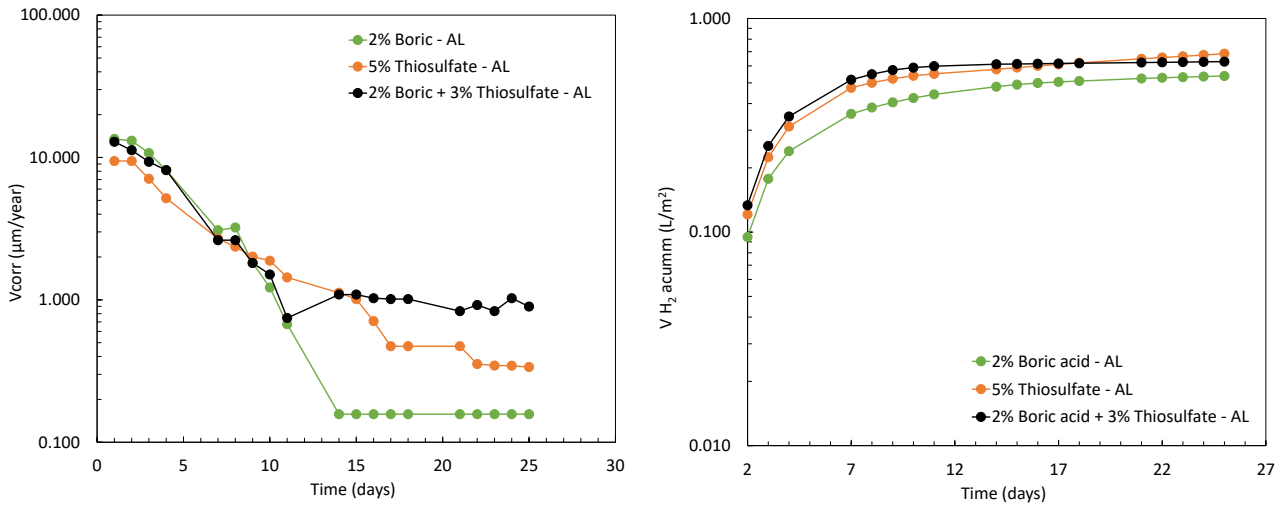

Figure 11. Corrosion rate (V_corr) (left) and H₂ risk (right) over time for boric and thiosulfate solutions

This evolution of the corrosion kinetic of the three aqueous solutions was confirmed with the Nyquist spectrums from EIS measurements in
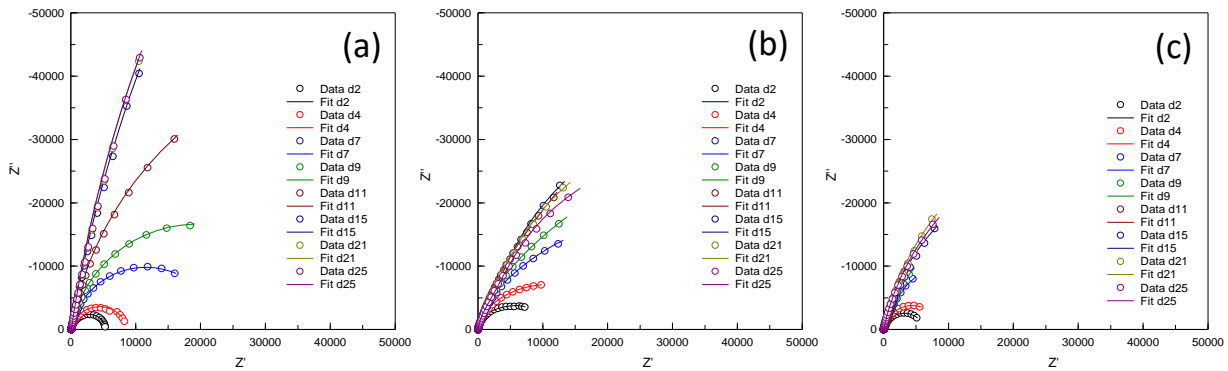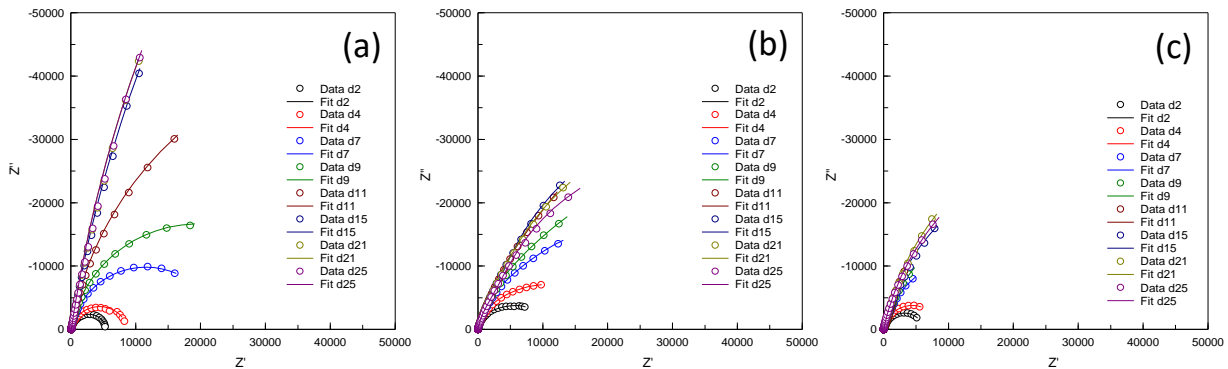

Figure *12*. As observed in

Figure *12*-a, a significant increase of the capacitive semicircles is detected in the boric acid solution showing the lowest corrosion risk over time due to an absorption phenomenon on the Al_2O_3 passive

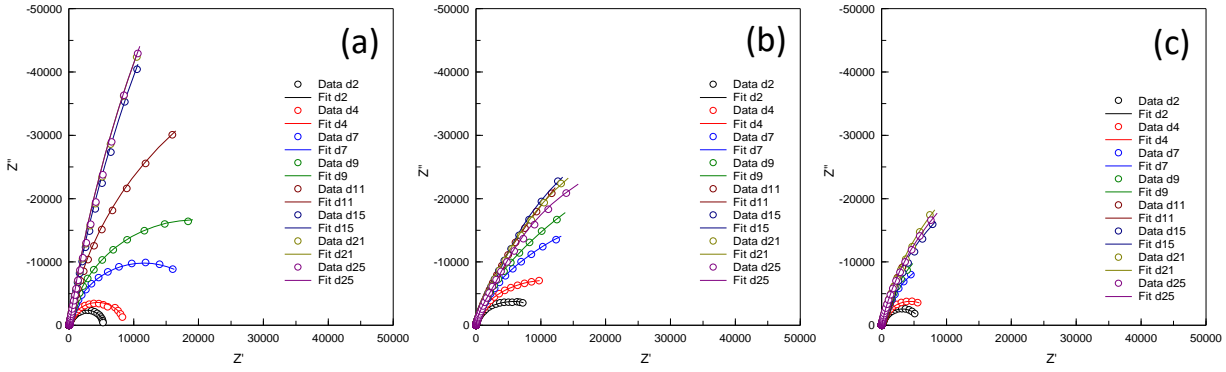film. The diameter of the Nyquist plots significantly decreases with the presence of thiosulfate (see

Figure *12*-b), lower when both retarders act as the same time (see
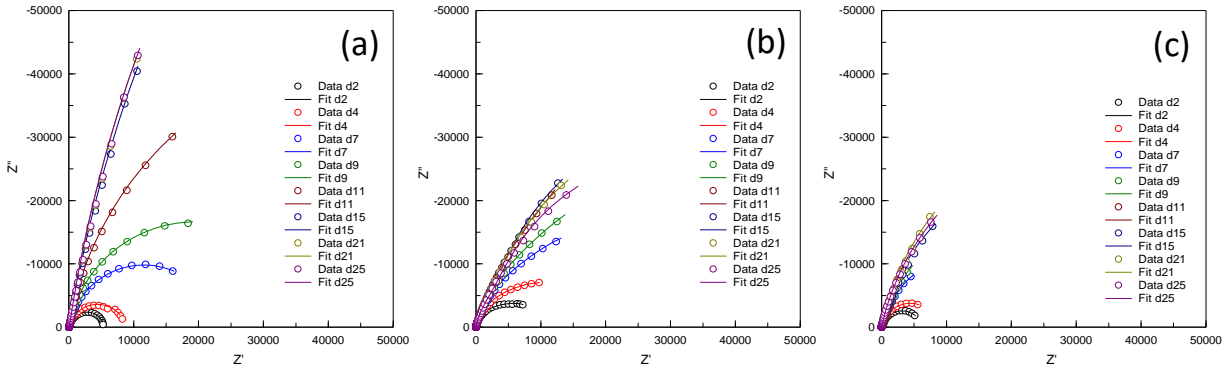

Figure *12*-c). These results confirm the calculated V_{corr} in Figure 11-left. Tails are detected in thiosulfate solutions (see
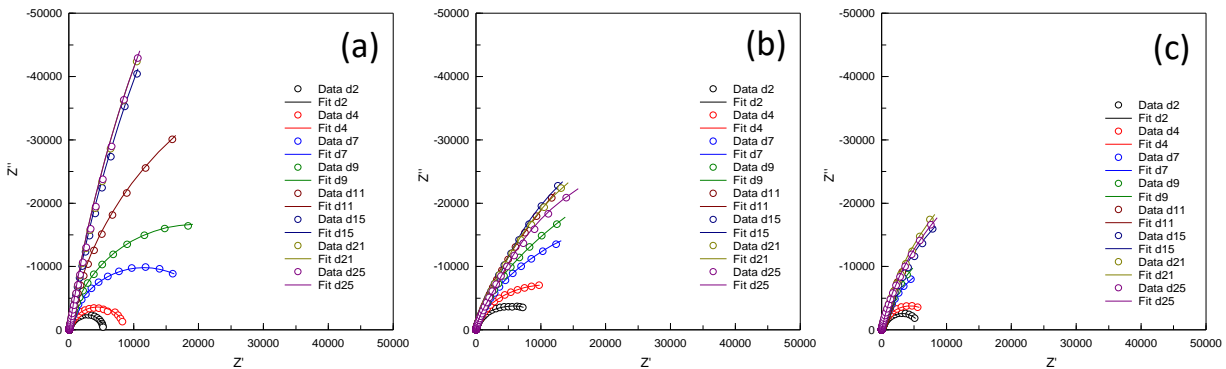

Figure *12*-b, c) which indicates that with this retarder a new film on Al surface is formed. The synergy effect of both retarders in
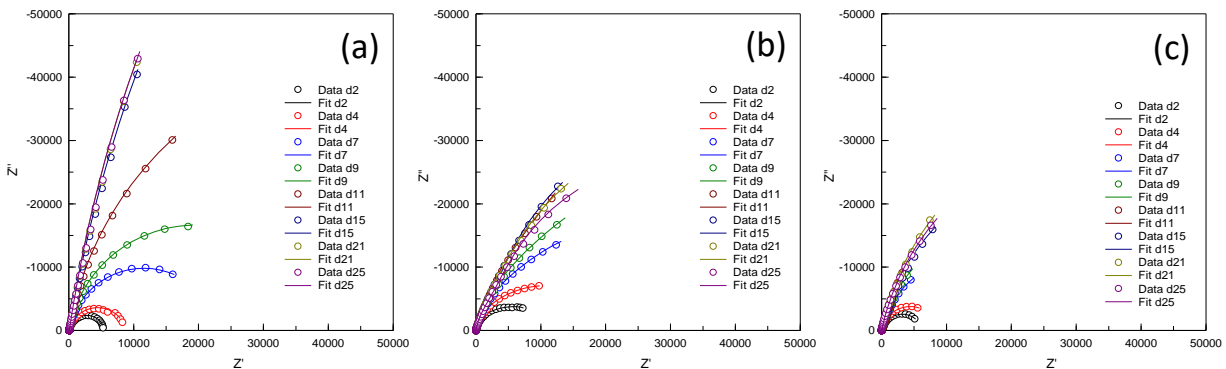

Figure *12*-c shows the lowest evolution over time, which suggests higher corrosion risk.
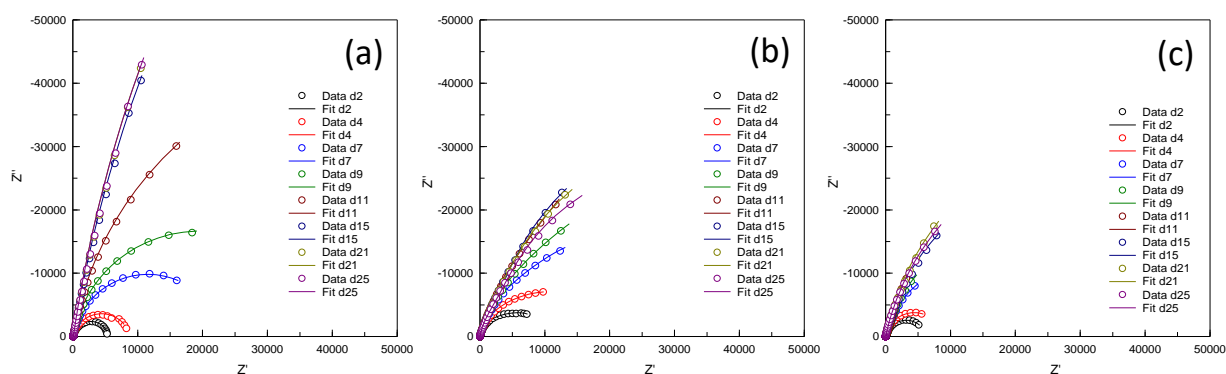
Figure 12. Nyquist diagrams from EIS measurements of: a) 2% boric acid, b) 5% thiosulfate, and c) 2% boric acid + 3% thiosulfate aqueous solutions

Table 12 summarises the corrosion rates and volumes of H_2 gas release in the Al solution system used in present study.

Table 12. Corrosion rates and H₂volumes of Al and AlMg alloy in aqueous solution systems

Solution	pH	Al			AlMg		
		V_{corr} (µm/year)		H_2 (L/m^2)	V_{corr} (µm/year)		H_2 (L/m^2)
		0d	*170d*	*170d*	*0d*	*170d*	*170d*
Ca(OH)$_2$ sat	12.50	1026.81	54.24	116.66	404.85	26.82	73.10
MPC/SPS	7.50	17.40	1.65	4.97	10.84	0.90	5.69
200 ppm K$_2$B$_4$O$_7$·4H$_2$O	8.40	3.66	0.44	0.54	3.32	0.31	0.42
6500 ppm KH$_2$PO$_4$	4.57	2.51	4.42	9.92	1.52	5.77	6.78
KH$_2$PO$_4$ + K$_2$B$_4$O$_7$·4H$_2$O	5.34	5.01	0.08	0.28	8.07	0.14	0.37
		0d	*25d*	*25d*	*-*	*-*	*-*
200 ppm K$_2$B$_4$O$_7$·4H$_2$O	8.40	15.57	0.54	0.38	-	-	-
300 ppm K$_2$B$_4$O$_7$·4H$_2$O	8.50	20.56	0.88	0.60	-	-	-
500 ppm K$_2$B$_4$O$_7$·4H$_2$O	8.70	21.85	2.28	1.03	-	-	-
500 ppm KH$_2$PO$_4$	4.28	1.61	2.39	0.85	-	-	-
3000 ppm KH$_2$PO$_4$	4.31	2.97	1.83	0.58	-	-	-
6500 ppm KH$_2$PO$_4$	4.57	5.45	2.08	0.54	-	-	-
10000 ppm KH$_2$PO$_4$	5.48	2.64	1.24	0.45	-	-	-
		0d	*25d*	*25d*	*-*	*-*	*-*
2% Boric acid	8.5	13.49	0.16	0.53	-	-	-
5% Thiosulfate	8.5	9.44	0.33	0.62	-	-	-
2% boric + 3% thiosulfate	8.5	12.88	0.89	0.68	-	-	-

- ENRESA:

ENRESA carried out corrosion test of aluminium in simulated pore alkaline waters at different pH: 7, 9, 11, 12 and 13. The results are shown in the Table 13 and Figure 13. Mean corrosion rates are obtained from gravimetric loss.

Table 13. Al corrosion rates in alkaline water under oxic and anoxic conditions at different pH

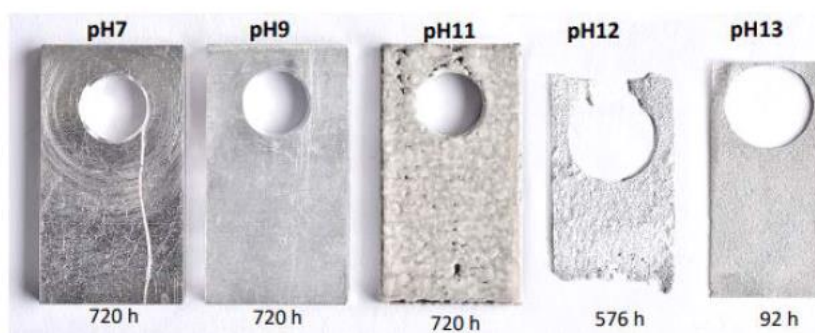| pH	H$_2$O + NaOH (oxic)	H$_2$O + NaOH (anoxic)
	Corrosion rates (mm/year)	Corrosion rates (mm/year)
7	0.0079	-
9	0.017	0.042
11	0.78	1.8
12	18	24
12.4	47	-
12.7	58	-
13	92	98

Figure 13. Aluminium surfaces after exposure to alkaline water at different pH values

In general, the data obtained do not show significant differences in the pH values obtained in oxic and anoxic media. Figure 14 shows the graphical representation of the corrosion rate (V_{corr}) values.

The instantaneous corrosion rate values are significantly lower than the values of average corrosion rate, obtained by gravimetric technique, especially for more alkaline pH values. At pH 7 or pH 9, the instantaneous corrosion rate values are similar to the average values of corrosion rate.
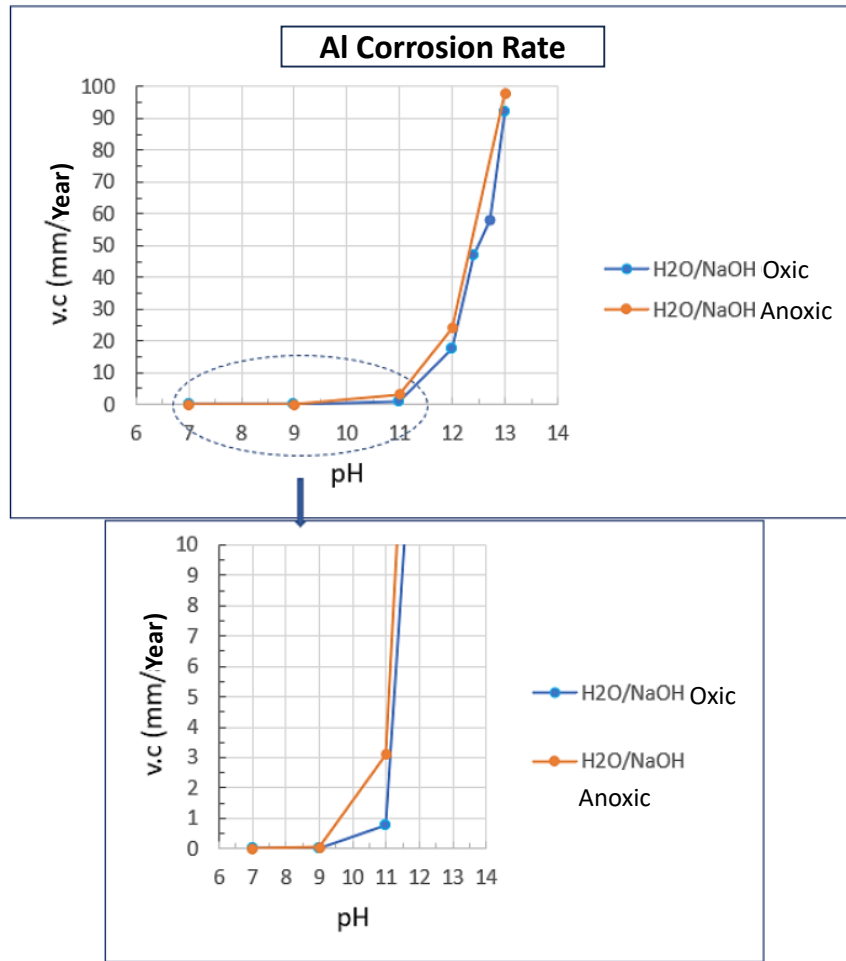

Figure 14. Graphical representation of the corrosion rate (V_{corr}) of pure Al in alkaline water at different pH under oxic and anoxic condition

After that, corrosion studies were conducted in synthetic water of the CABRIL (CEM II) and HORMISEC (CEM II) mortars following the results of lixiviation tests. As can be seen in Table 14, the corrosion rates measured for aluminium in the HORMISEC water are slightly higher than those measured in the synthetic water from EL CABRIL. This may be due to the slight difference in the pH value of the two synthetic waters, without discarding the fact that the amount of KOH and NaOH used to prepare 1L HORMISEC water is higher than that used in the preparation of 1L of CABRIL water.

Table 14. Corrosion rates in HORMISEC and CABRIL synthetic water in oxic and anoxic condition

Type of solution	Condition	Time (h)	Time (days)	Corrosion rate (mm/year)
CABRIL synthetic water (pH 12,6)	Oxic	240	10	1.2
		720	30	1.5
	Anoxic	240	10	1.3
		720	30	1,3
HORMISEC synthetic water (pH 12,6)	Oxic	240	10	2.1
		720	30	2.5
	Anoxic	240	10	2.3
		720	30	2.9

The most significant aspect is the decrease of the corrosion rates in the two synthetic waters, compared to that observed in the alkalized aqueous medium with NaOH (Table 13). The Figure 15

shows the corrosion rate values of Al in synthetic water of CABRIL and HORMISEC, as well as in H_2O at different alkalinity values.
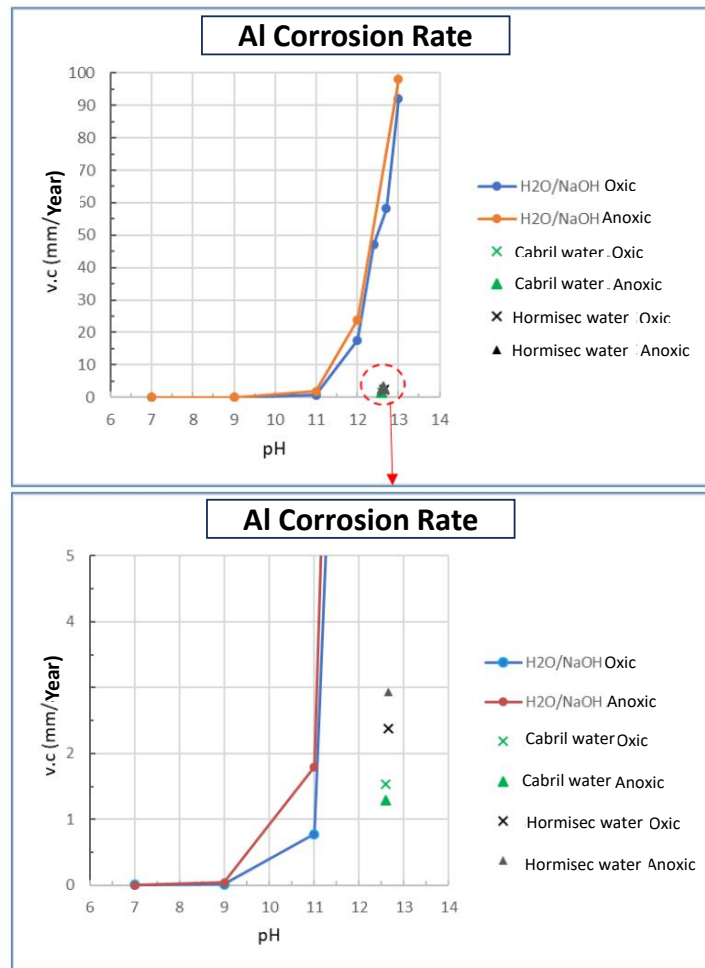

Figure 15. Graphical representation of the corrosion rate (V_{corr}) of pure Al in synthetic water of CABRIL and HORMISEC, and in alkaline water at different pH under oxic and anoxic conditions

Figure 16 shows the appearance of the Al specimens tested in synthetic water HORMISEC. The mode of corrosion observed in all specimens is of the generalized type non-uniform (Right side photo after pickling).

Figure 16. Aluminium surfaces after exposure to synthetic water HORMISEC

Analysing in details the layer of corrosion products generated, two areas can be observed clearly different (see Figure 17): a non-compact and non-adherent "outer" layer, and an "innermost" oxide layer, apparently well adhered to the aluminium substrate, thick and relatively uniform. X-ray EDS

technique was used to analyse these layers to determine its chemical composition. The EDS spectrum of the outermost layer contains majority of calcium (Ca) and aluminium (Al), as well as oxygen (O) and carbon (C). The innermost layer is mostly made of Al and O, as aluminium hydroxide.
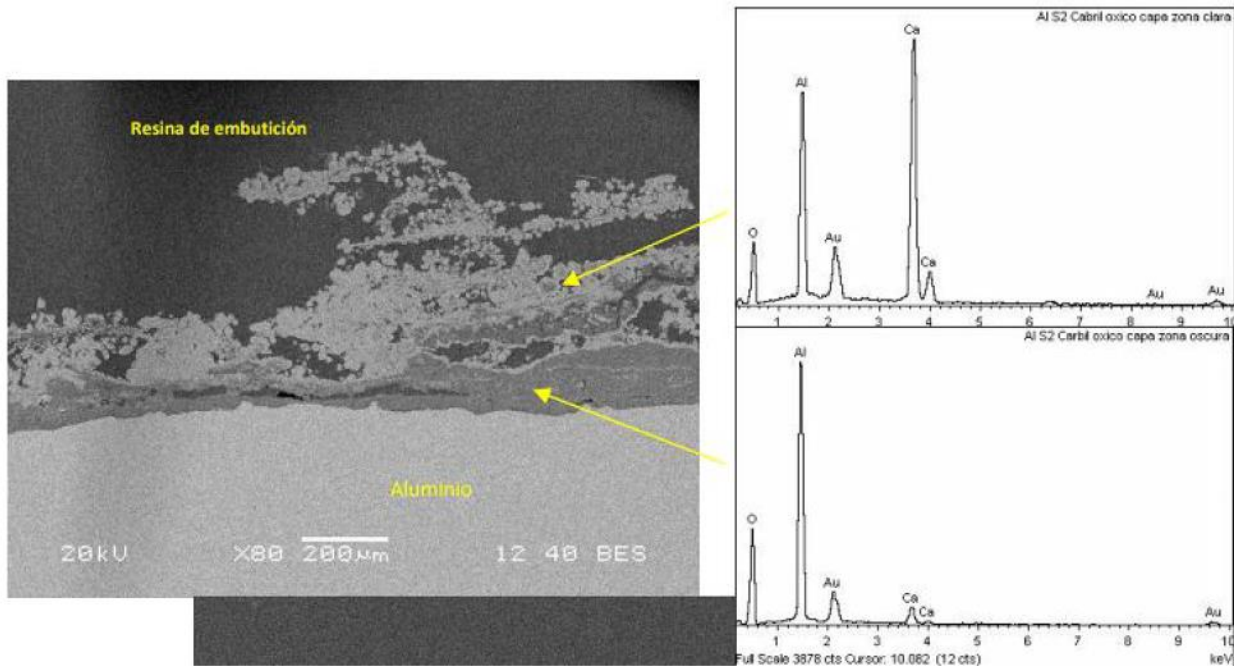

Figure 17. Corrosion product layer at the Al surface in synthetic water HORMISEC by BES/EDS

Figure 18 shows the variation in the corrosion rate evolution of Al from electrochemical measurements, with the simulated pore solution from CABRIL and HORMISEC pore media. The corrosion rate decreases as the test time increases, so the formation of a layer of corrosion products that brings passivity to the aluminium surface. Instantaneous corrosion rate values, especially those obtained in the oxic medium, are in line with the average corrosion rate obtained for aluminium in such a medium.
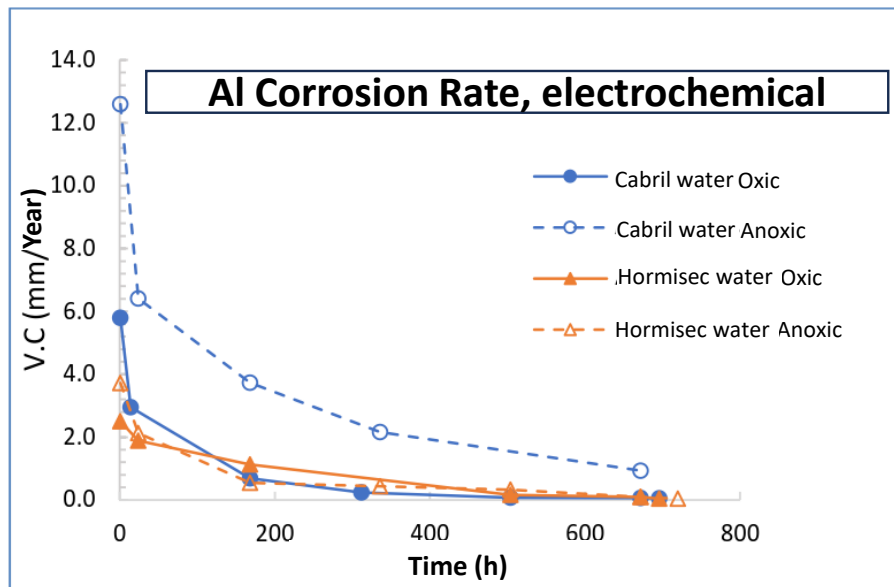

Figure 18. Graphical representation of the corrosion rate (V_{corr}) over time of pure Al in synthetic water of CABRIL and HORMISEC under oxic and anoxic conditions

The decrease in the corrosion rate of aluminium in synthetic water cements is attributed to the high presence of calcium ions (Ca^{2+}) in cement water. These cations are incorporated into the corrosion layer promoting passivity. For this reason, corrosion tests are carried out in distilled water to which $Ca(OH)_2$ is added, until pH values are reached between 11 and 13. The tests are carried out only for

aluminium and in air, for the sake of simplification with respect to tests under anoxic conditions, and especially by the fact that in the corrosion studies carried out for aluminium, no significant differences were observed between oxic and anoxic environments. These tests are performed at pH values of 11, 12, 12.6 and 13. The appearance of some of the Al tested specimens after 720 hours is shown in Figure 19.

Figure 19. Aluminium surfaces after 720 hours exposure to Ca(OH)$_2$ solutions at different pH

As a preliminary conclusion from the corrosion of Al in simulated pore alkaline waters at different pH and ion composition, summarised in

Table 15, it can be seen that the alkaline solutions containing Ca(OH)$_2$ result in significantly lower corrosion rates in aluminium than alkaline solutions with NaOH for a similar pH. The obtained values are somewhat higher than the corrosion rates obtained in synthetic pore waters from CABRIL and HORMISEC cements, the differences are not particularly significant. Significantly, at pH 11, the corrosion rates of Al in alkaline pore water with NaOH and alkaline pore water with Ca(OH)$_2$ coincide.

Table 15. Al corrosion rates values after 30 days in alkaline solutions and in simulated pore water of HORMISEC and CABRIL cements

pH	H$_2$O + Ca(OH)$_2$	Simulate CABRIL pore water	Simulated HORMISEC pore water	H$_2$O +NaOH
	Corrosion rates (mm/year) after 30 days			
11	0.79	-	-	0.8
12	1.2	-	-	18
12.6	4.5	1.5	2.4	582
13	43	-	-	92

- RATEN:

Electrochemical tests in simulated MPC pore solution:

The AlMg3 corrosion rate is 1.356 µm/y at the beginning of the test and decreases to 0.0105 µm/year on the last day of the test (Figure 20). The total calculated volume of hydrogen released at the end of the test is 0.355 L/m^2 (Figure 21).
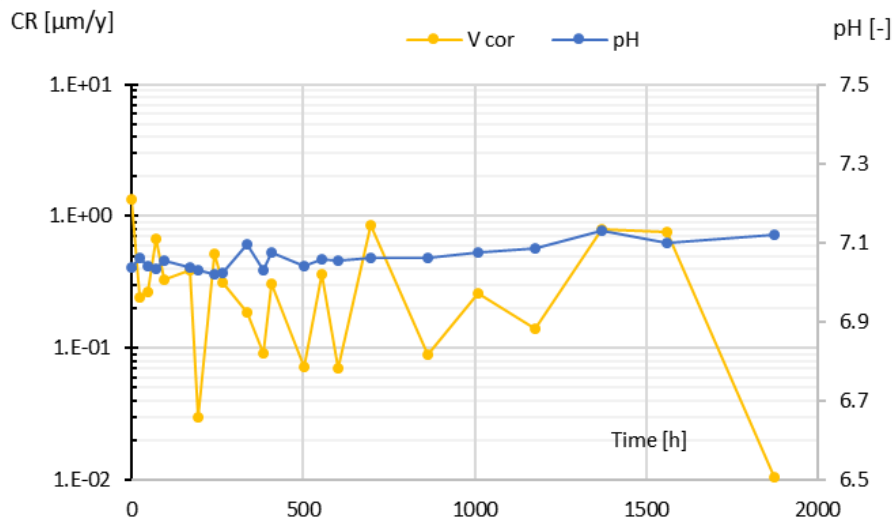

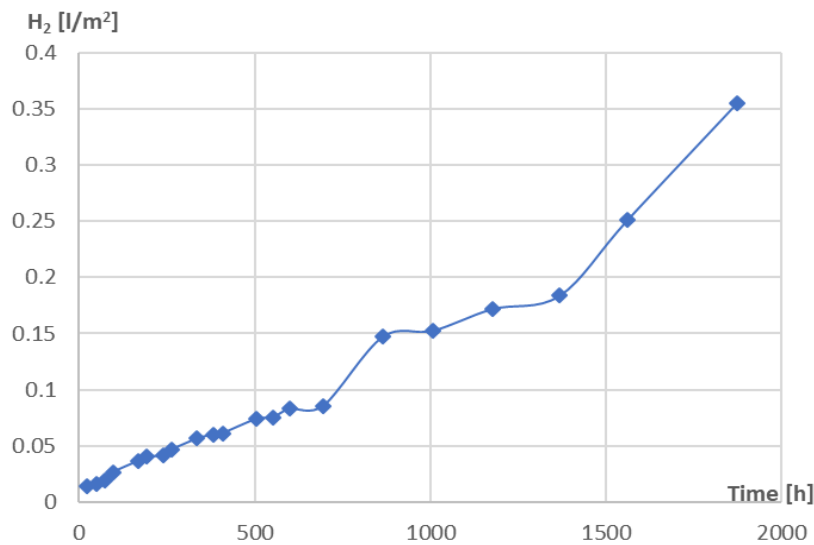*Figure 20. Corrosion rate(Vcor) and pH vs. time for the AlMg3 sample in the MPC pore solution*

Figure 21. Volume of H$_2$ from the electrochemical parameters (AlMg3 in MPC pore solution)

Chemical tests in simulated MPC pore solution:

The corrosion rate calculated from the volume of hydrogen released is 3.7 µm/year after 312h of testing and it maintains almost constant around this value until the end of the testing period of 85 days (Figure 22).

The hydrogen volume measured is 2.252 L/m^2 and its evolution is represented in Figure 23.

The comparative analysis of the corrosion rates obtained in the two tests (chemical and electrochemical) shows a difference, but the analysis of all the data obtained during the electrochemical tests shows a stabilization around the same corrosion rate. In the MPC pore solution, the corrosion rate in the first 400 hours tends to increase and decrease from interval to interval until it stabilizes.

Comparing the values of the H_2 volumes obtained in the two tests, we can say that there is practically no difference, the difference recorded coming from the different testing times, namely 2040 hours in the chemical test compared to 1872 hours in the electrochemical test.
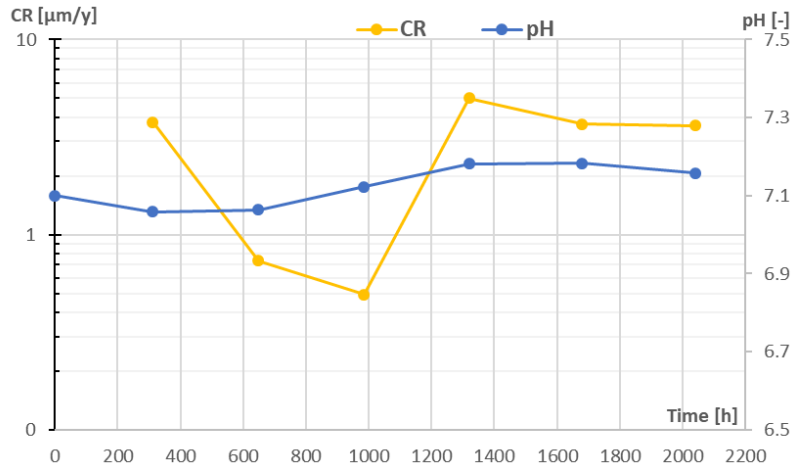

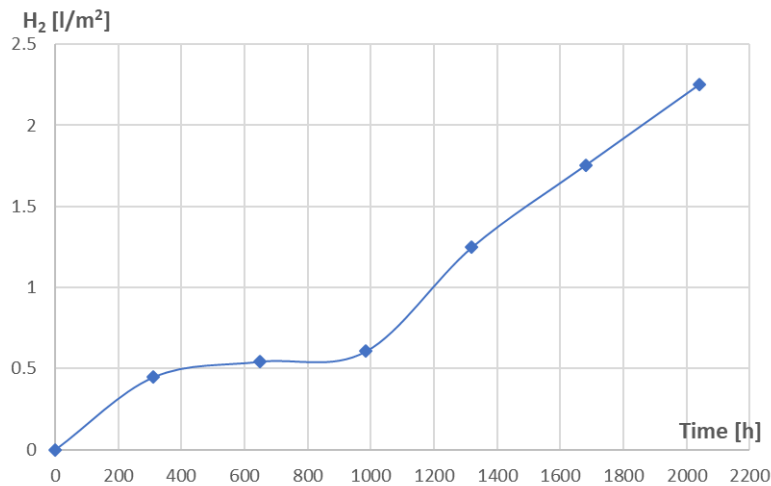*Figure 22. Corrosion rate and pH vs time (chemical test AlMg3 – MPC)*

Figure 23. Cumulative hydrogen volume (chemical test AlMg3 – MPC pore solution)

Electrochemical tests in Ca(OH)₂ solution (OPC simulated pore solution)

The corrosion rate was determined by the software based on the corrosion currents and its evolution is presented in Figure 24.
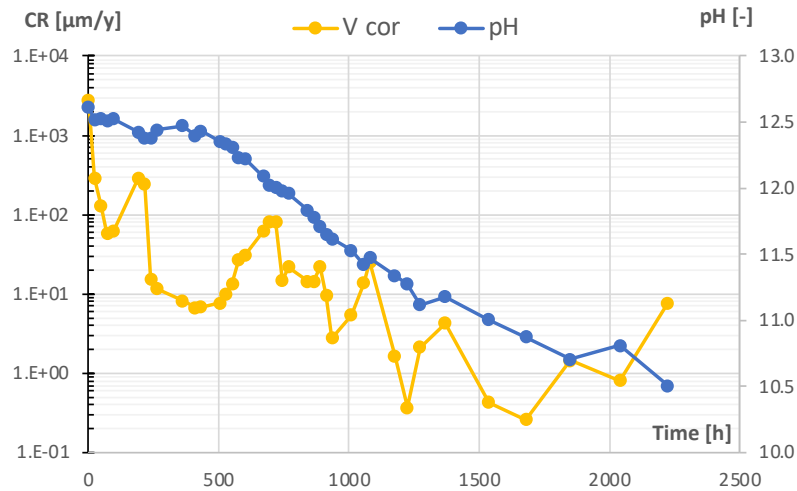
Figure 24. Corrosion rate (Vcor) and pH evolution for OCP pore solution

The total volume of hydrogen calculated based on the electrochemical parameters is 50.15 L/m^2 and its evolution can be seen in the Figure 25.
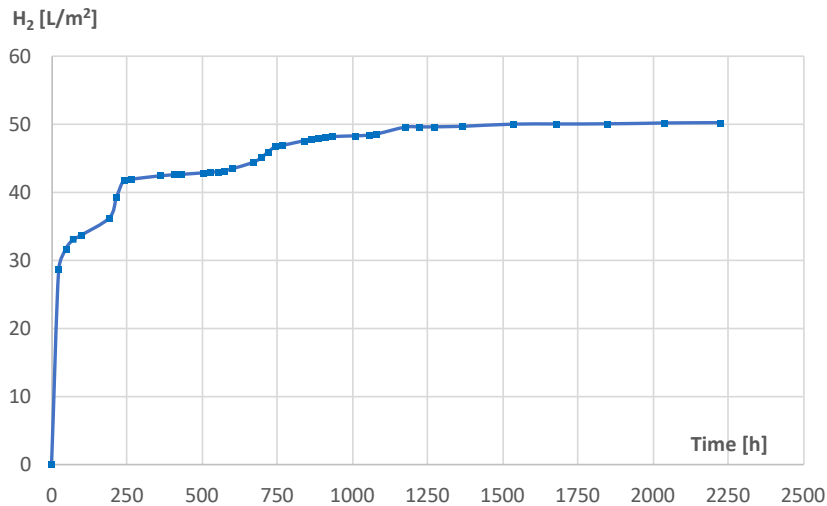
Figure 25. Volume of H$_2$ calculated from electrochemical parameters for OCP pore solution

Chemical tests in Ca(OH)$_2$ solution using AlMg3 samples:

The chemical tests for AlMg3 in OPC pore solution indicate an evolution of the corrosion rate directly proportional to the pH. The AlMg3 corrosion rate, estimated based on the measured hydrogen volume, decreases from 2.96E+03 µm/year, value recorded after 24 hours, to 0.9 µm/year after 91 days (Figure 26).

Figure 26. Corrosion rate (Vcor) and pH evolution in the OCP pore solution

The volume of released hydrogen measured in the same period is 94.98 L/m^2 expressed in normal conditions. Its evolution over time is presented in Figure 27.
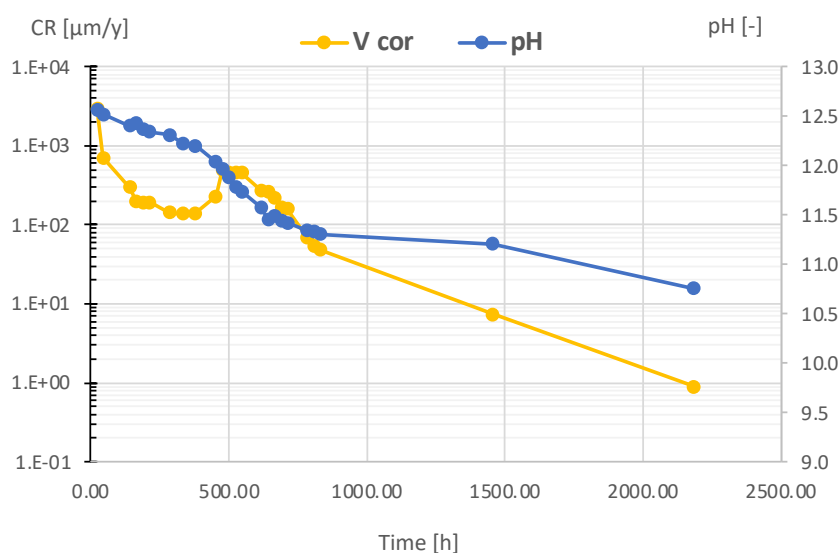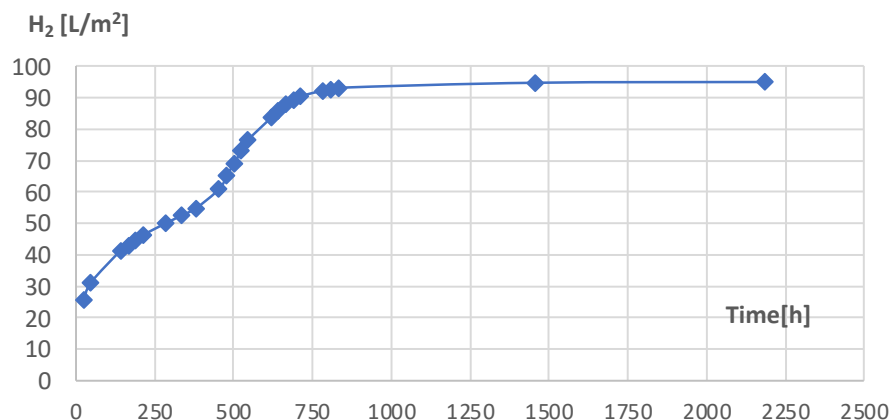

Figure 27. The cumulative H_{2n} volume obtained in the OCP pore solution

Table 16 summarises the corrosion rate and H_2 volumes from the RATEN studies in solutions.

Table 16. Corrosion rate and H_2 volume for AlMg3 in pore solutions

Testing environment	Measured method	Initial [h]	End [h]	$CR_{initial}$ [µm/y]	$H_{2-initial}$ [L/m²]	CR_{end} [µm/y]	$H_{2-Total}$ [L/m²]
MPC	LPR	0	1872	1.356	0.0139	0.0105	0.355
	Chemical	312	2040	3.763	0.45	3.612	2.252
Ca(OH)₂	LPR	0	2223	2751.3	28.86	7.7	50.15
	Chemical	24	2184	2955.3	25.562	0.9	94.98

The values of the hydrogen volume obtained by the two types of tests differ mainly because in the chemical test the released hydrogen is measured continuously, while in the electrochemical test the measurements are made only once a day, and the resulting hydrogen volume is calculated for that moment.

3.3.2 Cement matrix selection for Al immobilisation: Al alloy corrosion evolution

- CSIC:

The study of Al interaction with different cementitious matrices is necessary to understand the metal reactivity to find an optimal matrix for its immobilisation. Long-term corrosion studies were carried out on Al and AlMg alloys in 1M MPC and OPC blended mortars (CEM IV and CEM I+SF), to replace the commonly used CEM I matrix for Al immobilisation. Different evolution stages of the study were performed by the CSIC in present topic:

- First stage (0-300 days): 1-year under water immersion condition was performed in all cementitious matrices.
- After 1 year immersion: All samples were dried over 6 days and then coated with epoxy paint except one face of the mortar cube.
- Second stage (300 to 600 days): MPC and CEM I mortars were maintained for another year in water in individual and hermetic plastic containers. Another set of all the mortar matrices (CEM IV, CEMI+SF,1M MPC mortar and CEM I) were exposed to an alkaline simulated pore media (results in 1.4.6).

During the water immersion period, the pore pH and ions in the pore solution were periodically determined. The Al reactivity is analysed with E_{corr} and i_{corr} measurements.

Figure 28-left shows in a Pourbaix diagram, the E_{corr} of Al and AlMg alloy versus pore pH in MPC and OPC blended matrices over 1 year. For the MPC matrix with near neutral pore pH, CSIC found a significant evolution to more anodic values in the Al passive state. A shift towards more alkaline pH is detected in the long term under water immersion due to the leaching of phosphates and a decrease in the pore solution causing the increase of internal pore pH. In consequence, both Al alloys evolve to a more cathodic values suggesting higher corrosion risk and hydrogen evolution. In the case of CEM I and CEM IV matrices, Al and AlMg alloy are in the corrosion region with high risk for H_2 evolution. In contrast, the CEM I+SF matrix shows progressive evolution to lower E_{corr} values in the Al passive region as consequence of the decrease in the pore pH, close to 10 at the end of the test. This response suggests a reduction in corrosion risk and more controlled H_2 evolution than CEM I and CEM IV.

Figure 28-right shows the evolution of the corrosion rate under water immersion. In the first-year immersion, it was observed that all cement matrices show a tendency of decrease. Higher values are identified in CEM I, followed by CEM IV (2028 and 170 µm/year respectively). In contrast, MPC exhibits two order of magnitude lower corrosion rate than CEM I. In addition, CEM I+SF shows high initial corrosion rates, equalising with the MPC after 300 days (≈150 µm/year to 0.012 µm/year). No significant differences in corrosion rate are measured between both alloys. After 1 year, reactivation of the corrosion process is observed in MPC with an increase in V_{corr} and pore pH (pH 9.9), which remain constant over time (≈0.05 µm/year). No significant changes are observed for the CEM I mortar system, which maintains a constant V_{corr} for both alloys over time (≈0.81 µm/year) due to the pore pH remaining alkaline (pH 12.6).
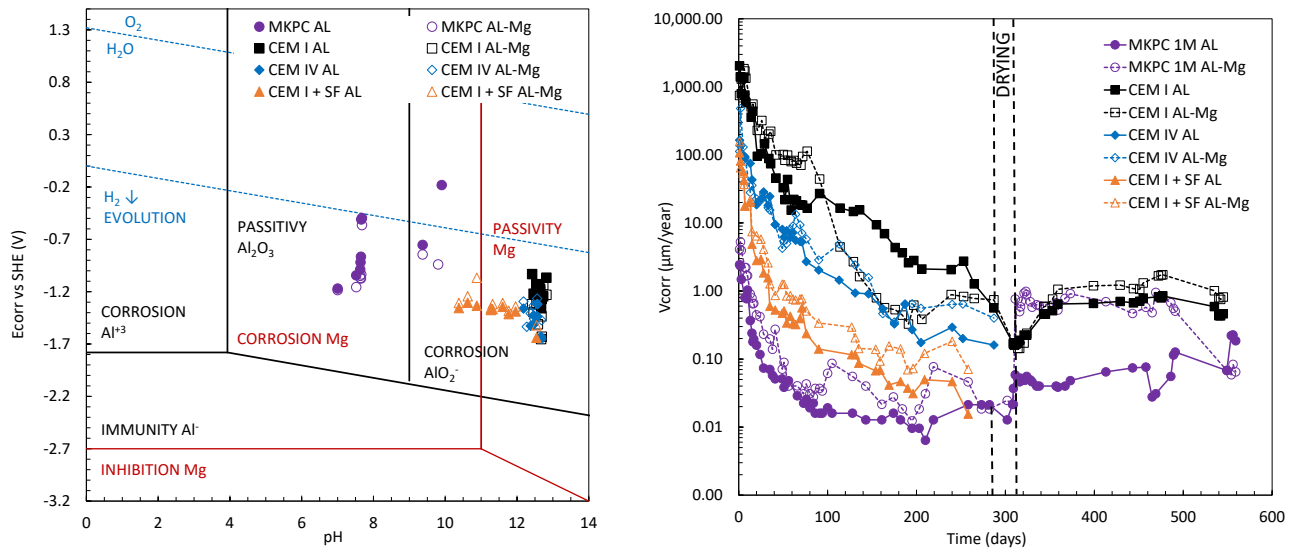
Figure 28. E_{corr} – pH for Mg and Al Pourbaix diagrams (left) and corrosion rate (V_{corr}) versus time (right) for Al and AlMg alloy in 1M MPC and OPC blended mortars under water immersion

From the i_{corr} data, the accumulated volume of H_2 released was estimated using Equations (6) and (7). Figure 29 shows the volume of H_2 released versus time. As expected, higher H_2 values are evolved in the OPC blended matrices. The highest volumes are calculated for CEM I and CEM IV mortars (≈25 L/m^2 at 1 year) related to their high alkalinity. In contrast, CEM I+SF shows lower volume of H_2 release (≈7.11 L/m^2 in 1 year) due to the lower pore pH over time. On the other hand, three order of magnitude lower volumes of H_2 are observed in MPC (≈0.02 L/m^2 at 1 year).

In all cases, the highest H_2 risk is detected in the early stages of Al/matrix interaction, which decreases significantly after 30 days, with an attenuate over exposure time. No significant difference is observed between Al and AlMg. In the second-year immersion, no significant effect in the volume of H_2 release is detected for CEM I mortar. However, in the case of MPC after 2-year immersion, an increase is identified which continues evolve over time (up to 0.20 and 0.04 L/m^2 for AlMg and Al respectively). This increase is related to the evolution of the pore pH in an MPC matrix in the long term under water immersion condition, giving a higher corrosion risk over time.

To understand if attenuation phenomena exist over immersion time, the amount of H_2 release was estimated at different periods: 0 to 30 days, 30 to 300 days, and 300 to 600 days in water for Al (see Figure 30-left) and AlMg alloy (see Figure 30-right). H_2 values at 2 years for CEM IV and CEM I+SF were estimated from the stabilised i_{corr} value at 1 year. As noted, the highest H_2 release occurs in the first month of interaction in all cementitious matrices, which slightly decreases after 1 year for Al and AlMg (30 to 300 days). However, the total volume of H_2 release is lower between 300 to 600 days, significantly for MPC and CEM I+SF (≈0.02 and 0.1 L/m$_2$ respectively). The attenuation process exists and increases with the time of the interaction with the matrix with the Al alloy.
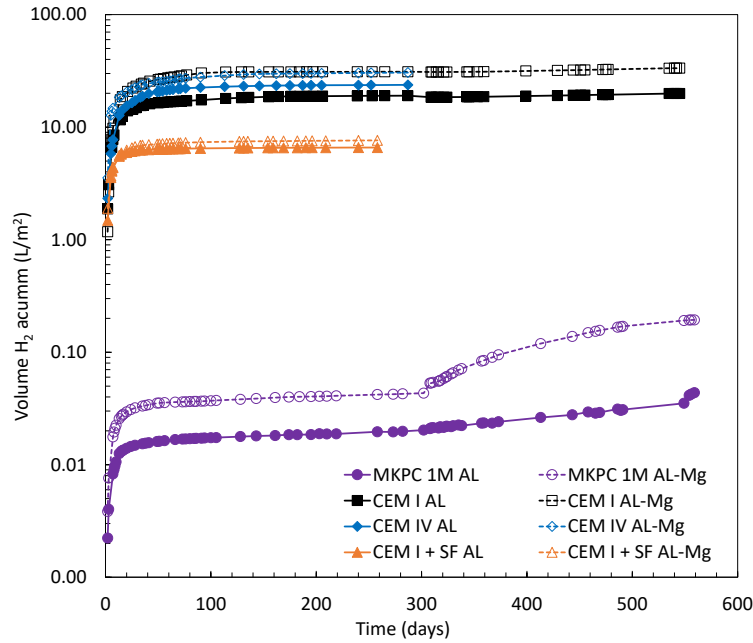
Figure 29. Accumulated H_2 over 2-years water immersion in MPC and OPC blended matrices
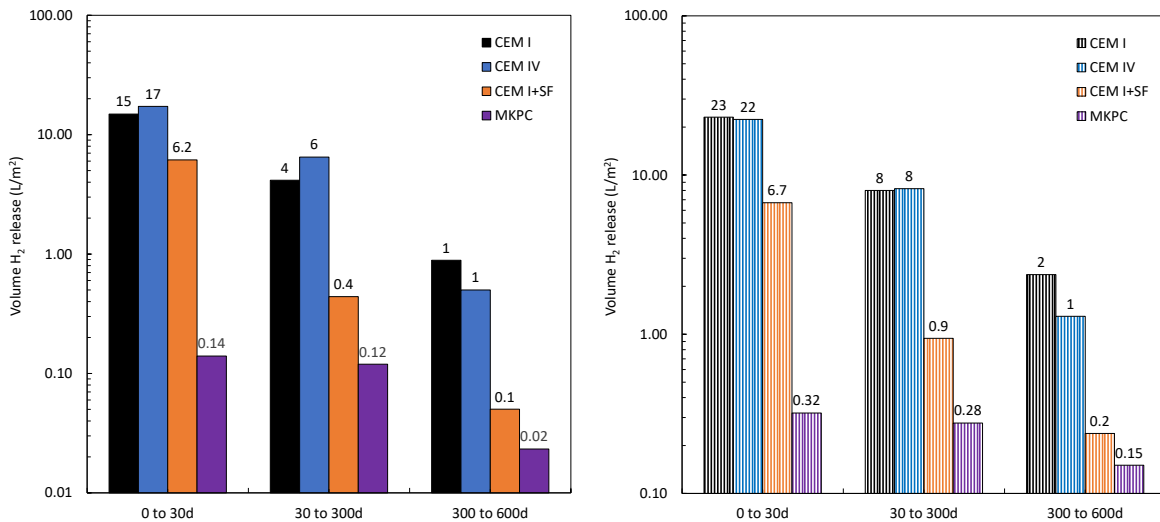

Figure 30. H_2 release in different periods: 0-30 days, 30-300 days, and 300-600 days in MPC and OPC blended mortars over 2-years under water immersion for pure Al (left) and AlMg alloy (right)

To understand the effect of the long-term corrosion performance of Al and AlMg alloy in cementitious matrices, Table 17 shows the pore pH and pore ion evolution analysed during the test. In the MPC mortar, a significant decrease in phosphate ions is observed due to the leaching process associated with immersion in water. In addition, the content of K and Mg ions decreases, to a lesser extent, up to 2 years of immersion in water. However, a significant increase in pore pH close to 10 is observed, which affects the Al corrosion response.

In the case of CEM I, a decrease of larger amounts of Ca ions is observed after 2 years in water immersion. In addition, a constant and higher pore pH is maintained over the test (≈12.6). Similar behaviour is observed for CEM IV (pH 12.56), while CEM I+SF shows a significant decrease in pore pH down to 10.88 after 1 year in water, with better corrosion behaviour over time.

Table 17. Pore ion and pH of the pore and external water of MPC and OPC blended matrices after 1 and 2 years under water immersion

Binder	Solution	Days	pH	P	B	Mg	K	Ca
CEM I	Pore	300	12.82	-	-	-	77	548
		600	12.58	-	0.4	-	165	343
	External	300	9.13	2	-	0.3	44	25
		600	8.68	0.8	0.2	0.3	100	29
CEM IV	Pore	300	12.56	-	-	-	120	309
	External	300	8.94	2	-	0.6	80	49
CEM I+SF	Pore	300	10.88	7	-	2	80	88
	External	300	8.94	1	-	0.3	16	50
MPC	Pore	7	7.00	6572	199	60	28108	19
		300	9.90	120	10	1	445	4
		600	9.37	226	18	16	841	3
	External	300	9.8	203	18	15	612	2
		600	9.40	548	48	5	2253	1

At the end of the experiment, after 2 years in water, MPC and CEM I mortar matrices were analysed by Mercury Intrusion Porosimetry (MIP) and XRD technique to understand the effect of the environment in the long-term mortar microstructure. The MPC microstructure consists of the main acid-base reaction product K-Struvite. In addition, CEM I matrix mainly contains portlandite as the main hydration product with secondary ettringite according to its alkaline pore pH (see Table 17). The MIP analysis gives a lower total porosity of 8.1% in CEM I, comparing with a 12.3% for MPC. A unimodal distribution with higher capillary pores (< 0.1 μm) is detected for CEM I matrix after 2 years under water immersion. Contrary, multimodal distribution is identified for MPC with larger intermediate and small pores (10-0.1μm).

SEM/EDX analyses were carried out to observe the changes at the Al/matrix interface.

In a CEM I matrix, a heterogeneous layer of aluminium oxide (Al_2O_3) with a thickness of 50 to 90 μm is identified on the Al surface (see Figure 31-a), which explains the high corrosion rates measured due to its high alkalinity [15]. The elemental distribution of the cement matrix near the Al interface in Figure 31-b shows an Al enrichment of the matrix up to a 1 mm depth. At that depth, Al ions formed by in contact with the highly alkaline matrix react with the matrix components (Ca and S) to form ettringite as the main hydration product [$(CaO)_6$-(Al_2O_3)-$(SO_3)_3$-$32H_2O$] also with XRD. Microcracks in the cement paste are detected, resulting from ettringite expansions, which affect the matrix stability.

The Al_2O_3 passive layer is not observed at the Al/MPC interface. For these near neutral matrices, a homogeneous layer of 30 μm thickness rich in phosphate is detected on the metal surface by EDX analysis (see Figure 31-c). However, the elemental distribution in Figure 31-d confirms that no Al enrichment is detected in the matrix, indicating the lower Al corrosion activity in contact with an MPC matrix. A composition of 25% phosphates, 29% MgO, 3% Al_2O_3 and 30% K_2O is identified, corresponding to the formation of the main reaction product K-struvite [$KMg(PO_4)$-$6(H_2O)$] as detected by XRD technique. The Al detected in the matrix is attributed to the FA in the MPC formulation.
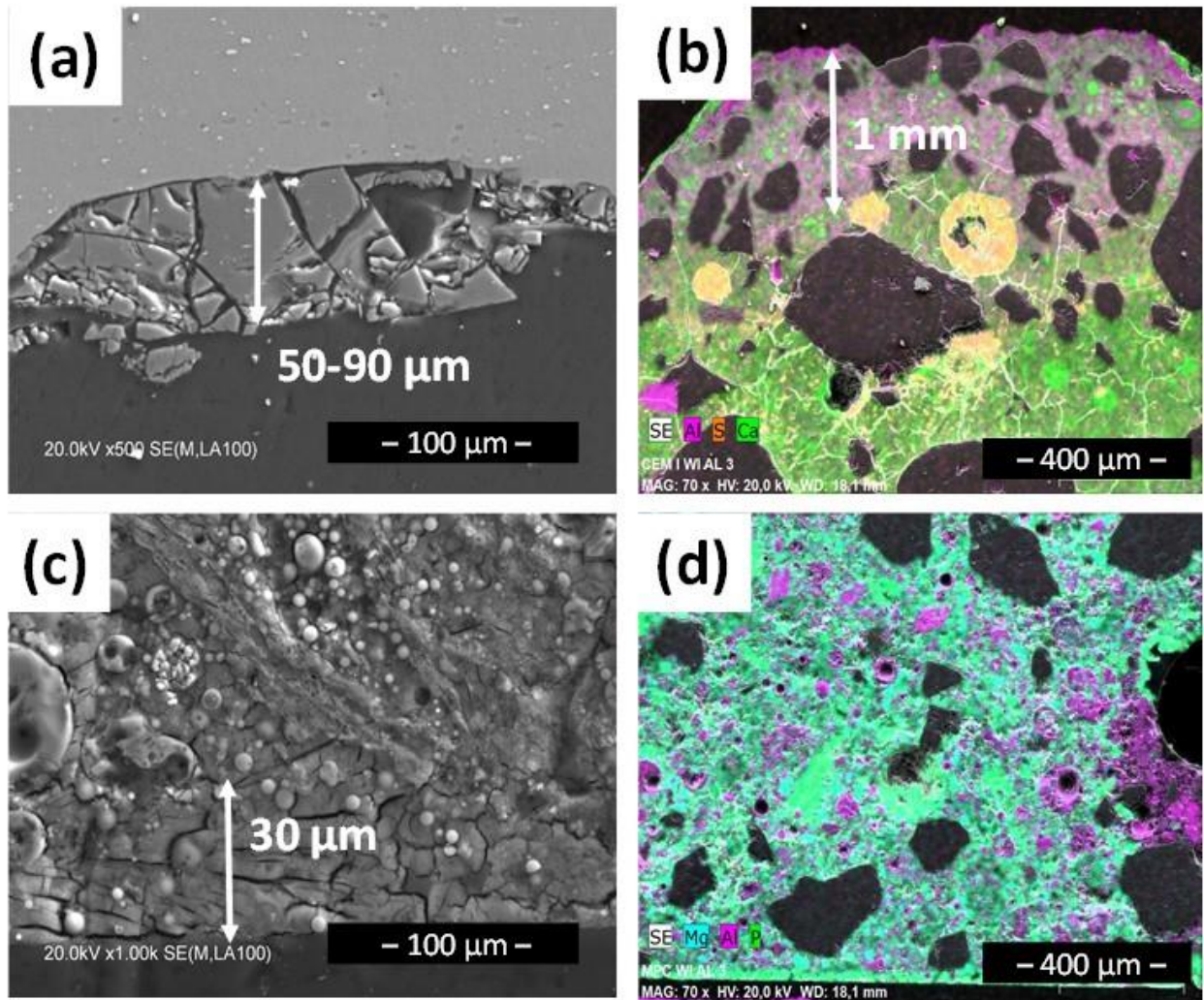
Figure 31. SEM/BS images of: a) Zoomed area of layer formation at the metal/CEM I interface, b) Mapping spectra of metal/CEM I interaction, c) Zoomed area of layer formation at the metal/MPC interface, and d) Mapping spectra of metal/MPC interaction

Table 18 summarizes the corrosion rate and H_2 volumes of MPC and OPC blended mortars under 1 or 2 years under water immersion. Corrosion and H_2 values are estimated for CEM IV and CEM I+SF using the stabilised i_{corr} value at 1-year immersion.

Table 18. Corrosion rates and accumulated volumes of H_2 of Al and AlMg alloy in MPC and OPC matrices in 1 and 2 years in water

Mortar	Al					AlMg				
	V_{corr} (µm/year)			Vol H_2 (L/m²)		V_{corr} (µm/year)			Vol H_2 (L/m²)	
	0d	1y	2y	1y	2y	0d	1y	2y	1y	2y
CEM I	2028	0.56	0.46	19.03	19.92	746	0.74	0.81	31.08	33.45
CEM IV	164	0.16	0.16	23.73	24.24	112	0.40	0.40	30.55	31.81
CEM I+SF	107	0.01	0.01	6.58	6.64	157	0.07	0.07	7.64	7.88
MPC	2.43	0.01	0.18	0.02	0.04	4.10	0.02	0.06	0.04	0.19

- ENRESA:

ENRESA carried out corrosion tests on aluminium embedded in CABRIL (CEM I) and HORMISEC (CEM II) mortars. After 24 hours of setting, a visual inspection of the mortar specimens was performed, and some holes were observed in CABRIL mortar specimens housing aluminium. These holes are attributed to the formation of channels of H_2 generated by the corrosion of aluminium during the setting stage (and perhaps during the first curing hours) of the mortar. In HORMISEC mortar specimens, with embedded aluminium, none of these channels was identified, most likely because of the higher porosity and lower mechanical resistance of this mortar, which facilitates the exit of the H_2 to the outside by multiple routes.

Table 19 shows the corrosion rate values measured for aluminium in CABRIL and HORMISEC mortars. The corrosion rate values obtained for aluminium are the lowest recorded in the different mediums, with values of average corrosion rate for aluminium in the CABRIL mortar of 0.058 mm/year, after 5450 hours of testing (7.4 months). For the HORMISEC mortar, the corrosion rate measured for the aluminium after 4200 hours of testing (5.7 months) is 0.086 mm/year.

Table 19. Corrosion rates of Al in HORMISEC and CABRIL mortars in oxic and anoxic conditions

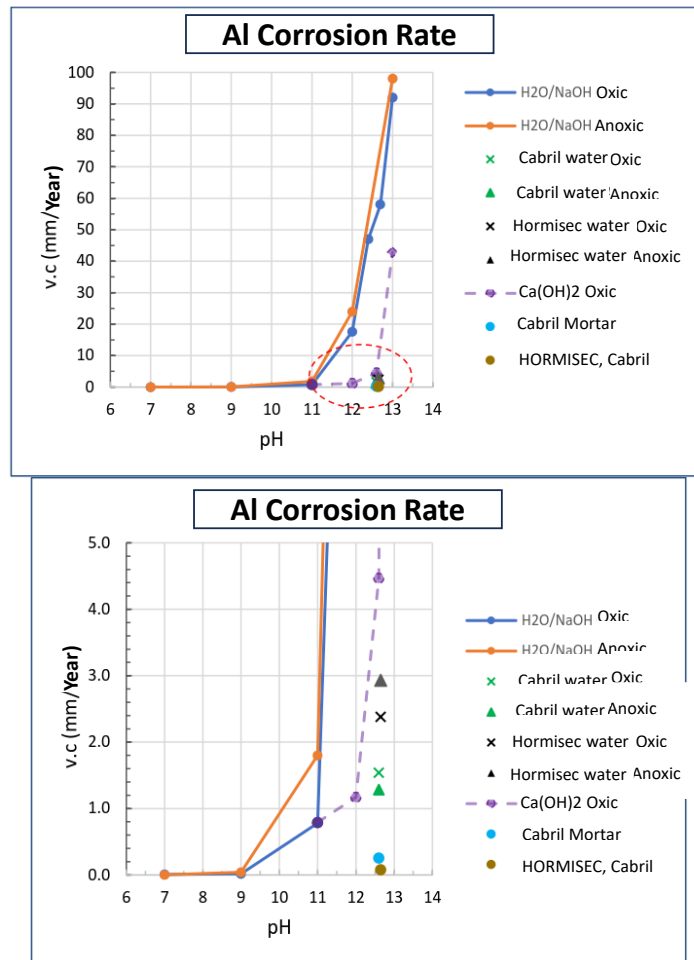|		CABRIL mortar		HORMISEC mortar		
	Test time (hours)	Test time (days)	Corrosion rate (mm/year)	Test time (hours)	Test time (days)	Corrosion rate (mm/year)
Anoxic	48	2	0.75	-	-	-
	144	6	0.41	-	-	-
	360	15	0.39	-	-	-
	672	≈28	0.26	-	-	-
	1654	≈69	0.16	-	-	-
	2397	≈100	0.11	2352	98	0.081
	3212	≈133	0.079	3887	≈162	0.083
	5447	≈227	0.058	4200	175	0.086
Oxic	5447	≈227	0.047	3215	≈134	0.062

Figure 32. Graphical representation of the corrosion rate (V_{corr}) of pure Al in CABRIL and HORMISEC mortars and synthetic pore water at different pH under oxic and anoxic conditions

There is hardly any significant difference in the corrosion rate values measured on aluminium specimens embedded in mortar and tested under anoxic or oxic conditions. It is possible that the carbonation of the water has little effect on the water that finally enters to the aluminium surface, after passing through the mortar barrier.

Figure 32 compares the average corrosion rate of Al in the different test media considered in this study, for a period of approximately 720 hours. The corrosion rate values measured for aluminium in the CABRIL and HORMISEC mortars are significantly lower than those obtained in the "synthetic" simulated pore water of such mortars.

The corrosion of aluminium in CABRIL and HORMISEC mortars generates a layer of corrosion products that is compact and relatively well adhered to the substrate as observed in Figure 33, providing effective protection for Al. The analysis by X-ray diffraction (XRD) indicates that this oxide is constituted, mainly, by $Al(OH)_3$. The fact that the mortar "confines" to some extent the corrosion products generated, contributes to the compaction of the corrosion products over the sample.

The corrosion rate evolution from the electrochemical measurements is somewhat lower than the average corrosion rate with values of 0.02 mm/year after 2110 hours of testing (as seen in Figure 34). This is mainly due to the fact that the aluminium specimen in the electrochemical test is based on a condition that has already been passivated, which makes the velocity values of instant corrosion lower.
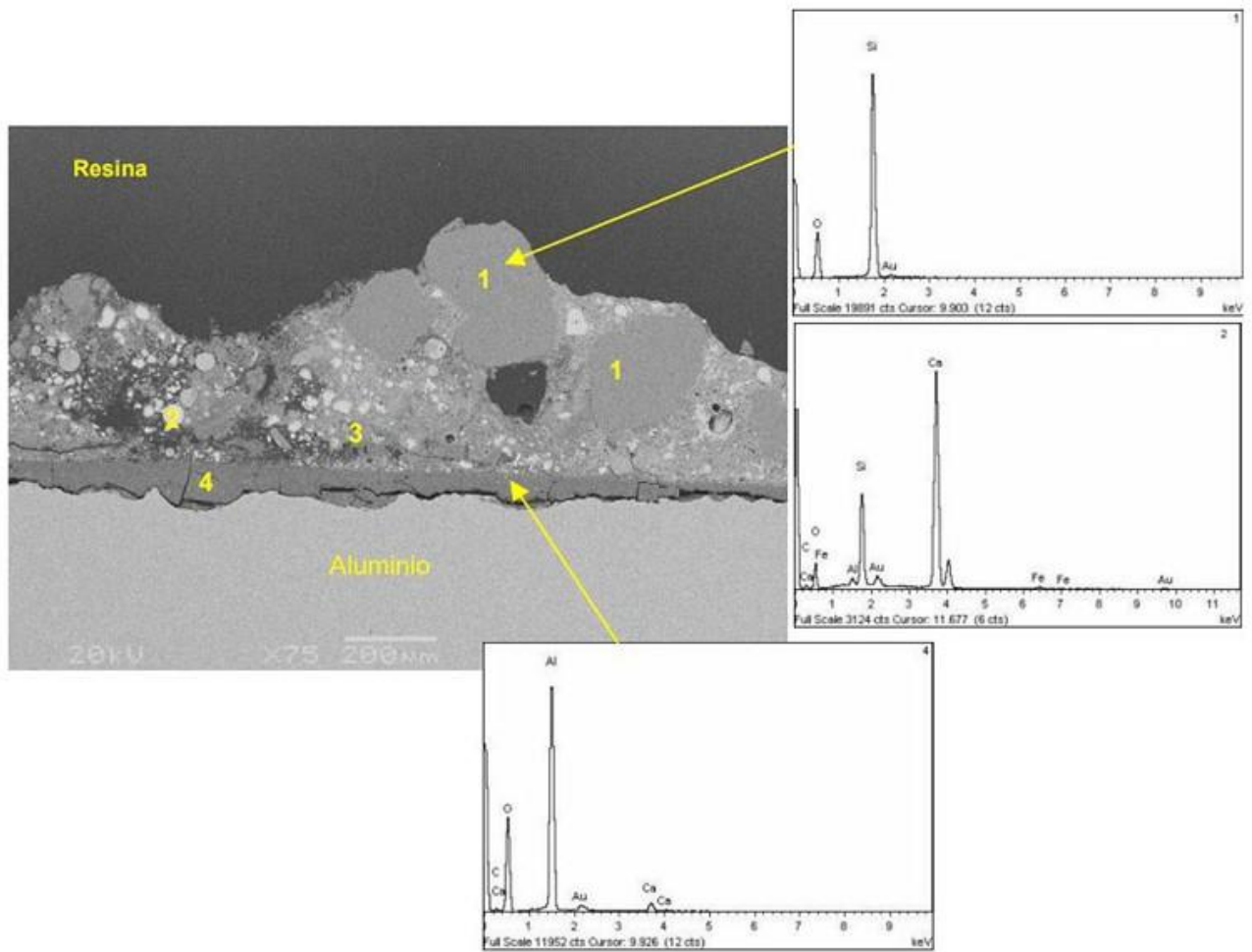
Figure 33. Corrosion product layer at the Al surface in CABRIL and HORMISEC mortars by BES/EDS technique
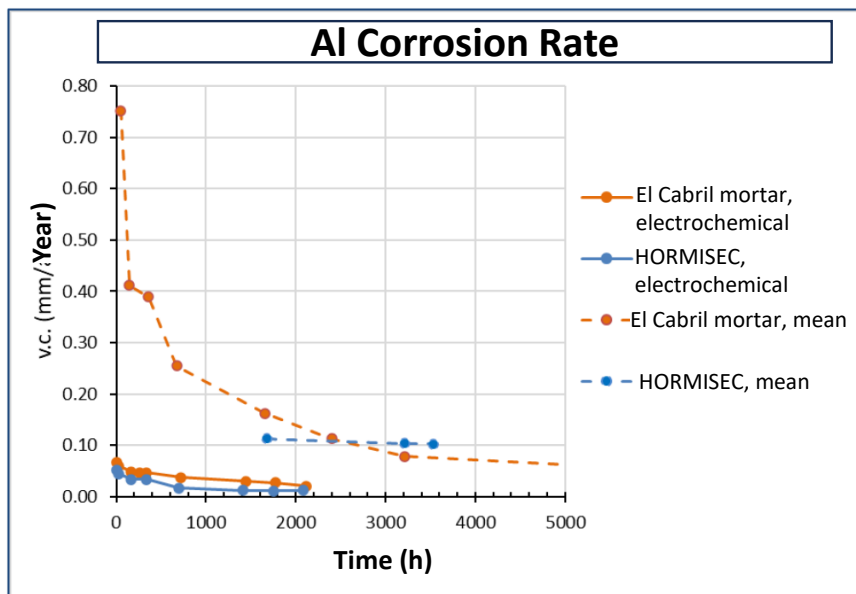

Figure 34. Corrosion rate (V_{corr}) over time from electrochemical test and mean values of pure Al in CABRIL and HORMISEC mortar specimens

Corrosion tests have been carried out by ENRESA on aluminium specimens embedded in MPC, in addition to those already mentioned in OPC (CABRIL and HORMISEC). Figure 35 compares a

specimen of CABRIL mortar with Al inside with a MPC specimen, also with aluminium, after the setting stage (24 hours). All the CABRIL specimens show holes due to the exit of the H_2 generated during the setting stage. On the contrary, none of the MPC specimens with Al show these holes, indicating that the corrosion of the aluminium embedded in the MMP is significantly lower.

Figure 35. Comparison between CABRIL (left) and MPC (right) mortar specimens with embedded Al. Holes from H_2 release in CABRIL mortar are appreciated (red circle)

Table 20 shows the corrosion rate values measured for aluminium in the MPC mortar. The corrosion rate of aluminium decreases significantly over time, due to the formation of a protective corrosion layers on the metal surface.

Table 20. Corrosion rates values of aluminium in MPC mortars under oxic and anoxic conditions

Ambient condition	Time (h)	Time (days)	Corrosion rate (mm/year)	Ambient condition	Time (h)	Time (days)	Corrosion rate (mm/year)
Anoxic	48	2	0.097	Oxic	5472	228	0.0023
	144	6	0.024				
	360	15	0.014				
	672	28	0.0071				
	1656	69	0.0060				
	2640	110	0.0027				
	4056	169	0.0024				
	5472	228	0.0011				

Figure 36 compares the average corrosion rate values of Al in the different test media contemplated in this project, for approximately 30 days. The measured values for aluminium in the MPC are the lowest on record, with average values for Al of 0.0071 mm/year after 28 days of testing (672 hours). For CABRIL mortar, the corrosion rate measured after 28 days of testing was 0.255 mm/year (almost 40 times higher). These Al corrosion rates correspond to an annual H_2 generation rate per m^2 of Al of 0.858 m^3/m^2 per year for the MPC.
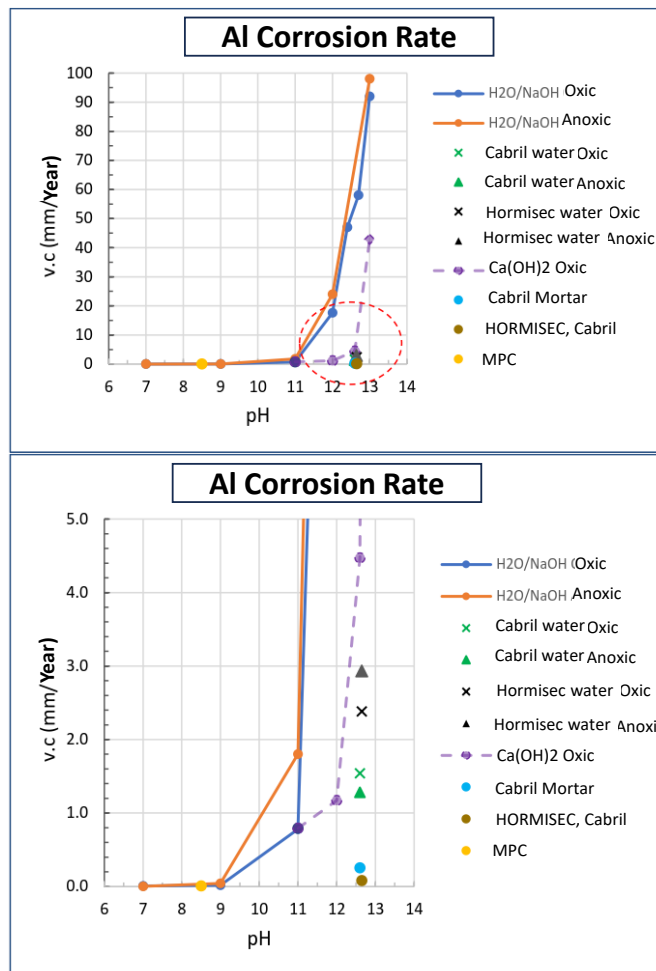
Figure 36. Corrosion rate (V_{corr}) for aluminium in all solution and mortar system at different pH

The corrosion of aluminium in the MPC mortar is uniform-generalized type. The BSE image in Figure 37 shows virtually no corrosion product layer.

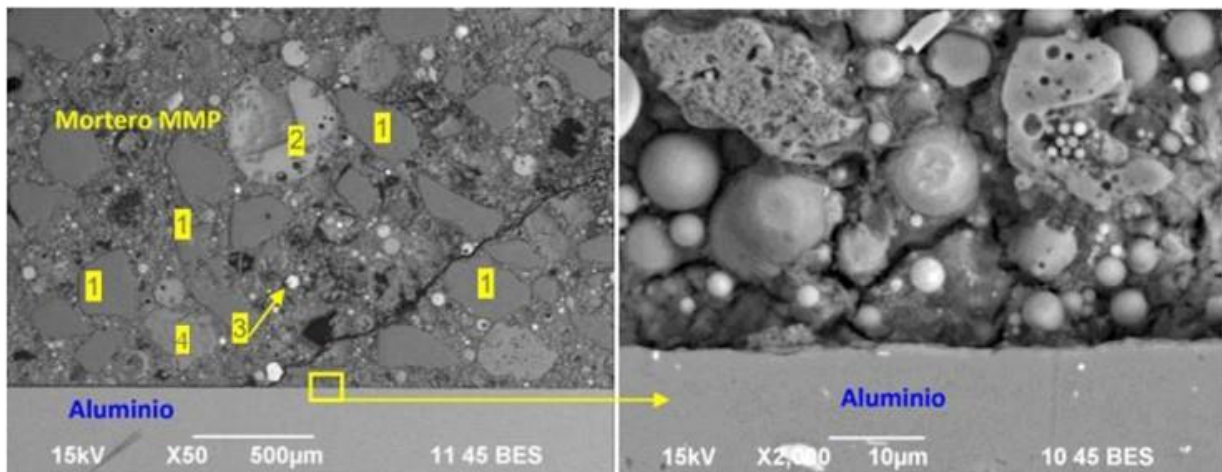*Figure 37. BSE image at the Al surface in the interaction with an MPC mortar*

- RATEN:

Electrochemical tests with AlMg3 coupon embedded in MPC and OPC pastes

(a) MPC paste   *(b) OPC paste*

Figure 38 presents the evolution of the hydrogen volume estimated based on the parameters measured in the electrochemical tests, for AlMg3 embedded MPC (a) and respectively in OPC (b).
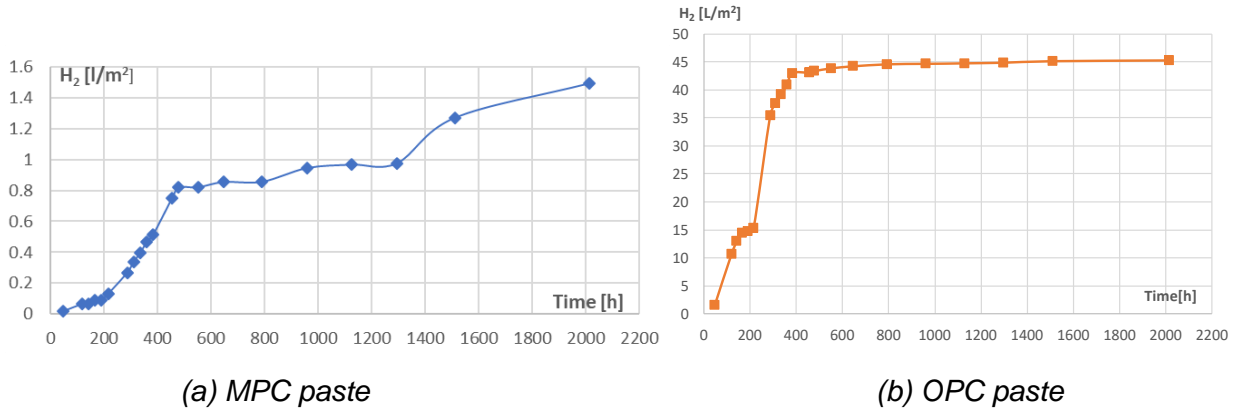
(a) MPC paste   *(b) OPC paste*

Figure 38. Volume of hydrogen calculated from the electrochemical test performed on AlMg3 embedded in the two matrices

As it is shown in (a) MPC paste   *(b) OPC paste*

Figure 39, the corrosion rate of AlMg3 embedded in MPC paste evolves from one moment to another, so the uncertainty on the total volume of hydrogen calculated assuming that the corrosion rate is constant during the entire time interval between two consecutive measurements is quite large. The value of the calculated hydrogen volume remains precise only for the moment in which the corrosion rate is measured.
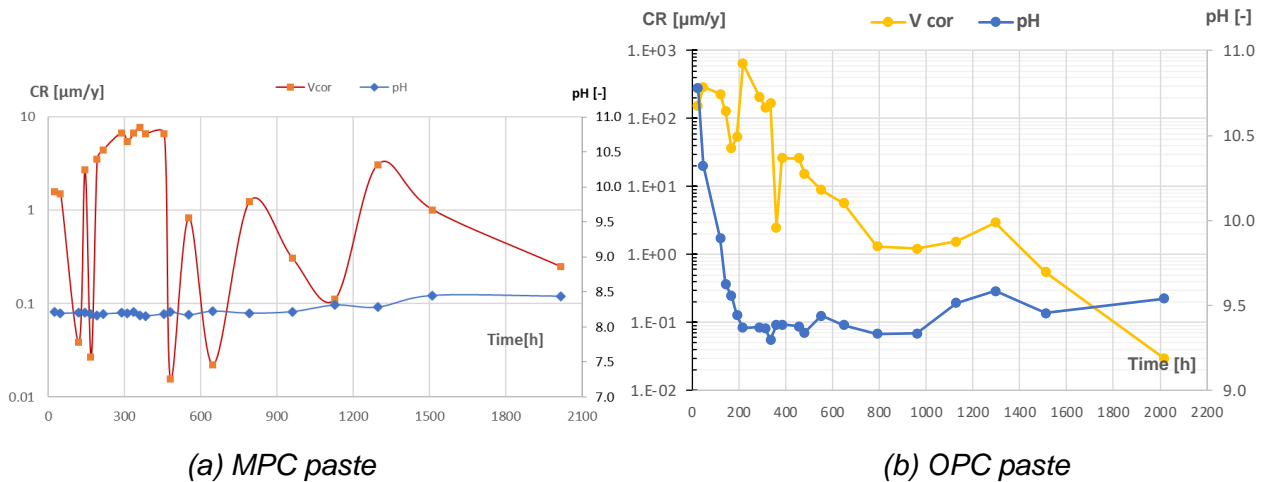

(a) MPC paste   *(b) OPC paste*

Figure 39. Corrosion rate and pH measured by electrochemical test on AlMg3 sample embedded in the two matrices

The evolution of the corrosion rate obtained for MPC paste ((a) MPC paste
(b) OPC paste

Figure 39-a) indicates transitions from an active state to a less active one through passivation. During the test, the corrosion rate registered low values, with repeated changes from one measurement to another, starting from 3.5 µm/year to 7.7µm/year at 360 hours of testing. The minimum corrosion rate value (0.016 µm/year) was recorded at 480 hours of testing.

For OPC paste ((a) MPC paste   *(b) OPC paste*

Figure 39 -b), the corrosion rate evolves also in several stages, reaching maximums for each stage, due to the transition to a passive zone with greater chemical stability compared to the created environment. In the first stage, the corrosion rate doubles its value, from 152.5 µm/year to 290

μm/year, after which it remains almost constant between 800 hours and 1300 hours of testing, and after 1300 hours it follows a downward trend. The maximum corrosion rate (642 μm/year) was recorded at 216 hours. The test was continued until there were no more significant jumps in the corrosion rate evolution, at the end of the test the recorded corrosion rate being 0.03 μm/year. All values recorded for AlMg3 corrosion rate in OPC paste are as expected higher compared to MPC.

Chemical test on AlMg3 coupon embedded in MPC and OPC pastes

The graphic representation of the volume of cumulative hydrogen, collected during this test, relative to the surface of the sample is shown in (a) MPC paste   (b) OPC paste

Figure 40.

(a) MPC paste   *(b) OPC paste*
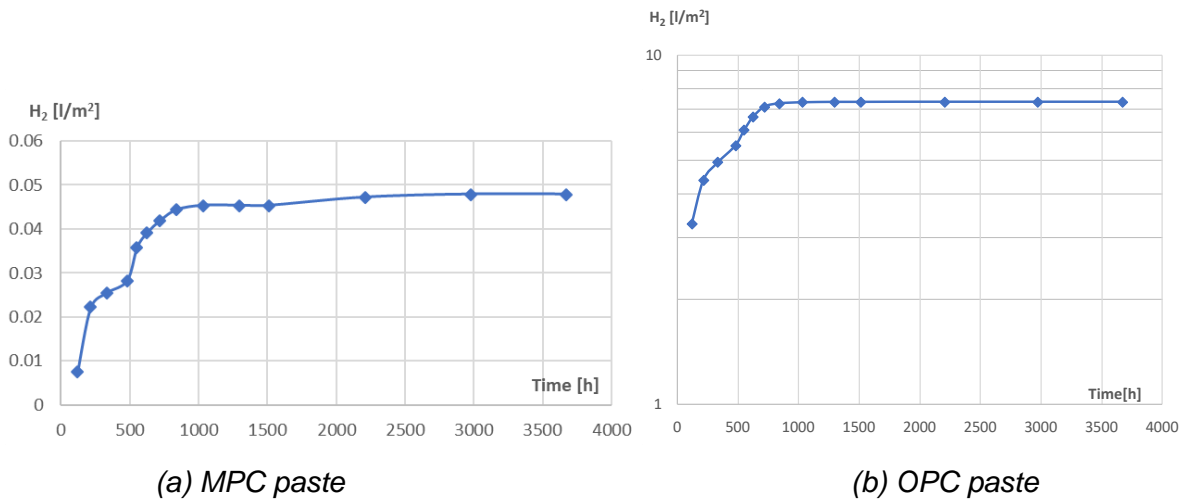
Figure 40. Cumulative hydrogen volume in chemical test (AlMg3 in MPC matrix)

The hydrogen volume released in the corrosion processes occurring for AlMg3 embedded in MPC is small and required that measurements be carried out at longer time intervals to avoid as much as possible reading errors and for comparison, the same time intervals were used also for OPC paste.

The evolution of the corrosion rate assessed based on the measured H_2 volume indicated that for MPC paste ((a) MPC paste   (b) OPC paste

Figure 41- a) the corrosion rate evolves within fairly small limits, with two picks one after 216 hours of the test (2.02 μm/year) and the second one after 555 hours (1μm/year), followed by a downward trend.
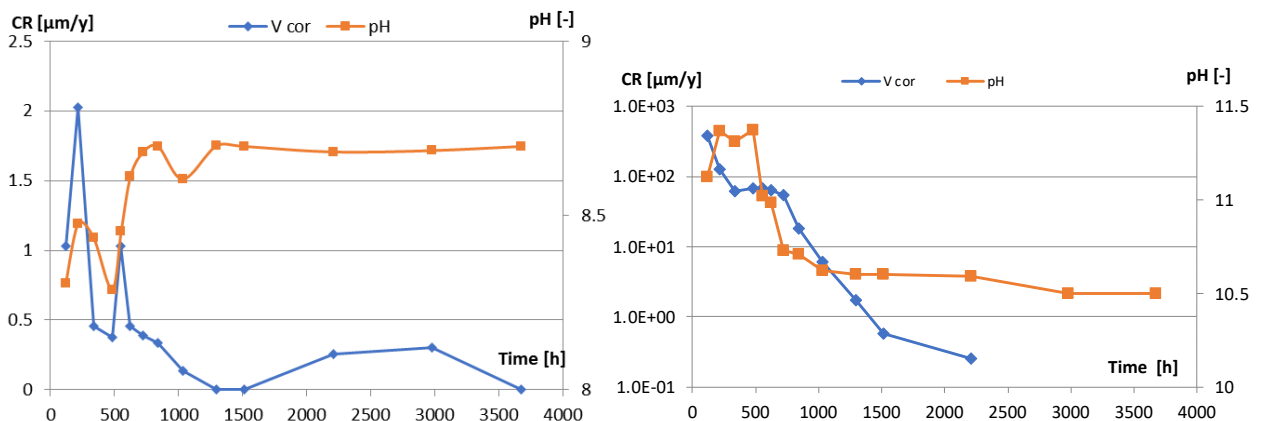
(a) MPC paste *(b) OPC paste*

Figure 41. Corrosion rate (Vcor) and pH vs time obtained in the chemical tests (AlMg3in MPC matrix).

For OPC matrix ((a) MPC paste *(b) OPC paste*

Figure 41- b), the corrosion rate has a two steps downward evolution and the corrosion values are significantly higher than in MPC paste.

Table 21 summarises the corrosion rate and H_2 volumes from the RATEN studies in cement pastes.

Table 21. Corrosion rate values and H_2 volumes from the RATEN studies for Al immobilisation

Testing environment	Measured method	Initial [h]	End [h]	$CR_{initial}$ [μm/y]	$H_{2-initial}$ [L/m^2]	CR_{end} [μm/y]	$H_{2-Total}$ [L/m^2]
MPC Paste	LPR	24	2016	1.59	0.015	0.249	1.495
	Chemical	120	3672	1.02	0.007	0.306	0.047
PC Paste	LPR	24	2016	152.5	1.59	0.03	45.19
	Chemical	120	3672	379.7	3.28	0.255	7.33

3.3.3   Effect of pore moisture content on Al alloy corrosion in MPC matrix

CSIC

Corrosion of metals in cementitious matrices is also dependent on the moisture content in the pores due to changes in electrical resistance and pore ion content, which can control the corrosion process. In the case of Al alloy, the corrosion kinetics, and the amount of H_2 released are affected. In order to verify this effect, CSIC studied different external curing conditions that allow variation in the pore water content. To explore this, 1M M/P ratio MPC mortars were examined during 90-day at 100%RH and isolated in a plastic container, as endogenous curing, which simulates the isolation into the steel drum container in the disposal repository. Replicate samples were used to allow the calculation of experimental errors.

In order to understand the Al corrosion response, changes in electrical resistivity (ρ) and pore water content were analysed in Figure 42.
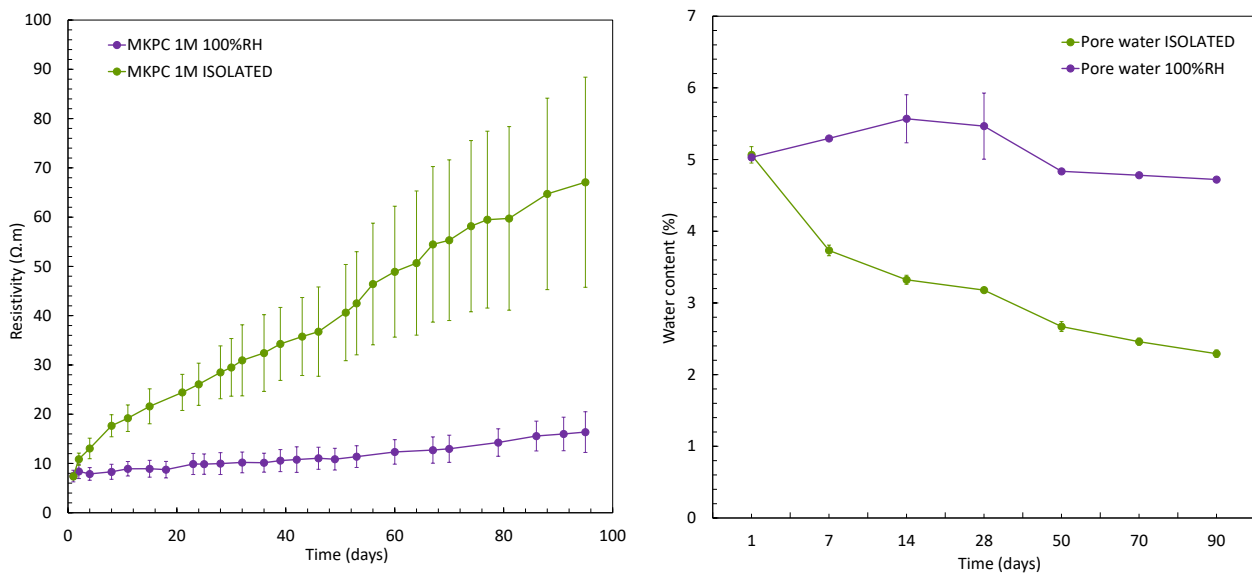

Figure 42. Electrical resistivity (left) and pore water content (wt.% by grams of sample) (right) over time for 1M M/P ratio MPC mortar under 100%RH and isolated condition

As observed in Figure 42-left, a significant increase in ρ is detected in isolated matrix (7.4 to 67.1 Ω.m) which is related to the progressive decrease in pore water content illustrated in Figure 42-right, which is consumed in the acid-base reaction progress of MPC (from 5.1 to 2.3 wt.%).This increase of ρ under isolated condition is related to a reduction of capillary pores and connectivity (more details in D4.8). However, under 100% RH condition, practically no change in ρ is detected (7.4 to 16.4 Ω.m) which is a consequence to more water content in pores due to a constant moisture supply by the environment which leads to a complete acid-base reaction (5.0 to 4.7 wt.%) (see Figure 422-right).

As discussed, alterations in the physical properties of the matrix due to the moisture content have a long-term impact on the Al corrosion rate (V_{corr}). As shown in Figure 43-left, at 100%RH, the V_{corr} exhibits three evolution stages over curing advance: up to 16 days (≈1.71μm/year), 62 days (≈1.26μm/year) and 90 days (≈1.27 μm/year). A stationary evolution is detected after 62 days when there is sufficient water availability in the media for the reaction to progress. In this case, phosphate ions content in the pore solution decrease over time due to the complete progress of the acid-base reaction. In contrast, under isolated condition with continuous pore water consumption for MPC reaction progress, there are higher unreacted phosphates ions in the pore solution resulting in a continuous decrease in the V_{corr}, with values of about one order of magnitude lower than at 100%RH (≈0.27 μm/year). A similar trend is identified for Al and AlMg in both environments.
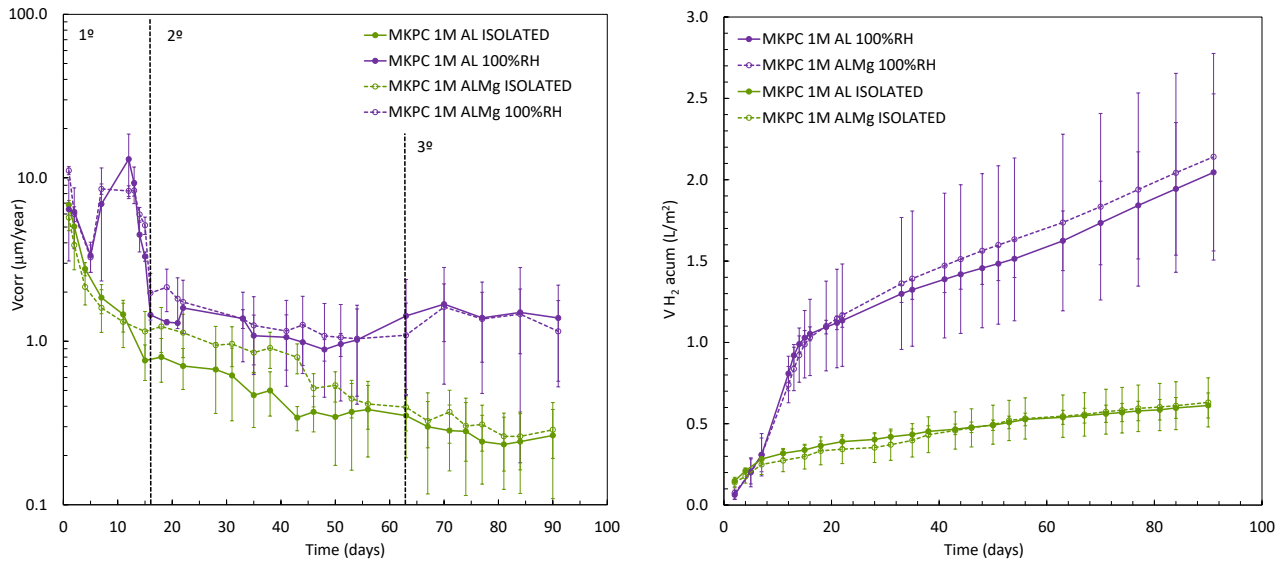

Figure 43. Corrosion rate (V_{corr}) (left) and accumulated H_2 release (right) versus time for 1M MPC mortars at 100%RH and isolated curing

The moisture content in the pores also has a significant influence on the amount of H_2 released of Al alloys. Figure 43-right illustrates the accumulated H_2 release in 1M MPC mortars under both moisture conditions. In both cases, the highest amount of H_2 gas release is measured in the first stage of interaction with the matrix (15 days), which continues to increase. Higher H_2 volumes are detected at 100%RH condition (≈2 L/m^{2}at day 90). Conversely, under isolated, lower H_2 release is observed with a constant evolution over time (≈0.60L/m^2 at day 90). This better behaviour against corrosion under isolated condition is related to the higher unreacted phosphate and borate ions in the pore solution, as a result of slight progression of the acid-base reaction over time due to the lower pore water content (described in D4.8).

To understand the impact of the pore water content on the corrosion of Al alloy, a second stage was conducted in which the moisture condition was changed. Some of the previously isolated samples were transferred to a chamber at 100%RH. This approach aimed to investigate whether Al and AlMg exhibit increase of the corrosion rate.

As previously noted, the pore water content has a significant influence on the Al corrosion response (V_{corr}). Figure 444-left shows lower V_{corr} values in isolated, under endogenous curing (≈0.33 to 0.11 μm/year up to 280 days). A decrease tendency is identified due to a lack of pore water content, which contributes to the electrochemical reaction progress. These lower corrosion rates of the Al alloys can be related to the higher concentration of unreacted phosphate and borate ions in the pore solution (results described in D4.8). However, a significant increase in V_{corr} is observed with the increase of

water content in pores due to the wetting of the matrix in the 100%RH compared to those kept in isolated condition ($\approx$0.15 to 6.64 L/m^2 at day 100). This reactivation process of the Al alloy corrosion response is related to the increase in water at the Al/matrix interface. However, a trend towards lower values is detected over time, indicating a recovery process of the passive state stabilisation to values of $\approx$1.51 L/m^2 at day 280.

This electrochemical response of Al alloy depending on the water content in pores can be observed in the accumulated H_2 release from 90 days to 280 days (see Figure 44-right). Lower H_2 release is observed when the samples are kept in isolated conditions, more significant for pure Al than for AlMg alloy (0.6 and 0.2 L/m^2 respectively). However, when the pore water content is higher, that occurs in the change at 100% RH, a significant increase is detected for Al and AlMg alloys (5.0 and 6.6 L/m^2, respectively).
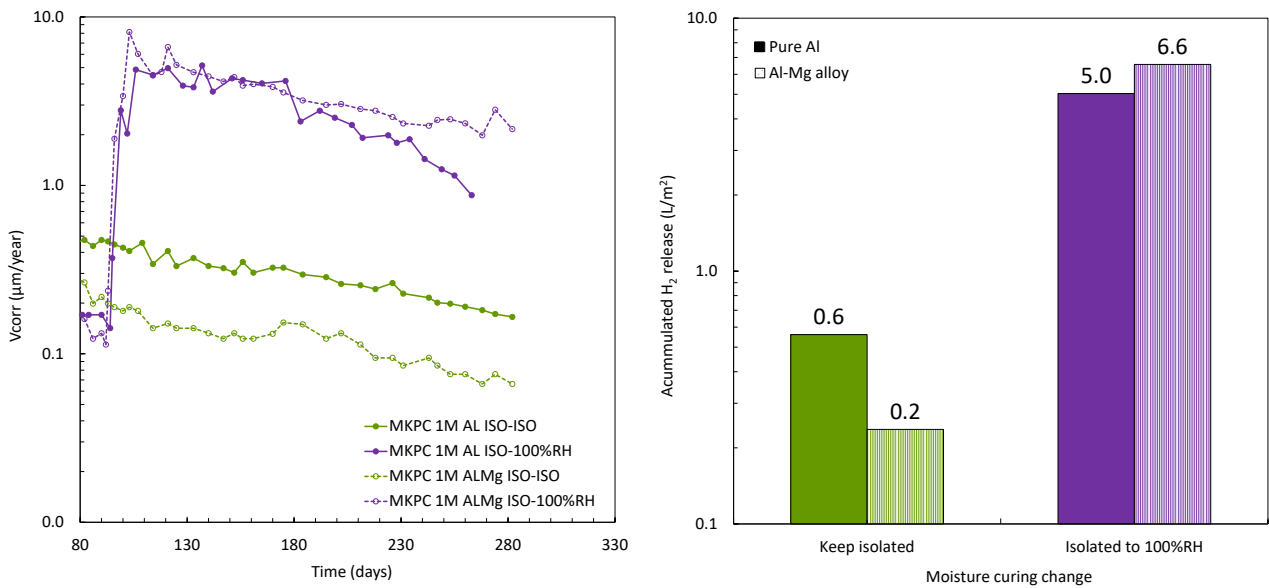

Figure 444. Corrosion rate (V_{corr}) (left) and accumulated H_2 release (right) from 90 to 280 days in 1M MPC mortars changing the moisture curing condition

Table 22 summarises the corrosion rates and H_2 values for the different moisture content influence.

Table 22. Corrosion rates and accumulated volumes of H_2 of Al and AlMg alloy in 1M MPC mortars under isolated and 100%RH condition

Curing	pH	Al					AlMg				
		(V_{corr}) (μm/year)			H_2 (L/m^2)		(V_{corr}) (μm/year)			H_2 (L/m^2)	
		1d	90d	280d	90d	280d	1d	90d	280d	90d	280d
Isolated	7.8	5.02	0.26	0.16	0.60	0.16	3.86	0.29	0.06	0.61	1.29
100%RH	8.6	6.40	1.39	0.87	2.05	0.87	11.06	1.15	2.15	2.14	5.57

3.3.4 Optimization of MPC matrix: Effect of MgO/KH$_2$PO$_4$ molar ratio

CSIC

Changes in the mix design, such as varying the MgO/KH$_2$PO$_4$ (M/P) ratio, play an important role in the physicochemical stability of MPC matrices as the presence of cracks and efflorescences (results from CSIC research included in D4.8) and in the Al reactivity at the matrix interface. In present study carried out by CSIC, different M/P ratios were examined in order to optimize the MPC formulation, with potential implications for aluminium corrosion and H_2 evolution. Due to this, 1, 2 and 3M M/P ratio MPC

mortar samples were examined over 90 days under 100%RH. Replicate samples were prepared to allow the calculation of experimental errors.

Results have indicated that differences in the pure Al and AlMg alloy corrosion response and in the volume of H_2 release are detected varying the M/P ratio in the MPC formulation. The corrosion potential (E_{corr}) was evaluated in function of the pore pH as observed in the Al Pourbaix diagram (see Figure 45-left). An evolution of E_{corr} to more anodic values is detected, more significant at lower M/P ratio (≈0.50 to 0.80 V). As described in D4.8, higher phosphate content in the pore solution and lower pore pH (≈8.5) in 1M leads to less Al alloy corrosion than at higher M/P ratios (pH>10). Due to this, both metal alloys in 2 and 3M are in the Al corrosion state, compared to the 1M M/P ratio that is located in a more clearly passive state (see Figure 45-left). However, as the pore pH of 1M is near neutral, Al and AlMg presented lower corrosion rate values than in 2 and 3M. This neutral pore pH is expected to allow the Al passivation. It is important to highlight that in all MPC systems, a risk of H_2 evolution exists, as all the experimental values were lower than the water reduction potential region.
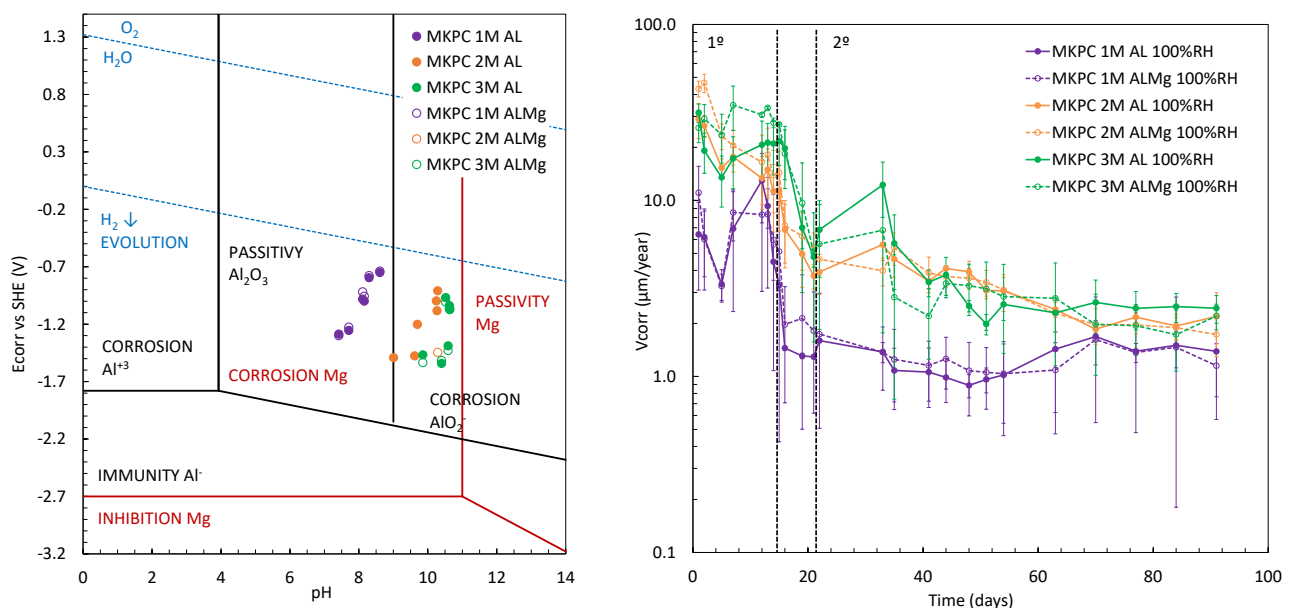

Figure 455. E_{corr} – pH for Mg and Al Pourbaix diagrams (left) and corrosion rate (V_{corr}) versus time (right) for Al and AlMg alloy in MPC mortars at 1, 2 and 3M M/P ratio under 100%RH condition

As the different M/P ratios have an influence on the evolution of the corrosion potential, the V_{corr} from i_{corr} measurements was also determined. Figure 45-right shows the evolution of the V_{corr} over time. Two stages of evolution are appreciated for the three M/P ratios that influence the passivation process of both alloys. Some higher corrosion rates (from 40 µm/year) are observed at higher M/P ratios in the first stages of interaction with the matrix related to the lower content of initial phosphate ions in the pore solution (from tests results described in D4.8). The second stage is followed by a decrease in the electrochemical corrosion response, which stabilises at long curing times and finally approaches the corrosion response of the three MPC matrices by a decrease of phosphate ions over acid-base reaction progress in all M/P ratio (2±0.4 µm/year at day 90).

As noted in previous results, variations in the MPC pore pH exhibit a significant impact on the Al alloy corrosion response (see Figure 46-left). As defined in D4.8, the pore pH increases at higher M/P ratio, resulting in a higher initial V_{corr} of Al alloy. However, in the long-term interaction a stabilisation of the corrosion rate occurs due to an increase in pore pH due to the progress of the acid-base reaction, indicating the potential positive influence of other ions in the pore solution on the corrosion response. Therefore, a significant influence in the V_{corr} of Al and AlMg is found with the phosphate (P) content evolution in the pore solution, defined in D4.8 (see Figure 46-right). As confirmed in 1.4.1 phosphates

attach to the metal surface and provide a protective effect against corrosion of Al. In addition, the evolution of borates (B), from the boric acid, with age is independent of the M/P ratio but also contributes to the control of Al corrosion response.
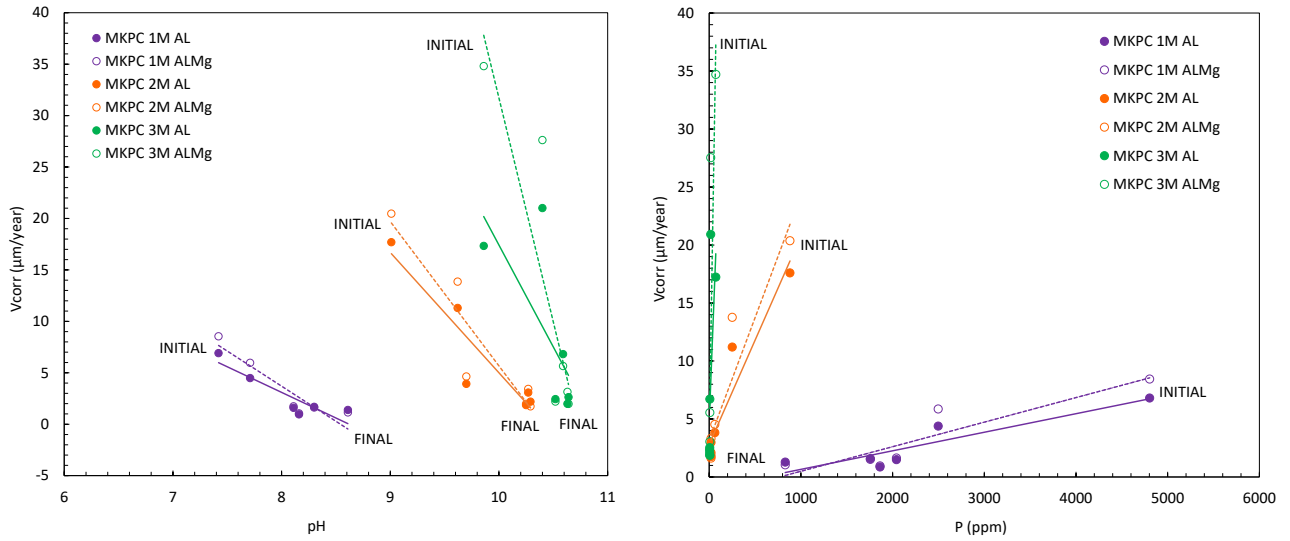

Figure 46. Corrosion rate (V_{corr}) versus pore pH (left) and P ion content (right) for MPC mortars at 1, 2 and 3M M/P ratio under 100%RH curing condition

As the corrosion rate is influenced by the M/P ratio in MPC formulation, changes in the H_2 evolution were also observed. Figure 46 illustrates the accumulated H_2 release over time.
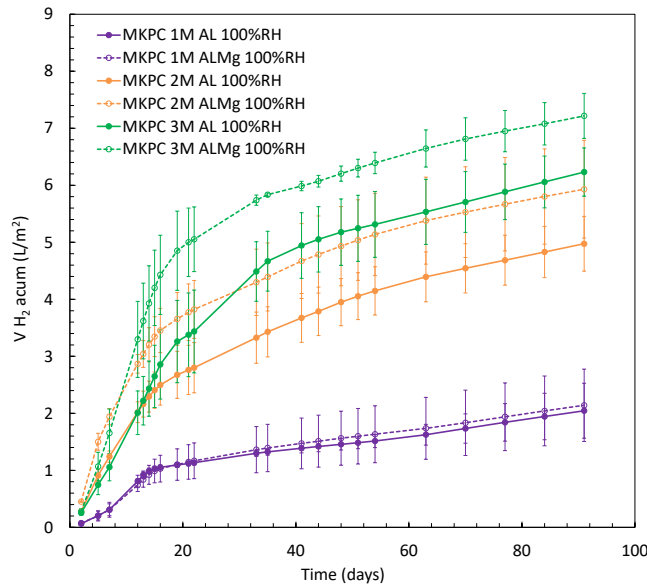
Figure 46. Accumulated H_2 over 90 days for 1, 2 and 3M MPC mortars at 100%RH curing

The higher volumes of H_2 for 2 and 3M are mainly related to the higher electrochemical activity of Al in the initial stage of interaction with the matrix. Higher values are identified over curing time at higher M/P ratios, with a difference of more than two orders of magnitude between 1M and 3M. The higher initial phosphate amount in MPC formulation at 1M allows for a lower amount of H_2 release over 90 days of testing due to the protection of the metal. In addition, a similar evolution was observed for Al and AlMg with 1M ratio. However, a higher evolution is identified for AlMg at 2M and 3M. The final accumulated average values were 2.04 and 2.14 L/m² for 1M, 4.97 and 5.93 L/m² for 2M, and 6.23 and 7.22 L/m² for 3M, for Al and AlMg, respectively. Experimental errors varying between ±0.4 to ±0.8 were detected.

Table 23 summarises the corrosion potential, corrosion rates and H_2 release values at different times over the test period.

Table 23. Summary of corrosion potential, corrosion rate and accumulated H_2 values of Al and AlMg alloy in 1, 2 and 3M M/P MPC mortars under 100%RH condition

| M/P ratio | Al | | | | | | AlMg | | | | |
| | E_{corr} (V) | | V_{corr} (µm/year) | | H_2 (L/m^2) | | E_{corr} (V) | | V_{corr} (µm/year) | | H_2(L/m^2) |
	1d	90d	1d	90d	90d		1d	90d	1d	90d	90d
1M	-0.90	-0.51	6.40	1.38	2.04		-1.01	-0.53	11.06	1.15	2.14
2M	-0.98	-0.70	28.97	2.19	4.97		-1.16	-0.73	43.11	1.73	5.93
3M	-1.04	-0.76	31.50	2.44	6.23		-1.26	-0.80	25.84	2.20	7.21

3.3.5   Influence of MgO and chemical retarders composition

CSIC-CNRS

In order to understand the effect of the different chemical retarders (boric acid and thiosulfate) and the type of MgO, CSIC and the CNRS studied the Al passivation process and corrosion response over 140 days of testing in cementitious matrices. For this purpose, isolated MPC mortar matrices were prepared following Table 6: 2% boric acid with HB-MgO, 5% of thiosulfate with LC-MgO and 2% boric acid + 3% thiosulfate with LC-MgO.

Figure 47-left shows the evolution of the corrosion rate as a function of time in the three MPC-based matrices. At initial stage, higher corrosion values are observed in presence of boric acid, compared to thiosulfate. A significant decrease evolution is detected in all samples due to the rapid formation of the Al_2O_3 passive layer in the first stage of interaction (up to 15 days). The worse behaviour and higher corrosion risk is identified with both retarders addition (from 7 to 0.07 µm/year), followed by only boric acid (6 to 0.04 µm/year), which continues to evolve over time. However, with only thiosulfate, a significant decrease in the corrosion rate is observed over time, by up to one order of magnitude (2 to 0.02 µm/year), and a stabilisation is also detected, contrary than in solution test probably due to the fact that thiosulfate reacts with the phosphate ions in mortar forming a new protective passive film against Al_2O_3 layer. No significant effect of the type of MgO was observed. In Figure 47-left, a similar trend and values in V_{corr} using R_p from LPR and R_t from EIS technique, confirming that both electrochemical methods are accurate for the evaluation of Al corrosion kinetic.

Figure 47-right shows the accumulated volume of H_2 release over time for the three MPC samples using Equation (6) and (7). Higher H_2 release is found in the early stage of interaction up to 30 days in the three systems. In the presence of boric acid, a similar evolution is detected, slightly higher when both retarders are used (5.5 and 4.9 L/m^2 respectively). This could be explained by the fact that boric acid would have a negative effect on Al corrosion in the presence of thiosulfate. In the case of only thiosulfate as retarder, an H_2 volume release of up to two orders of magnitude lower is identified (up to 0.58 L/m^2). However, an attenuation phenomenon is not observed, and a progressive evolution of H_2 release is found in all systems.
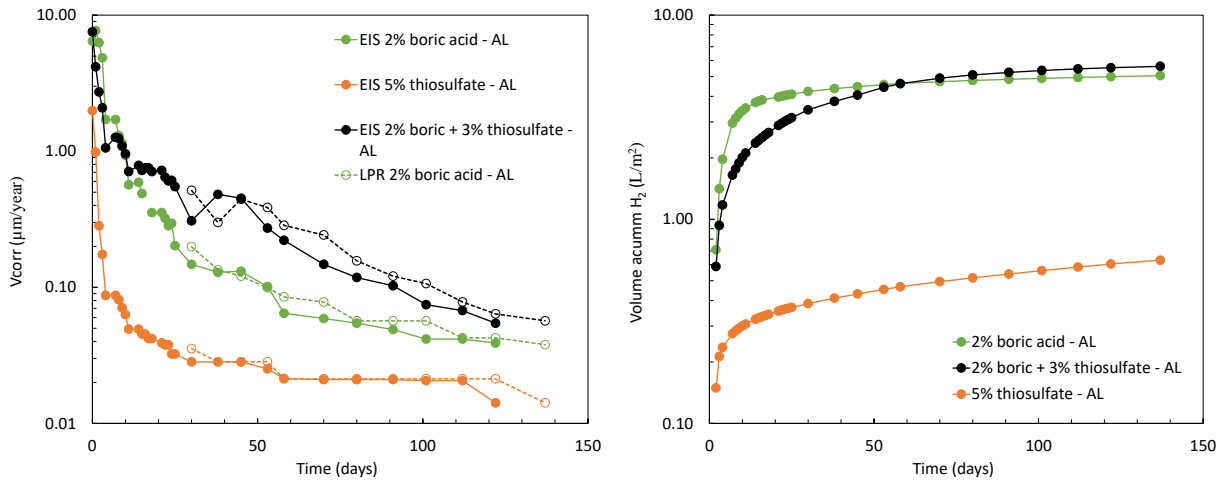
Figure 47. Evolution of the corrosion rate (V_{corr}) from EIS and LPR (left) and volume of H_2 release (right) over time for pure Al in low-cost mortar MPC Matrices

Table 24 summarises the corrosion rates and H_2 for the three MPC mortars in isolated condition.

Table 24. Summary of corrosion rate and H_2 release values of pure Al inlow cost MPC matrices

Mortar	Metal alloy	V_{corr} (µm/year)		H_2 release (L/m^2)
		0 days	140 days	140 days
5% thiosulfate, LC-MgO	Al	1.98	0.01	0.63
2% boric + 3% thiosulfate, LC-MgO	Al	7.53	0.05	5.62
2% boric acid, HB-MgO	Al	6.41	0.03	5.05

3.3.6 Al alloy corrosion in alkalinised MPC matrix

CSIC

- Alkalinisation of MPC matrix in pore alkaline water immersion

A reactivation process on Al corrosion can occur under disposal conditions by simulating the penetration of alkaline waters coming from the interaction of underground water with the concrete cells of the waste immobilisation system. A set of MPC and OPC blended mortars after 1 year under water immersion (see 1.4.2) were exposed to alkaline water over 250 days to follow the effect of matrix alkalinisation. For this purpose, after 1-year under water immersion, an air-drying process was performed reducing the pore water content in the matrix prior to transfer to an alkaline water (pH 12.6 with: K: 2800 ppm; Ca: 18 ppm; S: 361 ppm) in isolated and individual plastic containers.
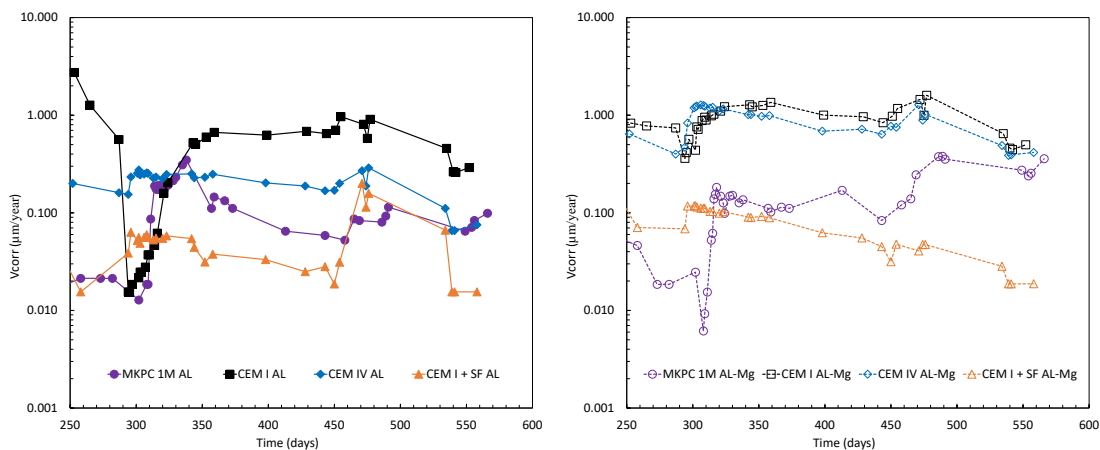

Figure 48. Corrosion rate (V_{corr}) versus time for Al (left) and AlMg alloy (right) in MPC and OPC blended mortars over 250 days in alkaline water

The evolution of the corrosion rate (V_{corr}) allows confirming the alkalinisation effect on the corrosion response (see Figure 48). An increase by two orders of magnitude is detected for Al (see Figure 48-left) and AlMg alloy (see Figure 48-right) in MPC matrix by a reactivation due to alkalinisation (≈0.01 to 1 µm/year). In addition, a rapid decrease in the Al corrosion rate is observed in the CEM I at day 300 in Figure 48-left, which is attributed to the drying stage prior to alkaline immersion. However, no effect of alkaline media is detected for AlMg (see Figure 48-right). An evolution towards its initial and higher corrosion rates (≈10 µm/year) is observed without any influence of the alkaline media, as also observed in CEM IV mortar evolution for both Al and AlMg. Contrary, Figure 48 shows the lowest corrosion rates over time for low-pH CEM I+SF mortar with final values of ≈0.01 µm/year. In addition, no effect of the alkaline environment is detected in the Al and AlMg corrosion evolution. Due to this, a better behaviour for Al immobilisation is detected in CEM I+SF followed by MPC mortar.

Figure 49-left illustrates the evolution of accumulated H_2 volume over time. In addition, Figure 49-right shows the accumulated H_2 release over this new alkaline immersion period. Due to the high alkaline pore pH in CEM I and CEM IV (>12), no effect of the external alkaline water is detected in Figure 49-left over time with H_2 final values of 20-30 L/m^2. A release of about 2 L/m^2 is measured in this new alkaline stage (see Figure 49-right). In addition, a non-evolution is observed in low-pH CEM I+SF with constant final values of 6.5 L/m^2 (see Figure 49-left) and lower H_2 release in this new stage is detected in Figure 49-right (0.16 L/m^2). This suggests that pure Al and AlMg alloy have not experienced a reactivation phenomenon under alkaline external conditions in OPC blended matrices. In the case for MPC, a reactivation due to alkalinisation is observed in Figure 49-left in both Al and AlMg alloys which exhibits an increase of 0.07 L/m^2 in the new alkaline condition (see Figure 49-right). These results confirm that MPC followed by CEM I+SF matrices are optimal alternatives for the Al immobilisation than CEM I due to lower H_2 release.
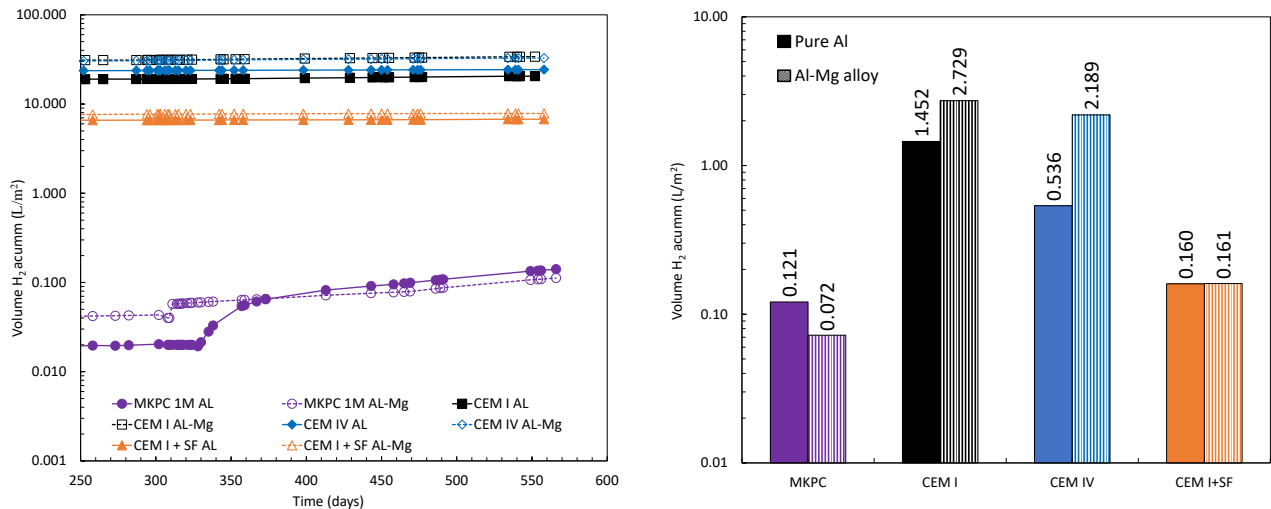

Figure 49. Accumulated H_2 release over time (left) and volume of H_2 release (right) for Al and AlMg alloy in MPC and CEM I matrix under alkaline water immersion

To understand the effect of the alkaline solution in the chemical stability of MPC and OPC matrices, Table 25 shows the pore pH and pore ion evolution analysed at the end of the test. In MPC mortar, a decrease in phosphate ions is observed, indicative that the acid-base reaction is progressing with time. In addition, low Ca alkaline ion concentrations are detected in contrast with MPC under water immersion in 4.2.1. Due to this, an increase in the pore pH from 9.9 to 10.6 confirms the alkalinisation of the matrix, also the phenolphthalein test in Figure 50-left. In the case of CEM I, a non-evolution of larger amounts of Ca ions is observed under the alkaline water immersion (see Table 25). In addition, a constant and higher pore pH is detected (≈12.6) confirmed in Figure 50-right by the phenolphthalein test, probably due to the alkaline external solution is not having a strong influence on this type of highly

alkaline matrices. In contrast, for CEM IV (pH 12.6) and CEM I+SF (pH 10.9), non-influence of the alkaline media on their pore ionic composition is identified in Table 25 with lower amount of Ca ions.

Table 25. Pore ion and pH over 250 days 1 under alkaline water immersion

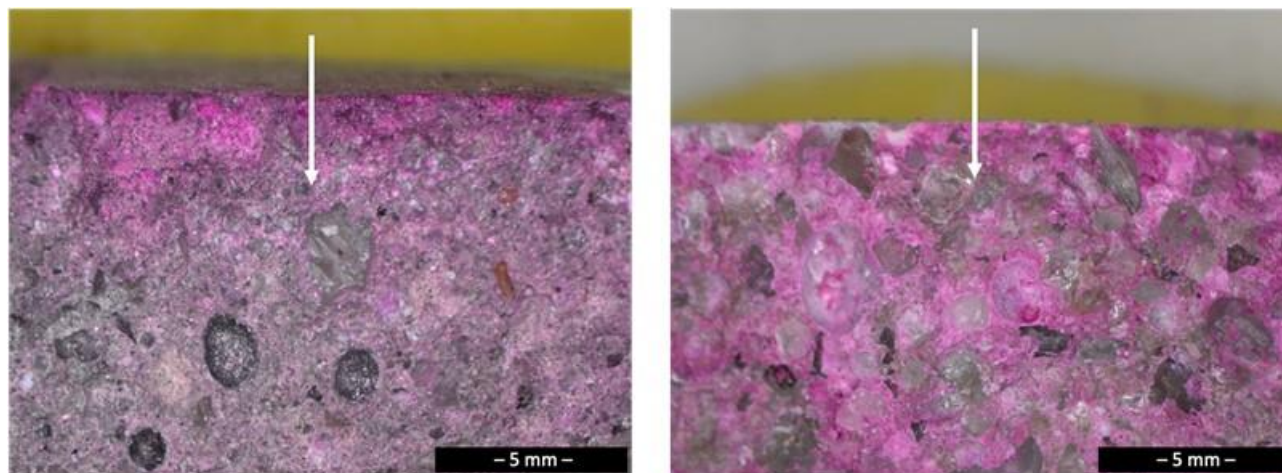| Binder	Days	pH	S	P	B	Mg	K	Ca
CEM I	250	12.6	5	-	0.2	-	110	409
CEM IV	250	12.5	350	-	5	1	2546	0.5
CEM I+SF	250	10.9	359	-	2	0.2	2477	0.7
MPC	250	10.6	31	49	8	4	540	3

Figure 50. Phenolphthalein test in MPC (left) and CEM I (right) matrices exposed to an alkaline solution for over 250 days. White arrows indicate the penetration of the media

At the end of the experiment, all MPC and OPC mortar matrices were analysed by MIP and XRD technique to understand the effect of the alkaline environment in the mortar microstructure. For MPC, main reaction product K-struvite forms due to less pore ion content as the reaction progresses over time. Conversely, in OPC-blended mortars with higher Ca-ion content which decreases over time, portlandite is formed as the main hydration product. However, in the case of CEM IV and CEM I, secondary ettringite is also detected.

In addition, the pore structure was analysed by MIP at the end of the test. CEM IV with 10.13 porosity show a unimodal distribution with large number of capillary pores (< 0.1 µm), making them less susceptible to media penetration, also observed in CEM I+SF. However, CEM I+SF also shows a significant increase in 1 and 0.1 µm pores with a 16.41 total porosity. A unimodal distribution with less capillary pores is detected in CEM I (7.24. porosity). Contrary, MPC with 13.05 porosity shows a multimodal distribution with larger number of small and intermediate pores (10 - 1 µm). Less capillary pores together with an increase in intermediate pores could lead to a MPC pore structure that is vulnerable to media penetration. This phenomenon could cause a reactivation of the Al corrosion due to the alkaline external conditions in MPC matrices.

To understand the effect of alkaline environment on the Al reactivity at the metal/matrix interface level, SEM/EDX analysis were conducted at the end of the test. In the Al/OPC interface (see Figure 51-a), a 50 µm homogeneous Al_2O_3 passive layer is also identified along the Al surface (1.4.2). However, as depicted in Figure 51-b, incrustations of Ca layers derived from alkaline media penetration are detected, having a negative effect on the passive layer. Despite this, a reactivation of the corrosion phenomenon due to re-alkalinisation has not been detected.

In the case of the MPC mortar in alkaline water, a 30 µm heterogeneous and dense layer of P, Mg, and K is also observed on Al surface (see Figure 51-c) (1.4.2). Al reacts less and no effect of alkaline media on the passive layer was observed. Figure 51-d displays a mapping image of the outer zone of the cube. The formation of an external layer rich in Ca and S is observed, which increases the pore pH by alkaline water penetration (see Table 25 and Figure 501-left). As a result, in MPC specimens there is alkalinisation in the outer zone, which slightly penetrates towards the core section, resulting in activation of the Al corrosion response.
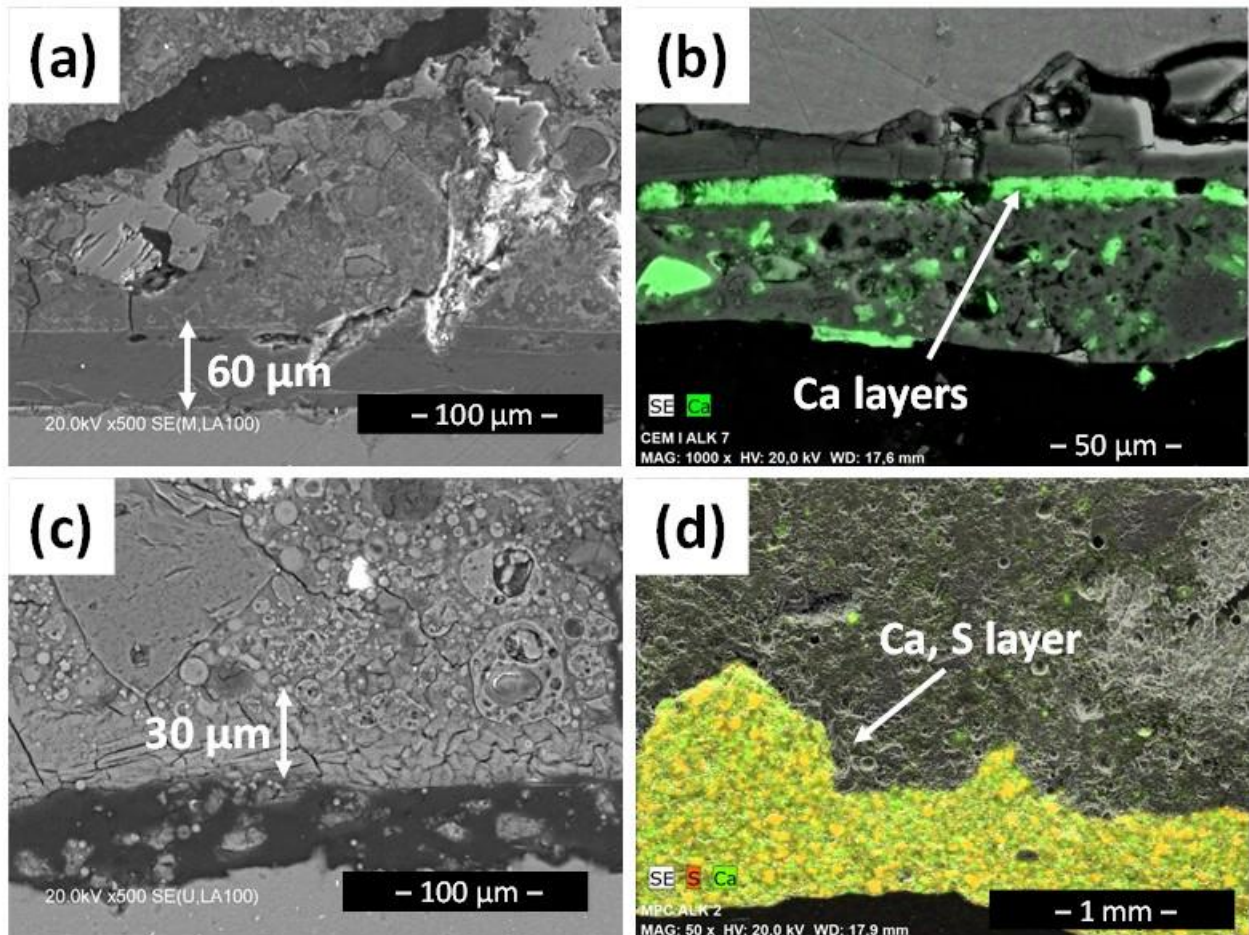

Figure 51. SEM/BS images after alkaline water immersion: a) Zoomed area of layer formation at the metal/OPC interface, b) Ca inclusions in passive layer in Al/OPC interaction, c) Zoomed area of layer formation at the metal/MPC interface, and d) External alkaline layer in MPC matrix

- <u>Alkalinisation of MPC matrix in contact with alkaline mortar</u>

This phenomenon of reactivation due to alkalinisation was also studied by the CSIC in a cylindrical 1M MPC mortar embedded in a prismatic CEM I mortar after curing under isolated condition over 90 days. Different curing conditions were considered to analyse the alkalinisation of the MPC matrix: 1) in a chamber at 100%RH curing condition (90 to 150 days), and 2) water immersion condition (up to 250 days).

As observed in Figure 52-left, an evolution of one order of magnitude is identified between 90 to 150 days probably due to the penetration of the alkaline pore solution of the fresh CEM I mortar and diffusion during the 90 days period at 100%RH (0.1 to 1 µm/year). At day 160, significant increase in the corrosion response of Al and AlMg alloy is detected under water immersion, higher for AlMg (10 and 100 µm/year, respectively). A stabilisation of the corrosion response is observed after 150 days of testing in water immersion. However, a recovering to lower V_{corr} values are identified in Al alloy (10 to 1µm/year).

Figure 52-right shows the volume of H_2 released for Al and AlMg alloy in MPC mortar in a CEM I external matrix for the different curing stages: 90-150 days (100%RH) and 150-250 days (water immersion). No influence of the CEM I mortar is detected in the volume of H_2 release under 100%RH curing for both metal alloys (≈0.40 L/m^2). However, after 150 days, the higher moisture content accelerates the alkaline diffusion in MPC matrix from the CEM I mortar, increasing the H_2 gas release on Al. In this curing period (150 to 250 days), significant differences between Al and AlMg alloy in the H_2 release is detected in Figure 52-right (Al: 4 L/m^2 and AlMg: 33 L/m^2) due to the less stability of AlMg under high alkaline conditions.
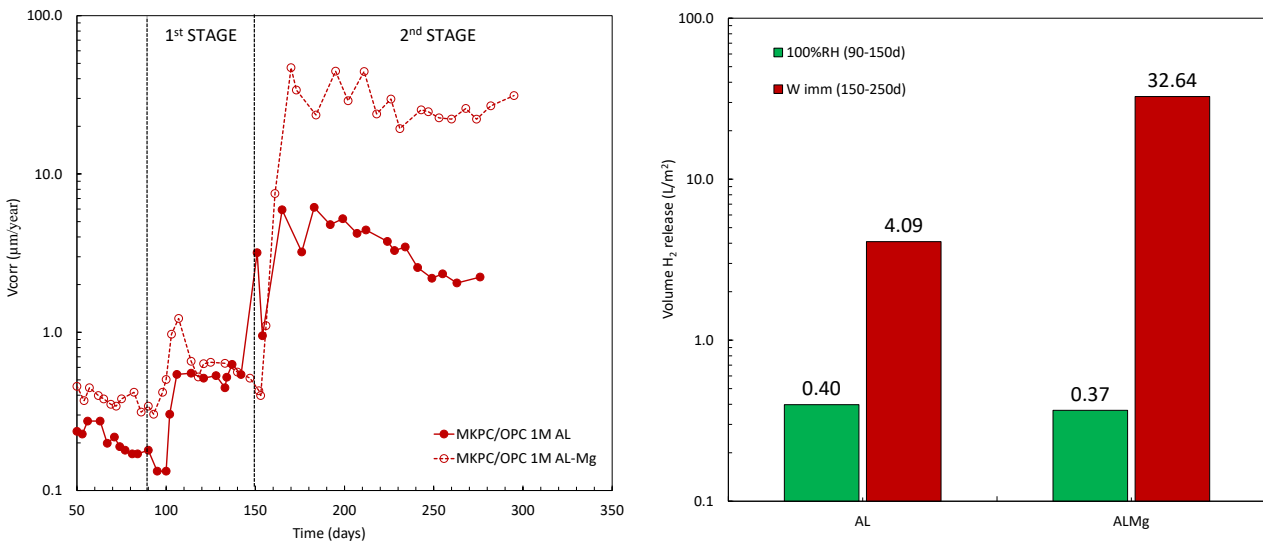

Figure 52. Corrosion rate (V_{corr}) versus time (left)) and volume of H_2 release in different curing periods: 90-150 days (100%RH), and 150-250 days (water immersion) (right) for Al and AlMg alloy in 1M MPC mortar with an external CEM I mortar

At the end of the test, the samples were dry cut to observe the alkaline penetration at the CEM I/MPC interface. Figure 53-a shows the interface prior to the phenolphthalein test. Some colour changes are detected in MPC sample. As observed in Figure 53-b, phenolphthalein test was sprayed. A significant penetration of about 1.5 cm of the alkaline media in the MPC matrix is observed reaching the Al level. Pore pH analysis of the core section near the Al coupon showed values of pH= 11.3. This test confirms that the reactivation of the corrosion rate in Figure 52-left is related to an alkalinisation of the MPC matrix in a CEM I mortar, accelerated by higher moisture conditions.
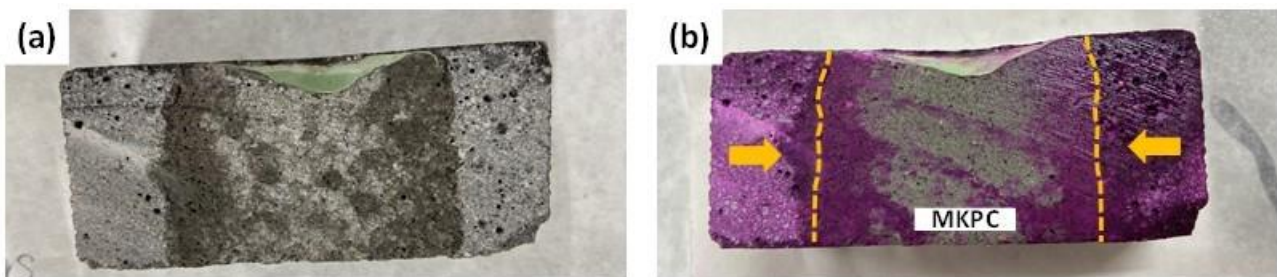

Figure 53. MPC matrix in an alkaline CEM I mortarafter 100%RH and water immersion condition: a) prior phenolphthalein test, and b) after phenolphthalein test. Yellow arrows indicate the penetration of the CEM I media

Table 26 summarises the corrosion rate values and H_2 release measured by the CSIC in 1.4.6.

Table 26. Summary of corrosion rate and H_2 release values of Al and AlMg alloy in 1M MPC and OPC blended matrices under alkaline conditions

Media	Mortar	Metal alloy	V_{corr}(µm/year)			Volume H_2(L/m^2)		
			250 days			**250 days**		
External alkaline solution	CEM I	Al	0.29			1.452		
		AlMg	0.49			2.728		
	CEM IV	Al	0.07			0.536		
		AlMg	0.41			2.188		
	CEM I+SF	Al	0.01			0.160		
		AlMg	0.01			0.160		
	MPC	Al	0.09			0.012		
		AlMg	0.35			0.072		
			60 days	**100 days**		**60 days**	**100 days**	
			100%RH	**Water imm**		**100%RH**	**Water imm**	
CEM I mortar cover	MPC	Al	3.18	2.23		0.40	4.09	
		AlMg	0.42	31.28		0.37	32.64	

3.4 Conclusions regarding the Al reactivity in MPC

CSIC
The main conclusions from CSIC contribution are described according to the five main objectives assessed for the research of Al and AlMg alloys immobilised in cementitious systems:

1) Conclusions derived from the ionic pore solutions studies suggest that:
    *   The kinetics of corrosion of the Al and AlMg alloy in $Ca(OH)_2$ alkaline solution simulating the OPC pore solution are too high, which suggests not recommending the use of OPC for Al immobilisation. Contrary, MPC pore solution shows significant lower corrosion kinetic, suggesting that MPC represents an alternative substitute for OPC for the Al immobilisation.
    *   Main ions in the MPC pore media play an important role in the Al passivation mechanism and have positive effect in the control of the H_2 release.
    *   Phosphate contributes to the passive layer formation, reducing the corrosion rate and hydrogen evolution. Higher phosphate concentration at low pH influences the Al passivation process due to the formation of a new passive film on the metal surface or an absorption phenomenon.
    *   Chemical retarders in MPC formulation influence the Al corrosion response. Better response is detected in the presence of boric acid than thiosulfate associated with an adsorption mechanism of interaction on the Al_2O_3 passive layer. A synergy effect is detected with both retarders are present.

2) Regarding the performance of Al immobilised in different matrices, CSIC can conclude:
    *   Alkaline Portland blended matrices such as CEM I and CEM IV show a degradation process with high H_2 risk demonstrated via LPR measurements.
    *   In the Al/CEM I matrix interface, a heterogeneous layer of Al_2O_3 is formed (50 to 90 µm). Al ions generated due to the high alkaline pore pH of CEM I diffuse up to 1 mm depth in the matrix with the formation of expansive ettringite, which may affect the further integrity of the waste form.

- Lower corrosion rates and H_2 values are detected in 1M MPC matrix, followed by low pH CEM I+SF, making them optimal alternatives for Al alloy immobilization compared to CEM I. More than two order of magnitude difference have been found.
- No significant differences are identified for Al and AlMg alloy in the OPC blended cements. However, the AlMg alloy shows higher corrosion rates over time in MPC due to an increase in the pore pH by a leaching phenomenon in water (up to 9).
- Not significant metal reactivity exists in an MPC mortar due to their lower pore pH in the Al passive domain. A protective effect of the phosphate content was observed. In the presence of phosphate ions, the internal pH decreases and a 30 μm dense microlayer at the Al/matrix interface is observed.

3) In the evaluation of the pore moisture content and the optimisation of MPC matrix on Al alloy corrosion response, CSIC can conclude:
- The corrosion process and the volume of H_2 release are affected by the pore moisture content and the evolution of the acid-base reaction process in MPC matrix.
- The presence of unreacted phosphates and borates in the pore solution inhibits the corrosion process and the release of H_2 gas, which is more pronounced in the absence of water in isolated, endogenous curing, due to a slight evolution of the MPC reaction process.
- Changes in the moisture in pores reactivate the corrosion process for Al and AlMg alloys but both Al and AlMg alloys recover the passive state over time.
- The optimisation of the initial MPC formulation by changing the M/P ratio due to the presence of cracks and efflorescences affects the corrosion response and H_2 released of pure Al and AlMg alloy.
- The corrosion response is influenced by the pore pH and the evolution of phosphate ions in the pore solution.
- The increases of pore pH at higher M/P ratio duplicate or triplicate the initial corrosion rate of Al alloys that equalise at long-term of interaction due to the evolution to less phosphate ions in the pore solution by the progress of the acid-base reaction.

4) Regarding the effect of chemical retarders and type of MgO in low-cost MPC on the Al passivation mechanism, main conclusions from the CSIC and CNRS are:
- Significant influence of the boric acid and thiosulfate as chemical retarders in the MPC formulation on the Al corrosion was identified.
- An effect of the different type of MgO was not appreciated in Al corrosion due to a similar chemical composition and microstructure.
- In cementitious systems, thiosulfate has a better effect than boric acid on the Al passivation mechanism probably due to the fact that this chemical retarder reacts with the phosphate in the matrix forming a new passive film against Al_2O_3 layer, which shows the lowest H_2 release.
- When both retarders are present, the synergy between the two products is not clear and it appears that boric acid has a negative effect on the action of thiosulfate, showing the highest corrosion and H_2 values.

5) In the evaluation of the reactivation of the Al corrosion response due to alkalinisation in cementitious matrices, main conclusion are:
- Under alkaline immersion conditions, the MPC matrix shows a reactivation of the corrosion process due to alkalinisation compared to the OPC blended matrices.
- The lowest H_2 release values are observed in MPC followed by CEM I+SF.
- When in contact of MPC with CEM I mortar there is diffusion of the alkaline environment into the MPC matrix. A pore pH of 11.3 is detected and reaching the Al interface.
- A reactivation of the corrosion process of Al and AlMg was observed in MPC alkalinised matrix.

ENRESA

The main conclusions derived from the ENRESA study are:

- In alkaline water by addition of NaOH, the highest corrosion rates are obtained for Al, with values close to 100 mm/year at pH 13 and 60 mm/year at pH values of 12.6, in tests lasting approximately 30 days. In the other hand, test carried out on synthetic water of the CABRIL and OPC mortars with a pH of 12.6, the corrosion rate "falls" to values between 1 and 3 mm/year, mainly due to the formation of a layer of corrosion products. Corrosion tests of aluminium in alkalized water with $Ca(OH)_2$, yield corrosion rates similar to those obtained by corrosion tests of aluminium in synthetic water of the tested OPC mortars, for similar test times (30 days).
- The corrosion rates of the Al embedded in the tested OPC mortars are significantly lower than those measured in synthetic waters, with corrosion kinetics decreasing as the duration of the trial increases. In CABRIL mortar, corrosion velocities of 0.058 mm/year, are obtained after 227 days of testing and for the mortar HORMISEC corrosion velocities of 0.086 mm/year, are measured after 175 days of testing. The highest rates of corrosion in Al, and therefore the highest corrosion velocity in the hydrogen gas generation takes place mainly in the first hours of contact of Al with mortar paste, during the setting stage, with the formation of H_2 gas outlet channels. Corrosion of Al in CABRIL and OPC mortars generates a compact and relatively well-adhered layer of corrosion products on the substrate, which effectively protects the Al.
- On the other hand, MPC mortar results in corrosion rates for aluminium that are significantly lower than those obtained in CABRIL mortar, with values of 0.0011 mm/year, after 228 days of testing. Similarly to what was observed with CABRIL and OPC mortars, the highest corrosion rates and therefore, the more H_2 production, takes place, mainly, in the first few hours of contact of the aluminium with the mortar paste.
- These results are the starting point for the analysis and development of specific Waste Acceptance Criteria for aluminium. The maximum aluminium surface area allowed in a container, based on the maximum pressure permitted, beyond which cracking occurs. This pressure is caused by the corrosion rate evaluated, which must be as realistic as possible.

RATEN
The main conclusions of the RATEN study are:

- The AlMg3 samples tested show different corrosion rates depending on the environment in which they were immersed, resulting in a volume of hydrogen proportional to the mass of aluminum transformed into corrosion products.
- Between the two environments in which these samples were tested, by far the most aggressive is the alkaline environment developed by the Portland cement-based matrix: the corrosion rate varied between 0.05 μm/y and 9 μm/y in MPC and between 0.05 μm/y and 500 μm/y in OPC. The total hydrogen normalized volume in MPC matrix was estimated at ~ 1.5 L/m^2 from the electrochemical parameters, while in the chemical test the normalized volume of hydrogen was 0.05 L/m^2, significat lower than in OPC (45 L/m^2 estimated from electrochemical parameters and ~8 L/m^2 measured from chemical test).

INTEGRATED ANALYSIS
The integrated analyses of the main parameters obtained from the study of the corrosion response of Al alloy considered the corrosion rate (in μm/year) and volume of hydrogen release. The result of the value assessment is summarised in

Table 27and Table 28 for the initial state (1day) and after 100 days of exposure derived from the studies carried out for each partner in pore solutions and mortar/paste test, respectively.

Table 27. Corrosion rates and H₂ volume released derived from each partner test in solution test

Partner	Method	Alloy	Ca(OH)₂ sat. solution					MPC SPS				
			V_{corr} (µm/year)		pH		H_2 (L/m²)	V_{corr} (µm/year)		pH		H_2 (L/m²)
			1d	100d	1d	100d	100d	1d	100d	1d	100d	100d
RATEN	LPR	AlMg3	2751	8	12.5	10.5	50	1.4	0.01	7	7.1	0.4
	Chem.		2955	0.9			95	3.7	3.6			2.25
ENRESA	LPR	Al	600	50	12.6	12.6	-	-	-	-	-	-
CSIC	LPR	Al	1027	54	12.6	12.8	117	17	1.6	7.6	7.8	4.9
		AlMg3.5	405	27			73	11	0.9			5.7

Table 28. Corrosion rates and H₂ volume released derived from each partner test in mortar test

Partner	Method	Alloy	OPC mortar					MPC mortar				
			V_{corr} (µm/year)		Internal pore pH		H_2 (L/m²)	V_{corr} (µm/year)		Internal pore pH		H_2 (L/m²)
			1d	100d	1d	100d	100d	1d	100d	1d	100d	100d
RATEN	LPR	AlMg3	153	0.03	11	9	45.2	1.6	0.25	8.6	8	1.5
	Chem.		380	0.25			7.33	1.02	0.24			0.05
ENRESA	LPR	Al	750	110	12.6	12.6	-	9.7	2.7	8.5	8.5	0.86
CSIC	LPR	Al	1047	16.5	12.6	12.8	17.9	2.4	0.02	7	9.8	0.02
		AlMg3.5	1047	44			30.2	5.2	0.04			0.04

Although similar trends are observed for the three partners in the same environment, significant differences are noted, particularly in the mortar. The corrosion process in the pore solution is more active than in the mortar as a consequence of the higher electrical resistance of the matrix and the evolution over time of the pore ion content as a consequence of the cement hydration evolution. Differences are also appreciated with the method to determine the volume of hydrogen, higher with chemical (direct measurement) than from electrochemical estimation in the case of pore solution that change the trend in mortar. There is no method to measure the volume of hydrogen as that exist from the determination of the corrosion rate. In addition, the differences observed are probably related to the design of the surface preparation of the Al alloy, the pH stability of the system, mainly in alkaline conditions, or the determination method used in the case of mortar, or the different type of samples and number of measurements to determine the variability of the corrosion process.

4 Steel reactivity in magnesium phosphate cement (MPC)

Two partners (CNRS/IJCLab and RATEN) performed experimental tests to evaluate the steel reactivity in MPC matrices, including low-cost formulations and their results are summarized in this chapter.

4.1 Work carried out

To assess and understand the steel reactivity across different MPC formulations and to estimate corrosion rates and the volume of H_2 generated, chemical tests and electrochemical measurements, such as Electrochemical Impedance Spectroscopy (EIS) and Open Circuit Potential (OCP), were applied for steel corrosion in mortars of reference MPC and LC-MPC formulations, and in mortar based on Portland cement (OPC). Furthermore, steel reactivity in solutions containing boric acid and/or thiosulfate was examined by immersion tests. Characterization of the corrosion products were carried out through SEM/EDX and XRD.

4.1.1 Materials used and samples description

4.1.1.1 CNRS/IJCLab

Both reference MPC formulation and LC-MPC formulations were tested by CNRS/IJCLab. The LC-MPC formulations have been developed using the same parameters as the MPC reference (see Table 29), but with reactive MgO replacing DB MgO, and incorporating thiosulfate, either alone or combined with H_3BO_3, as retarders. Experimental results from sub-task 6.2 suggest that for MPC mortars prepared with reactive MgO, the optimal mass ratio of retarders to cement is 0.05. As a result, two formulations were chosen for corrosion studies: one containing only thiosulfate at 5 wt% (referred to as B0T5), and the other containing of 2 wt% boric acid and 3 wt% thiosulfate (referred to as B2T3). The raw materials used are listed in Table 30 and the LC-MPC formulations are detailed in Table 31.

Table 29. MPC formulation defined as a reference for all the studies (mass of components is expressed to obtain 1 L of mortar) [6]

MPC reference starting reagents	Mass (g)	Mass ratio reagent/(MgO+KH$_2$PO$_4$)
DB MgO	131.39	-
KH$_2$PO$_4$ (Yara KristaTM, 98 wt.%)	443.58	-
Sand	574.97	1
Fly ash	574.97	1
H$_3$BO$_3$	11.50	0.02
Water	293.24	0.51

Table 30. Raw materials

Reagent	Reference, Supplier	Purity	Specific surface (m²/g)
Reactive MgO	AK98VHR, Timab	97.3%	90
Dead Burned MgO	Magchem 10 CR, Martin Marietta Magnesia	98.3%	0.9
KH_2PO_4	ACS reagent, Sigma-Aldrich	99%	
Fly ash	Class F- low CaO content, EDF CORDEMAIS		1.5
Boric acid	VWR	> 99.5%	
Sodium thiosulphate pentahydrate	ACS reagent, Sigma-Aldrich	99.5%	
Sand	MIOS 0.1-1.2 mm, SIBELCO	$SiO_2 \geq 98\%$	
Distilled water			

Table 301. LC-MPC formulations (mass of components is expressed to obtain 1 L of mortar)

Starting reagents	B0T5		B2T3	
	Mass (g)	Mass ratio reagent/(MgO+KH_2PO_4)	Mass (g)	Mass ratio reagent/(MgO+KH_2PO_4)
Reactive MgO	128.72	-	128.55	-
KH_2PO_4	437.13	-	436.56	-
Sand	565.86	1	565.12	1
Fly ash	565.86	1	565.12	1
Sodium thiosulfate	28.30	0.05	16.95	0.03
Water	288.59	0.51	288.21	0.51
Boric acid	0	0	11.30	0.02

The chemical composition (wt%) of steel used in this work is given in Table 32. A section of steel 10x0.4x0.1 cm was employed for electrochemical measurements. Steel electrode was degreased then washed with HCl 0.1M, ultrasonic cleaned with ethanol and distilled water to remove all impurities on surface. Steel surface of 4 cm² was immersed in mortar.
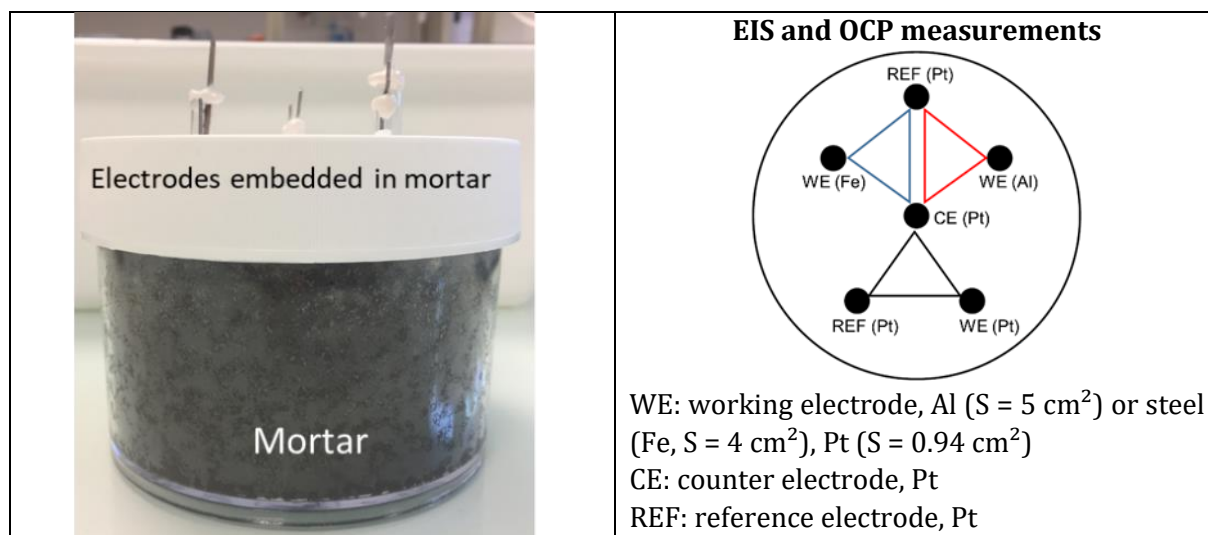
Details on the electrochemical setups used for steel embedded in mortar are given in Table 33.

OCP and EIS plots were measured by a PARSTAT4000 potentiostat. EIS measurements were conducted at open circuit potentials (OCP) in a frequency range from 10^6 to 10^{-2} Hz at an AC amplitude of 10 mV.

Table 32. Chemical composition (wt%) of steel

Element	Fe	C	Si	Mn	P	S	Cr	Mo	Ni	Cu
Amount (wt.%)	98.2	0.122	0.206	0.641	0.016	0.013	0.118	0.02	0.011	0.451

Table 33.Electrochemical setups details

EIS and OCP measurements

WE: working electrode, Al (S = 5 cm^2) or steel (Fe, S = 4 cm^2), Pt (S = 0.94 cm^2)
CE: counter electrode, Pt
REF: reference electrode, Pt

4.1.1.2   RATEN

Similar tests (chemical and electrochemical) as described in Chapter 3 for Al reactivity were performed by RATEN to assess the steel reactivity and H$_2$ evolution in chemical conditions relevant for MPC matrix compared to OPC matrix. DC01 carbon steel (equivalent with EN 10130 or Werkstoff number 1.0330) with the standard composition given in Table 33 was used. The experimental tests were performed both with DC01 coupons immersed in solutions simulating the pore water of MPC and OPC, and also with DC01 coupons embedded in MPC and OPC pastes.

Table 33 Chemical composition of the DC01 carbon steel, [wt.%] [16]

Chemical composition	C	Mn	P	S	Fe
Nominal	≤ 0,12	≤ 0,6	≤ 0,045	≤ 0,045	up to 100%

For OPC pore water a saturated Ca(OH)$_2$ solution was used, while the MPC pore solution composition is indicated in Table 9.

The OPC and MPC paste compositions are given in Table 10 and respectively Table 11 (sub-chapter 3.2.1.3). It has to be noted here that the formulation for the magnesium phosphate cement was adapted after the reference one, as it was difficult for RATEN to purchase the dead burned magnesia, to allow reasonable setting times by using reactive magnesium oxide (chemical grade oxide).

The experimental conditions and experimental set-ups used for chemical and electrochemical tests are the same as those presented in sub-chapter 3.2.1.3.

4.2 Main findings: Steel corrosion and H₂ evolution

4.2.1   Steel corrosion in LC-MPC mortars

CNRS/IJCLab performed electrochemical tests to assess steel corrosion in low cost MPC matrices. The plots of the open circuit potential (OCP) vs. immersion time for steel in MPC mortars are shown in Figure 55.

OCP of steel immersed in these mortars remains at an almost constant value for the immersion duration. Information from OCP measurements did not allow concluding on steel behaviour in contact with these two MPC mortars because the difference of OCP values is small (~100mV).
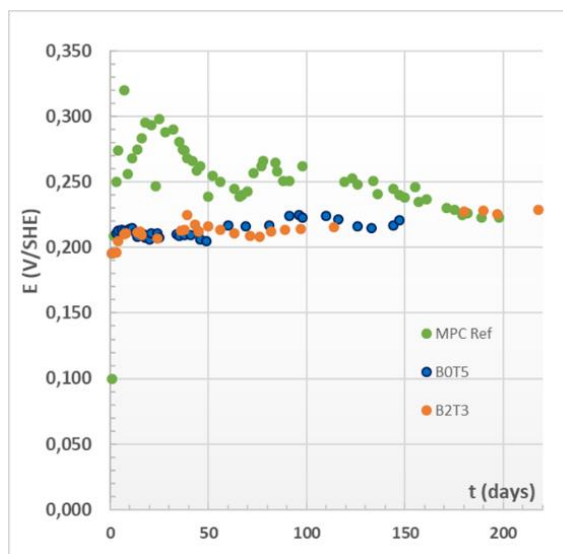
Figure 55. Variation of the open circuit potential of steel with the time immersion in MPC ref, B0T5 and B2T3

Nyquist diagrams of steel measured at OCP in MPC mortars are shown in Figure . Nyquist plots put in evidence a more capacitive behaviour, like an inert electrode, for the steel immersed in MPC ref, suggesting limited corrosion. In contrast, in LC-MPC mortars, the behaviour differs, suggesting more corrosion. This observation is supported by the impedance modulus $|Z|$ measured at 0.01 Hz, which is higher in MPC ref (approximately 5.10^5 (Ohm.cm²) compared to LC-MPC mortars (approximately 1.10^5(Ohm.cm²)). Furthermore, the overall impedance in LC-MPCs increases with prolonged exposure, suggesting a potential enhancement in corrosion resistance. The significant difference in loop amplitudes at high frequencies between LC- MPC and MPC ref prompts investigation into the specific contributions of the mortar matrix and corrosion layer to this phenomenon.
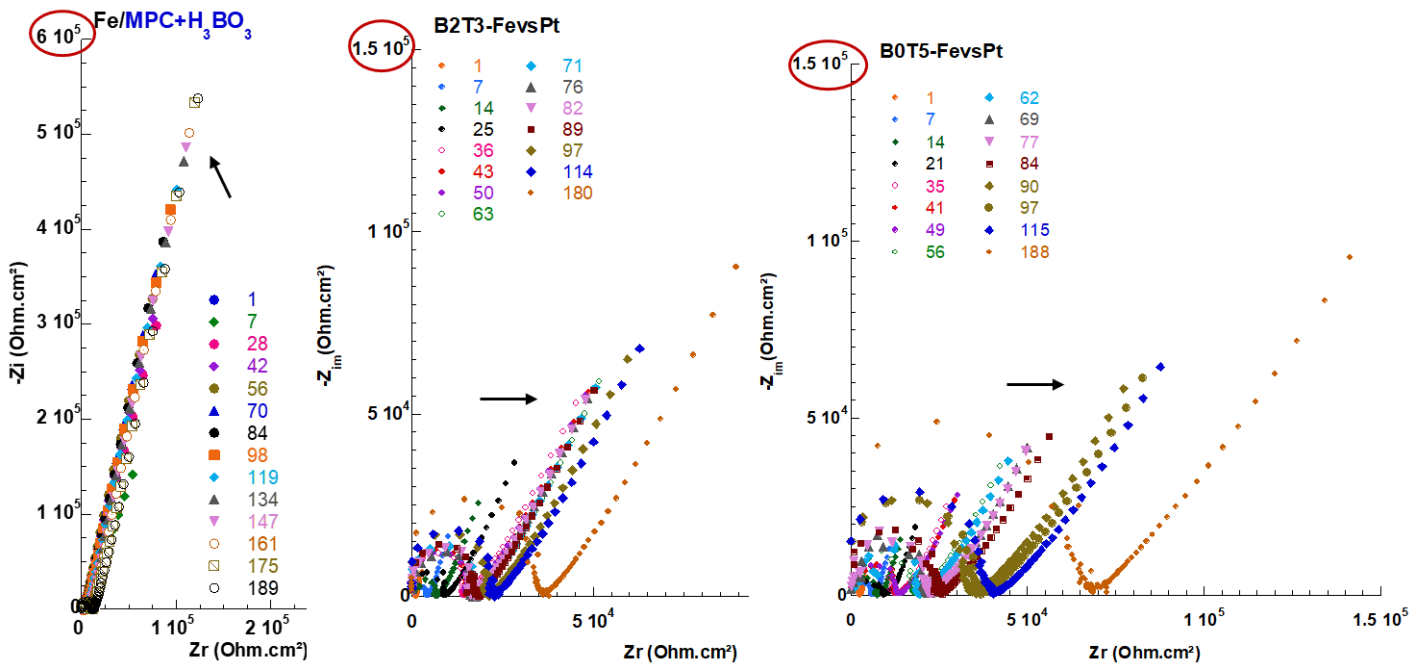
Figure 56. Nyquist diagrams of steel measured at OCP, from 10^6 to 10^{-2} Hz in MPC and LC MPC mortars

More EIS measurements need to be performed in the long term and EIS plots need to be fitted to determine a corrosion mechanism of steel in these MPC mortars.
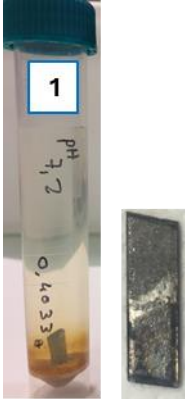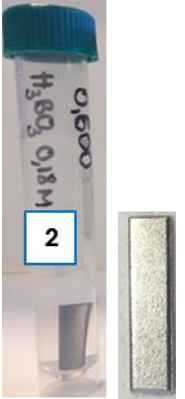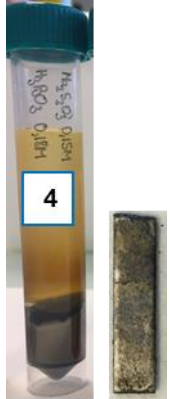
4.2.2 Reactivity of steel in thiosulfate solution with and without boric acid

To assess the effect of the retarder used in MPC formulations on steel corrosion, CNRS/IJCLab performed simple corrosion tests, in aerated solutions, using the following protocol and parameters:

- Sodium thiosulfate pentahydrate $Na_2S_2O_3.5H_2O$ was used for these tests.
- The pH of all test's solutions was set at 7.2 by adding NaOH solution.
- Each tube contains a plate of metal and 9 mL of solution.
- Before introducing the plates in the tubes, they are cleaned and weighed.
- Once removed from the tube (immersed time = 17 days), the plate is thoroughly rinsed with distilled water, gently dried and weighed.

Visual observations of samples immersed in solutions with pH 7.2, solution containing only H_3BO_3, solutions containing only sodium thiosulfate, and solution containing both additives are presented Table . The concentration of boric acid and thiosulfate in the solution was calculated directly from the quantities in the B0T5 and B2T3 mortars. Although this concentration may be overestimated, this study assumes that retarders do not participate in the formation reaction of K-struvite. Therefore, we presume that the entire concentration of retarders is contained within the pore solution.

Table 34. Observations of steel sample in different solutions after 17 days of immersion
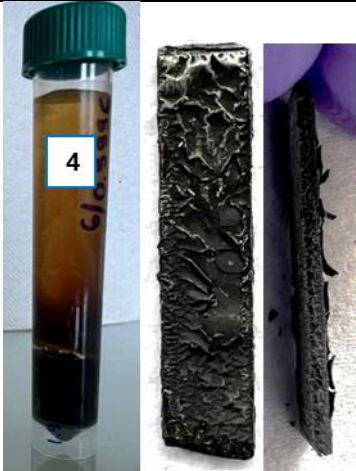

Visual observations				
Solution composition	pH 7.2	pH 7.2, H_3BO_3 0.18 M	pH 7.2, $Na_2S_2O_3$ 0.18 M	pH 7.2, H_3BO_3 0.18M, $Na_2S_2O_3$ 0.11 M

After 17 days of immersion, it was observed that the steel sample in solution 2, containing H_3BO_3, exhibited no signs of corrosion compared to the sample in solution 1, which lacked H_3BO_3. This suggests that the presence of H_3BO_3 effectively protects the steel from corrosion. Conversely, sodium thiosulfate does not exhibit a similar inhibitory effect on steel corrosion. Notably, in solution 3 containing only thiosulfate, the formation of a black layer on the sample surface was observed, indicative of mackinawite film formation, as documented in the literature [16].

The steel sample immersed in solution 4, which contained both H_3BO_3 and thiosulfate, demonstrated that the protective effect of H_3BO_3 is compromised in the presence of thiosulfate. In this case, a significant mass loss was recorded, accompanied by the observation of an orange precipitate in the solution. Furthermore, the steel surface exhibited a non-adherent black layer, suggesting the formation of a mixture of Fe_2O_3 and Fe_3O_4.

Continuing the experiments for 120 days, samples in solutions 3 and 4 exhibited distinct corrosion behaviours. A photograph of the samples before removing the corrosion layer is provided in Table 35.

Table 35. Observations of steel samples in different aerated solutions after 120 days of immersion

Visual observations		
Solution composition	$pH_{initial}$ 7.2, $Na_2S_2O_3$ 0.18 M	$pH_{initial}$ 7.2, H_3BO_3 0.18M, $Na_2S_2O_3$ 0.11 M

In solution 3, the corrosion layer, although non-homogeneous, demonstrated adhesion, with a reduced presence of orange precipitate in the solution. In contrast, sample in solution 4 displayed a non-adherent black corrosion layer, accompanied by a significantly higher amount of orange precipitate compared to solution 3. Additionally, a noticeable change in pH was observed in these solutions at 120 days. Solution 3 exhibited a pH increase from 7.2 to 9, while solution 4 showed a pH increase from 7.2 to 7.8.

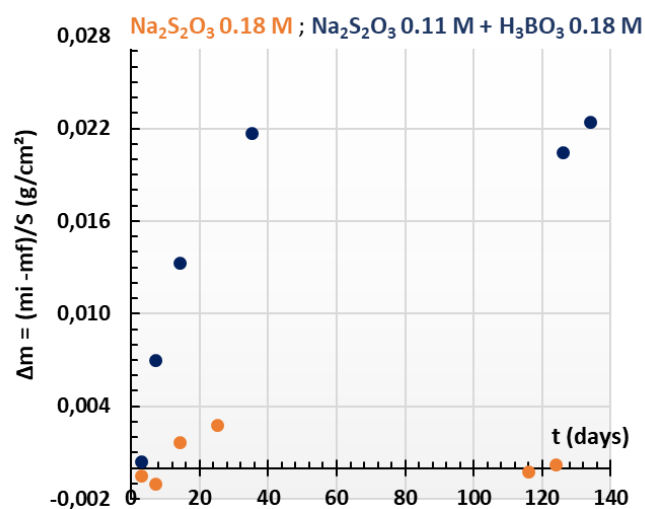Weight loss measurements for samples immersed in these aerated solutions are presented in Figure .

Figure 57. Weight loss measurements before removal of corrosion products

The above plot illustrates distinct corrosion behaviours of the steel samples in the two solutions. This difference may be attributed to the adherence of the corrosion layer. In solution containing only thiosulfate, the corrosion product adheres to the surface, potentially limiting the access of oxygen and water to the steel surface, thus retarding the corrosion process. In contrast, the corrosion layer formed in solutions containing both boric acid and thiosulfate is non-adherent. Previous studies have indicated that exposure of Fe_xS_y film to borate media induces significant modifications, potentially leading to the formation of additional corrosion products in this environment [17]. Corrosion rates will be determined post-removal of corrosion products. Additional analyses, including XRD and SEM/EDX, will be conducted to identify the corrosion products formed. At present, corrosion rates have not been determined. However, based on the plot, it is anticipated that the corrosion rate of steel immersed in boric acid with thiosulfate will be higher compared to that in solutions containing only thiosulfate.

Surfaces analysis by XRD and SEM/EDX were performed to identify the corrosion products. The diffractograms of samples after 120 days of immersion in thiosulfate solutions with and without boric acid are given in Figure 58. The XRD analysis of the samples immersed in solution 3, containing only thiosulfate, revealed the presence of FeS Mackinawite, characterized by its black coloration. Additionally, alpha-goethite (FeOOH) was identified, which typically appears as an orange zone in the sample. In contrast, in solutions containing both boric acid and thiosulfate, XRD results also confirmed the presence of FeS. However, alongside FeS, the analysis detected the presence of Fe_2O_3 and/or Fe_3O_4. It is important to note that the XRD technique employed cannot differentiate between Fe_3O_4 and Fe_2O_3, necessitating further characterization for precise identification.

Mackinawite, syn

FeS

Fe$_3$O$_4$/Fe$_2$O$_3$

2-Theta - Scale

Solution composition	pH$_{initial}$ 7.2, H$_3$BO$_3$ 0.18M, Na$_2$S$_2$O$_3$ 0.11M

Goethite α-FeOOH

FeS

2-Theta - Scale

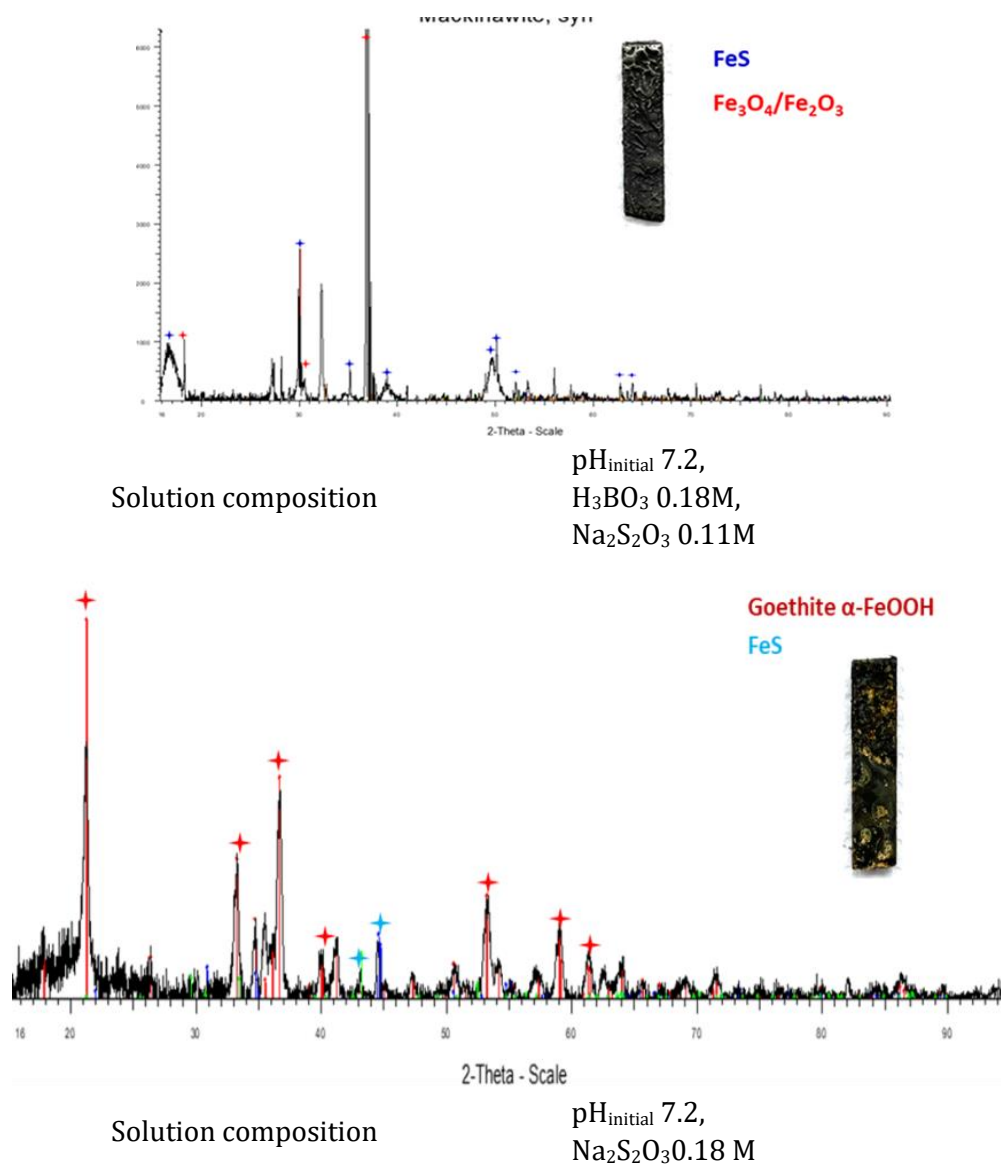| Solution composition	pH$_{initial}$ 7.2, Na$_2$S$_2$O$_3$ 0.18 M

Figure 58. XRD characterization of samples after 120 days of immersion

SEM photographs, as presented in Figure 549, provide a global observation of the morphology and composition of the corrosion layers formed on the steel samples before and after immersion in solutions containing both thiosulfate and boric acid, as well as in solutions containing only thiosulfate. To prepare the samples for SEM analysis, they were embedded in resin, longitudinally cut, and polished to a mirror finish to facilitate the observation of the transition between the metal substrate and the corrosion layer.

The average thickness of the corrosion layer ranges from 60 to 80 µm. In the SEM images, the corrosion layer appears porous, indicative of its complex microstructure. Notably, two distinct types of corrosion products are observed in the solution containing both boric acid and thiosulfate, suggesting a heterogeneous corrosion process. In contrast, the corrosion layer appears thinner in the solution containing only thiosulfate.
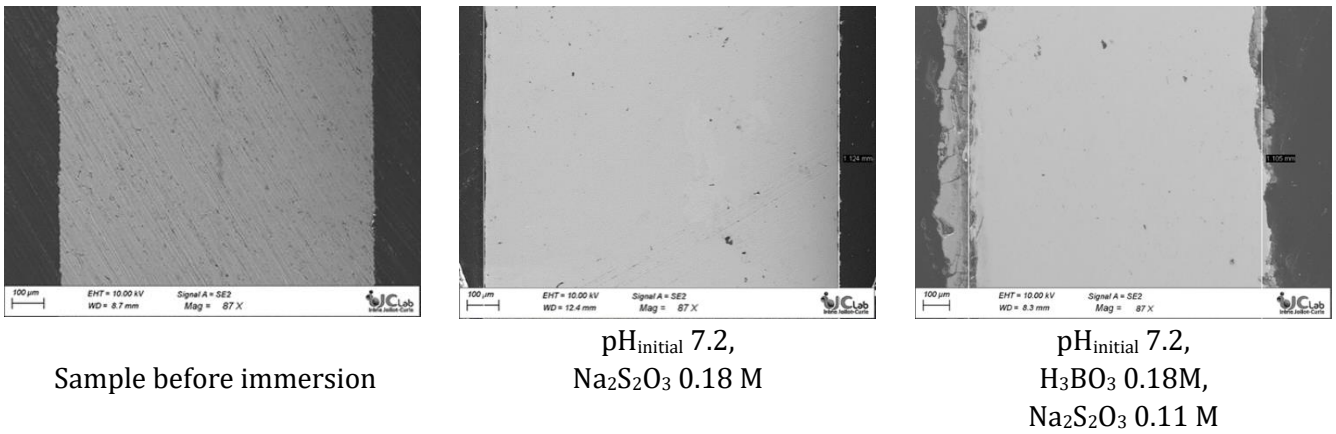
| Sample before immersion | pH$_{initial}$ 7.2, Na$_2$S$_2$O$_3$ 0.18 M | pH$_{initial}$ 7.2, H$_3$BO$_3$ 0.18M, Na$_2$S$_2$O$_3$ 0.11 M |

Figure 549. SEM photos of steel samples before and after 120 days of immersion in aerated thiosulfate solutions without and with boric acid

The EDX analysis presented in Figure 550 shows the elemental composition of the corrosion layer formed on the steel sample immersed in a solution containing boric acid and thiosulfate (120 days). Three distinct points were analysed: Point A, representing the outer layer of the corrosion product, Point B, located in the middle of the corrosion layer, and Point C, which corresponds to the steel substrate.

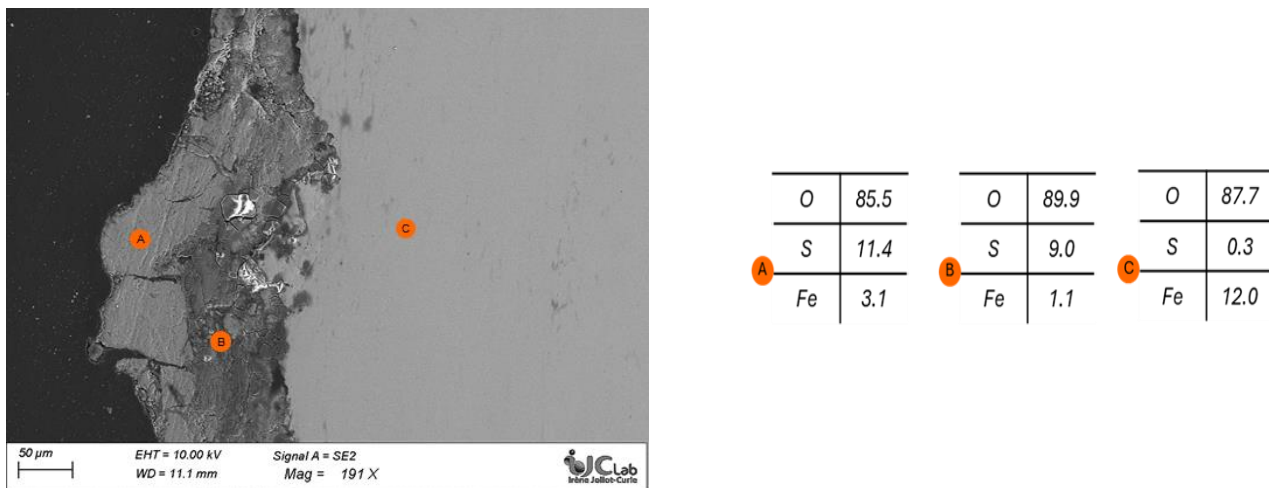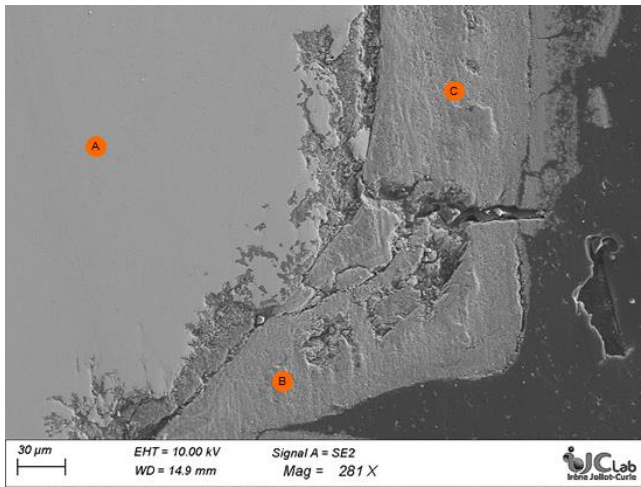| A	O	85.5		B	O	89.9		C	O	87.7
	S	11.4			S	9.0			S	0.3
	Fe	3.1			Fe	1.1			Fe	12.0

Figure 550. Elemental composition (wt%) by EDX analysis of corrosion layer in steel sample after 120 days of immersion in aerated thiosulfate solution with boric acid

At Point A, the elemental composition reveals a high oxygen content of 85.5%, followed by sulphur at 11.4%, and iron at 3.1%. This composition suggests the presence of oxidized species at the surface, possibly indicating the formation of iron oxides. In contrast, at Point B, the oxygen content remains high at 89%, with a reduced sulphur content of 9% and a minimal iron content of 1.1%. This composition suggests a transition zone within the corrosion layer, where oxygen-rich compounds dominate. Finally, at Point C, representing the steel substrate, the elemental composition shows a lower oxygen content, with a predominant iron content of 12% and a minimal sulphur content of 0.3%. These findings suggest a gradual transition from the steel substrate to the outer corrosion layer, with oxygen-rich species accumulating towards the surface. Overall, the EDX analysis highlights the heterogeneous nature of the corrosion layer.

Figure 61 presents the elemental composition (wt%) obtained through EDX analysis of the corrosion layer formed on steel samples after 120 days of immersion in aerated thiosulfate solution. Three distinct points were analysed: Point A, representing the steel substrate, and Points B and C, located within the corrosion layer.

A			B			C		
O	39.1		O	92.2		O	90.4
S	0.2		S	5.8		S	7.6
Fe	60.7		Fe	2.0		Fe	2.0

Figure 61. Elemental composition (wt%) by EDX analysis of corrosion layer in steel sample after 120 days of immersion in aerated thiosulfate solution

At Point A, which corresponds to the substrate, the elemental composition reveals a high iron content of 60%, with a lower oxygen content of 39% and minimal sulphur content of 0.2%.

In contrast, Points B and C, situated within the corrosion layer, show different elemental composition. At Point B, the oxygen content is significantly higher at 92.2%, accompanied by a sulphur content of 5.8% and a minimal iron content of 2%. Similarly, at Point C, the oxygen content remains elevated at 90.4%, with a higher sulphur content of 7.6% and a lower iron content of 2%. These findings indicate the formation of corrosion products rich in oxygen and sulphur.

4.2.3 Reactivity of DC01 carbon steel and H_2 evolution in MPC and OPC pore solution

The evolution of the corrosion rate measured in the electrochemical tests performed by RATEN on steel immersed in pore solution characteristic for MPC and OPC matrices is presented in Figure 62, together with the pH evolution during the electrochemical tests.
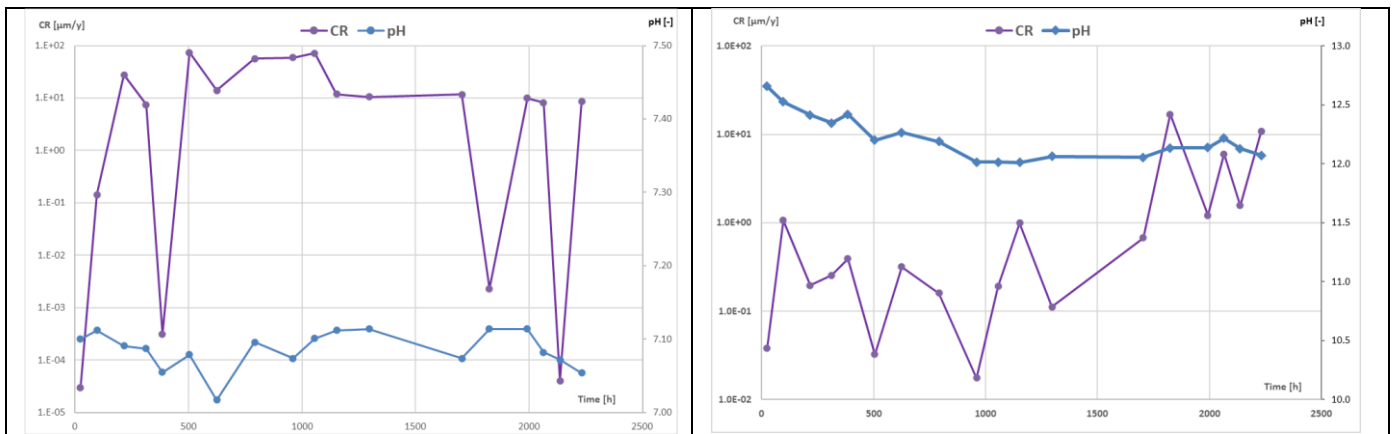

Figure 62. Corrosion rate and pH in the electrochemical tests performed on DC01 in MPC (left) and OPC (right) pore solution

During the electrochemical tests, the pH remained almost constant (around 7.1) for MPC pore solution and registered a decrease (from 12.7 to ~ 12.1) at the beginning of the test in OPC pore solution. An increase of the corrosion rate can be observed for DC01 immersed both in the MPC pore solution and in the OPC pore solution, but the increase is larger for MPC pore solution (to 50 and even 100 µm/year) compared to OPC pore solution (~ 1 µm/year). In MPC pore solution, after initial increase of corrosion rate (characteristic for activation), a short relative passivation period in which the corrosion rate registered a sharp decrease is followed by a longer activation period (from 500 h up to ~1700 h) characterized by high corrosion rate. In the last part of the test, successive relative passivation (in which the corrosion rate sharply decreased from ~ 1 µm/year to almost 1 nm/y) and activation transitions were observed. Similar "saw teeth" behaviour of corrosion rate was observed for DC01 immersed in OPC pore water, but with a much smaller increase or decrease amplitude.

The evolutions of the normalized hydrogen volumes calculated from the electrochemical parameters for steel immersed in MPC and OPC pore water are presented in Figure 63 (left figure for MPC pore water and right figure for OPC pore water).
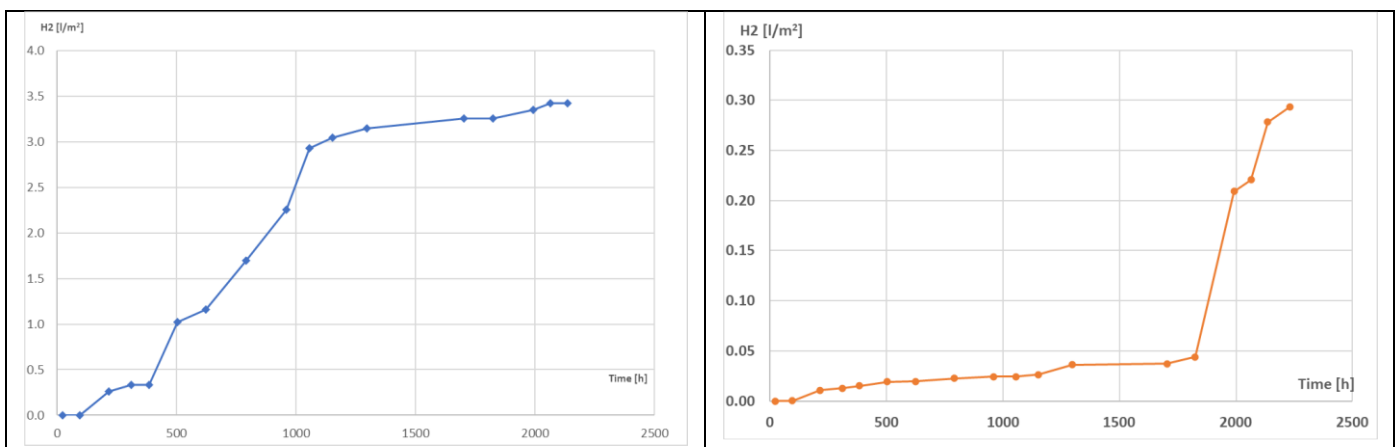

Figure 63. Hydrogen normalized volume calculated from the electrochemical parameters for DC01 immersed in MPC (left) and OPC (right) pore solution

If in OPC pore water the hydrogen volume slowly increased in the first 1800 hours of testing (to 0.05 L/m^2), in MPC pore water the hydrogen volume increased steeper, reaching after ~ 1000 hours of testing 3 L/m^2. After this period, in MPC the hydrogen volume slowly increased (up to 3.5 L/m^2), while in OPC pore water a sharp increase was obtained (up to 0.3 L/m^2).

In the chemical tests, the hydrogen volume was directly measured, and its evolution is presented in Figure 64 for the two pore solutions (MPC – left and OPC – right).
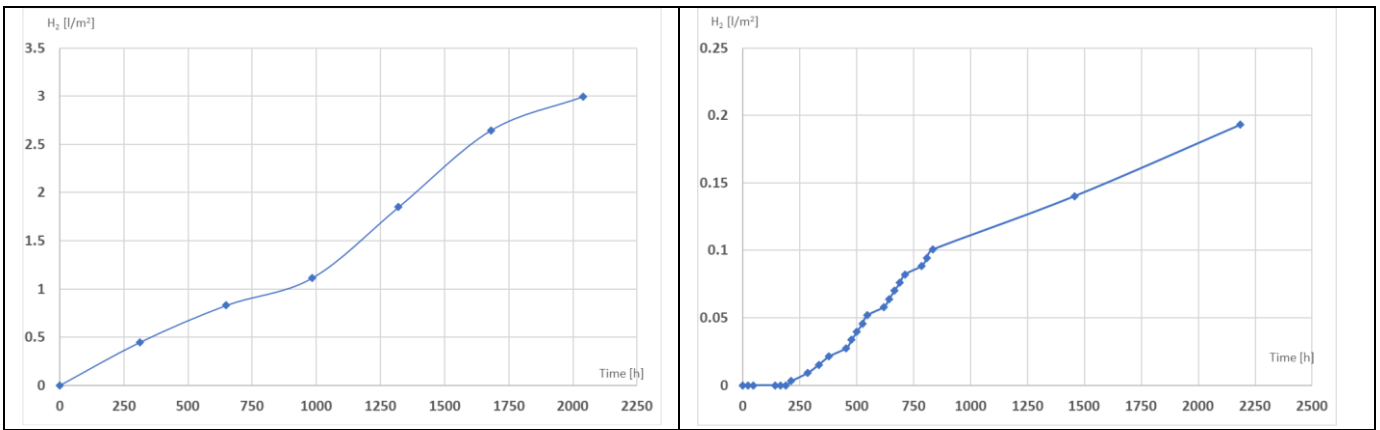
Figure 64. Hydrogen normalized volume measured from the chemical tests on DC01 in MPC (left) and OPC (right) pore solution

As it can be observed in Figures 63 and 64, at the end of the tests, the normalized hydrogen volume generated by DC01 corrosion in MPC pore water is more than one order of magnitude higher that that generated in OPC pore water and good estimates for hydrogen volume based on the electrochemical parameters were obtained.

Based on the hydrogen volume measured, the corrosion rate was calculated and its evolution is presented in Figure 65 together with the solution pH evolution during the chemical tests.
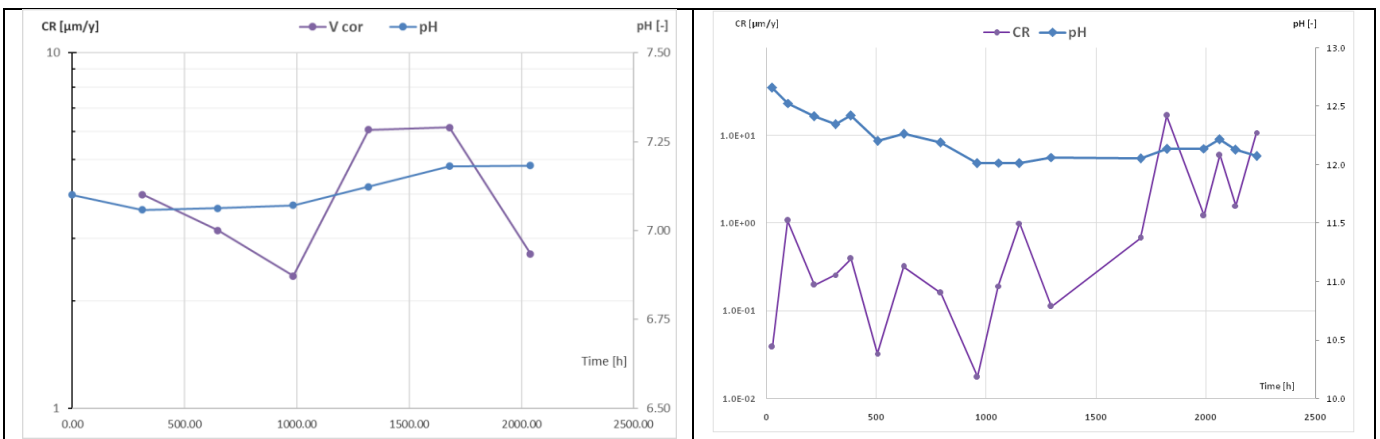

Figure 65. Corrosion rate estimated from the chemical tests performed on DC01 immersed in MPC (left) and OPC (right) pore solution

During the chemical test, the pH of the two solutions had a similar behaviour as in the electrochemical tests: remained almost constant for the tests performed in MPC pore solution (with a slight increase after 1000 hours of testing from 7.1 to ~ 7.2), while for the pore solution characteristic for OPC, the pH decreased to ~ 12 in the first part of the test (up to ~ 1000 h) and kept constant after that.

For the carbon steel immersed in MPC pore water, the initiation of the corrosion process took place immediately after the start of the test (indicated by the appearance of hydrogen bubbles on the surface of the sample). However, the corrosion did not develop much, as the volume of hydrogen collected was small, most probably the corrosion process was inhibited by black deposit that was observed on the sample surface (this deposit is going to be analysed by SEM/EDS) that limited the contact of the sample with the solution.

As stated in Chapter 3.2 where the tests are described for AlMg3 samples, we considered the possible gasses enclosed in the matrix by analysing in parallel a sample without metal and a sample with the metal embedded in the matrix. Our assumption was that all the gas developed during chemical reaction is only hydrogen. The steel corrosion is more complex than aluminium corrosion. If in the case of Aluminium, corrosion occurs mainly by reaction with water, generating H_2 due to the simultaneous water reduction, in case of steel corrosion mechanism involves a first oxidation step by water and a second step by dioxygen, with the kinetic of the second step depending on the O_2 content.

In OPC pore water, the semi-pasive state observed for the first period of testing (~800h) is followed by an increase of corrosion rate that is acomplised by a decrease of solution pH (Figure 65-right).

4.2.4   Reactivity of DC01 carbon steel and H_2 evolution in MPC and OPC pastes

The corrosion rates and the pH registered during the electrochemical tests performed by **RATEN** on steel embedded in MPC and OPC matrices are presented in Figure 66.
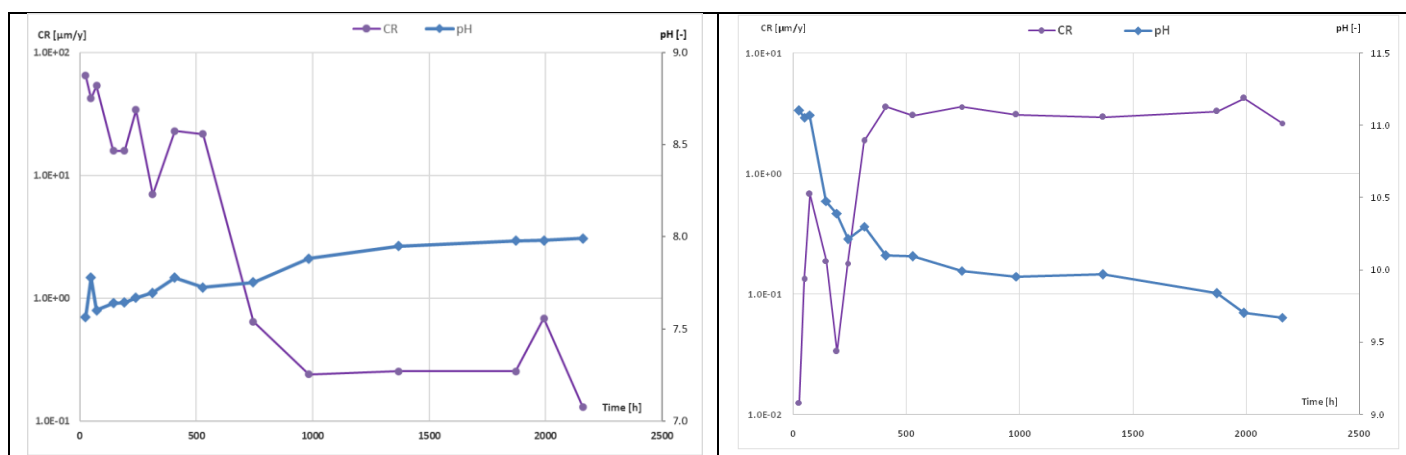

Figure 66. Corrosion rate measured in the electrochemical tests performed on DC01 embedded in MPC (left) and OPC (right) paste

For steel embedded in MPC paste, a gradual decrease in corrosion rate was observed (Figure 66-left) with two short periods of reactivation in the first 408 h. Contrary, for steel embedded in OPC paste, a gradual increase in corrosion rate was observed at the beginning of testing (~400 hours), with 2 activation and partial passivation sequences, accompanied by the pH decreased from ~ 11.2 to ~ 10.2. After this period, both the corrosion rate and the pH remain almost constant.

The hydrogen evolution, determined based on the electrochemical parameters and respectively directly measured from the chemical tests performed on steel embedded in the two matrices (MPC and OPC paste) is represented Figures 67 and 68. The hydrogen volumes estimated based on the electrochemical parameters for steel embedded in MPC and OPC are similar with those obtained in the pore solutions corresponding to the two matrices (Figures 63 and 64). From the chemical tests, the hydrogen volumes (that are directly measured) are similar for both matrices.
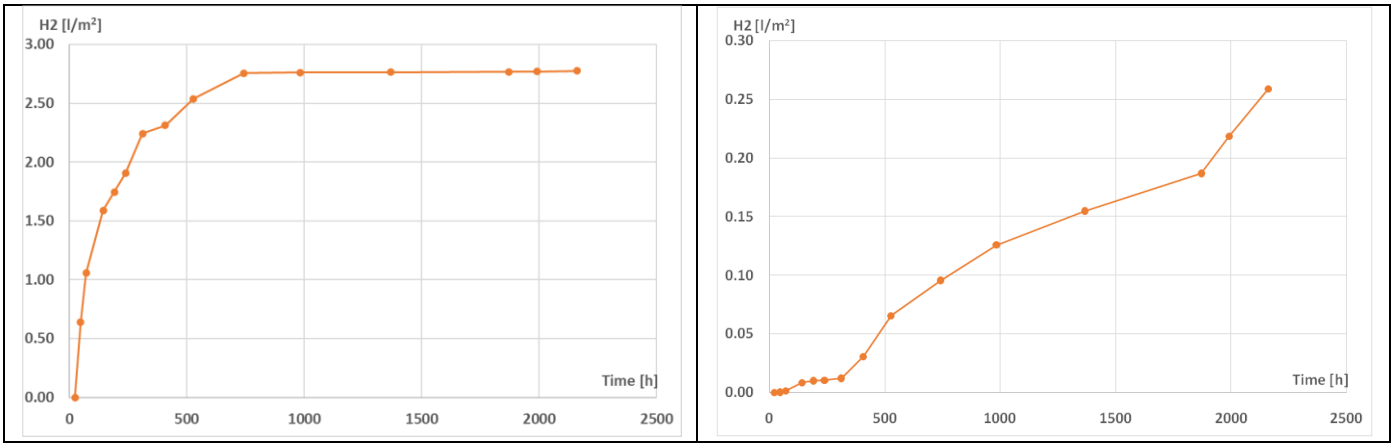
Figure 67. Hydrogen normalized volume calculated from the electrochemical parameters for DC01 embedded in MPC (left) and OPC (right) paste
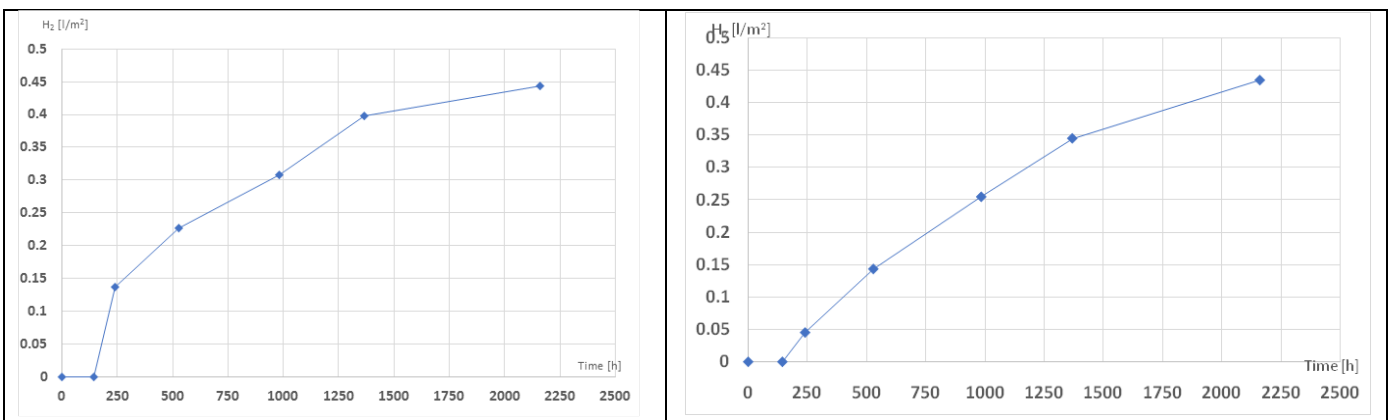

Figure 68. Hydrogen normalized volume measured during the chemical tests on DC01 embedded in MPC (left) and OPC (right) paste

By the electrochemical tests the instantaneous measurements of the corrosion rate are performed and to estimate the volume of hydrogen released between two successive electrochemical measurements the corrosion rate was assumed to be constant and this assumption can generate large uncertainties associated to the volume of hydrogen. On the other hand, in the chemical tests, the volume of hydrogen is measured over a certain period, but the measurement corresponds only to the first oxidation (steel reaction with water). Furthermore, as mentioned, the electrochemical tests for embedded steel samples were performed in open environment, while the chemical tests were performed under Ar blanket.

Figure 69 presents the pH evolution during the chemical tests and the corrosion rate estimated based on the H_2 volume measured in these tests. As it can be observed from the electrochemical test and chemical test on samples embedded in MPC and OPC paste, the corrosion rate has a decreasing trend in MPC and increasing one in OPC.
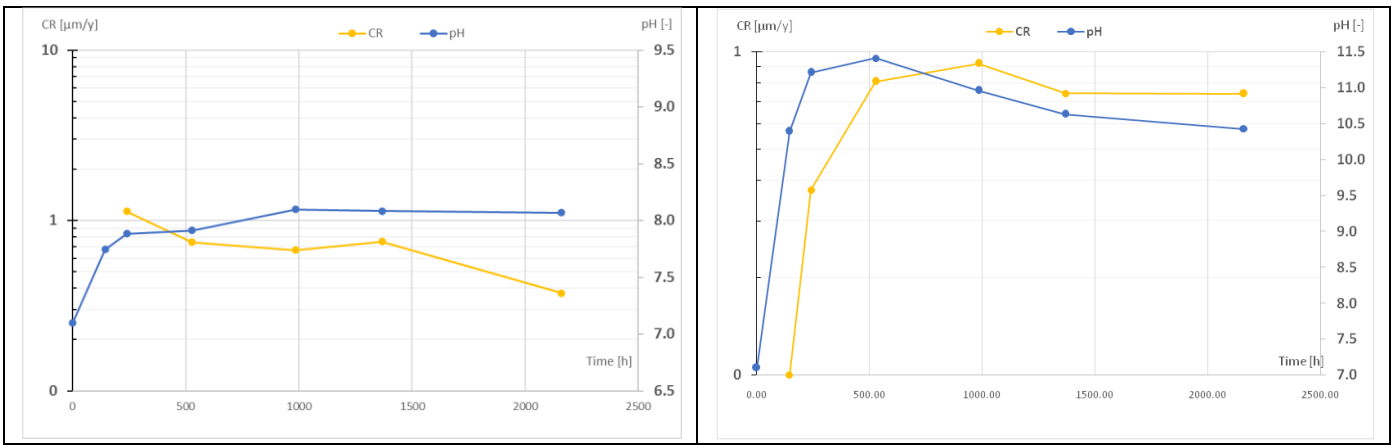
Figure 69. Corrosion rate estimated from the chemical tests performed on DC01 embedded in MPC (left) and OPC (right) paste

A summary of the corrosion rates and H_2 volumes determined through the two methods applied by RATEN on DC01 immersed in MPC and OPC pore solution and embedded in MPC and OPC pastes is given in Table 36.

Table 36. Summary for parameters measured in the electrochemical and chemical tests performed on CD01 carbon steel

Matrix type	Testing environment	Method	Initial time [h]	End of testing [h]	CR [µm/y] initial	H_2 [L/m^2] initial	CR [µm/y] end of test	Total H_2 [L/m^2]
MPC	pore solution	LPR	96	2232	0.143	0.00135	8.55	3.50
		Chemical	312	2040	3.99	0.447	2.71	2.99
	paste	LPR	48	2160	42.3	0.64	0.13	2.77
		Chemical	240	2160	1.13	0.137	0.37	0.44
OPC	Ca(OH)$_2$ solution	LPR	96	2232	1.06	3.7E-4	10.7	0.29
		Chemical	213	2184	0.39	3E-3	7.38	0.19
	paste	LPR	48	2160	0.13	1.2E-4	2.61	0.26
		Chemical	240	2160	0.374	0.045	0.743	0.43

It has to be mentioned again here that the tests performed with carbon steel embedded in the two pastes, were started after the pastes were cured at room temperature for 24 days and during these days the H_2 generated was not collected.

4.3   Conclusions regarding the steel reactivity in MPC

The corrosion of steel in sodium thiosulfate solution is evident, and the addition of boric acid does not provide protection against this corrosion but contrary, their combination appears to exacerbate the corrosion process. For future research, kinetic measurements have to be conducted to determine if the corrosion layer formed with sodium thiosulfate is stable or follows a logarithmic or linear kinetic corrosion pattern.

Furthermore, EIS measurements during 200-days immersion of steel electrodes in mortars reveal significant corrosion of steel in low cost MPC formulation compared to the reference one, although the differences between mortar compositions B0T5 and B2T3 are minimal. However, the overall impedance of LC-MPC formulations increases with prolonged exposure, suggesting a potential enhancement in corrosion resistance. Additional EIS measurements should be conducted over the long term, and the EIS plots need to be fitted to determine the corrosion mechanism of steel in these low cost MPC mortars.

From the tests performed on DC01 steel in MPC compared with OPC, in the limit of the associated errors, experimental data obtained clearly indicates that for MPC matrix the total hydrogen volume generated by DC01 type carbon steel is more than 10 times higher than the hydrogen volume generated in OPC matrix, due to the corrosion rate significant higher in MPC compared to OPC matrix.

The behaviour of carbon steel in MPC matrix was similar to that in OPC with the only difference that initially the corrosion rate was higher in MPC and towards the end of the test it decreased and in OPC it was the opposite.

To overcome the higher corrosion of steel in MPC compared to OPC matrix, concrete drums cam be used for aluminium embedding in low cost MPC.
In cases where the corrosion of steel in the presence of thiosulfate exhibits linear kinetic corrosion, the consideration of concrete drums over steel ones could be warranted. The decrease in the cost of cement manufacturing could offset the high cost of concrete drums compared to steel drums.

DC01 seems to be more reactive in the solutions simulating the pore water of MPC (prepared with light burned magnesia) but has similar reactivity when embedded in the two types of conditioning matrices.

5 Conclusions

For aluminium and its alloys embedded in MPC, the corrosion rates measured by all partners are significantly lower (around 2 orders of magnitude) than in OPC and consequently the volume of hydrogen generated is lower in MPC compared to OPC.

Phosphate contributes to the passive layer reducing the corrosion rate and hydrogen evolution. Higher phosphate concentration at low pH influences the Al passivation process due to the formation of a new passive film on the metal surface or an absorption phenomenon.

Chemical retarders in MPC formulation influence the Al corrosion response. Better response is detected in the presence of boric acid than thiosulfate associated with an adsorption mechanism of interaction on the Al_2O_3 passive layer. A synergy effect is detected with both retarders are present. Main ions in the MPC pore media play an important role in the Al passivation mechanism and have positive effect in control the H_2 release.

6 Dissemination

The results obtained in Subtasks 4.6.5 and 4.6.6 were diseminated by publishing 4 articles in international journals (3 of them WOS indexed), 3 reports in the proceedings of PREDIS workshops and 11 presentation in international conferences.

- o Papers:
    - Perona, R., Fernández-García, C., García-Lodeiro, I., Criado, M., Bastidas, J. M., & Alonso, M. C. (2023). Corrosion behavior and immobilization of pure aluminum and Al−Mg alloy LLRW in magnesium potassium phosphate cements. Journal of Nuclear Materials, 582. https://doi.org/10.1016/j.jnucmat.2023.154501 (Q1, I. F. = 3.11).

    - Fernández-García, C., Alonso, M. C., Bastidas, J. M., García-Lodeiro, I., & Fernández, R. (2024). MgO/KH2PO4 and Curing Moisture Content in MPC Matrices to Optimize the Immobilization of Pure Al and Al-Mg Alloys. Materials, 17(6), 1263. https://doi.org/10.3390/ma17061263 (Q2, I. F. = 3.4).

    - Fernández-García, C., Padilla-Encinas, P., Fernández, R., & Alonso, M. C. (2024). Interaction of aluminium alloys with MPC and OPC blended cements on the metal – matrix interface. Applied Geochemistry Journal (*under review*). (Q2, I. F. = 3.4).

    - David, A., Lautaru, V., Samarineanu, C. (2004). Corrosion behaviour of aluminium alloys immobilized in MPC mortar.Journal of Nuclear Research and Development (under publication)

- o Reports:
    - Alonso, M.C. and Fernández-García, C. (2022) "Al corrosion in magnesium phosphate cements (MPC)", PREDIS Proceedings of April Workshop 2022, Espoo, Finland.

    - Alonso, M.C. and Fernández-García, C. (2023) "Al corrosion in magnesium phosphate cements (MPC)", PREDIS Proceedings of May Workshop 2023, Mechelen, Belgium.

    - David, A., Lăutaru, L., Fulger, M., Bucur, C., Le, K., Delpech, S., Rodrigues D., Cannes, C. (2023). Steel corrosion in magnesium phosphate cements. PREDIS Proceedings of May Workshop 2023, Mechelen, Belgium

- o Presentations in conferences:
    - WP4 CSIC presentation: Encapsulation of reactive metals in MPC matrices. Second PREDIS Workshop Meeting, April 25-28, 2022, Espoo, Finland.

    - Fernández-García, C. and Alonso, M. C. Corrosion of aluminum alloy in simulated pore systems of magnesium phosphate cements for hydrogen inhibition. IV national congress of construction materials (CNMAT22). Abstracts book, ISBN: 978-84-09-38118-0. June 28 to July 1, 2022, Ciudad Real, Spain.

    - Fernández-García, C. and Alonso, M. C. Corrosion, and hydrogen evolution of Al/AlMg alloy in mortar of magnesium phosphate and Portland base binders. XLII national congress of RSEQ electrochemistry specialist group meeting (GERSEQ22). Abstracts book, ISBN: 978-84-09-42511-2. July 6-8, 2022, Santander, Spain.

    - CSIC. WP4: Encapsulation of reactive metals in MPC cement matrices. Third PREDIS Workshop Meeting, May 22-26, 2023, Mechelen, Belgium.

- Fernández-García, C. and Alonso, M. C. Physico-chemical stability of Magnesium Potassium Phosphate Cements (MPC) for aluminium alloy inmobilization. 48 Annual meeting of the Spanish Nuclear Society (SNE48). Abstracts book, ISBN: 978-84-090-01616-7. October 4-6, 2023, Toledo, Spain.

- Fernández-García, C., Padilla-Encinas, P., Alonso, M. C. and Fernández, R. Interaction of Al alloys with MPC and OPC based binders on the metal-matrix interface. 6th International Workshop on Mechanisms and Modelling of Waste / Cement Interactions (JCCW2023). Abstracts book. November 20-24, 2023, Prague, Check Republic.

- WP4 CSIC presentation. Intermediate WP4 PREDIS Workshop Meeting, November 24th, 2023, Paris, France.

- Lăutaru, V., David, A. Corrosion Behaviour of DC01 Carbon Steel in Environments that Simulate the Chemical Conditions of the Pore fluids of some Conditioning Matrices. The 15th Biennial International Conference on Sustainable Development through Nuclear Research and Education, May 29-31, 2024.

- David , A., Lăutaru, V., Assessment of Corrosion Behavior of AlMg3 in Two Conditioning Matrices with Different Chemistry: Portland Cement Matrix and MPC Matrix. The 15th Biennial International Conference on Sustainable Development through Nuclear Research and Education, May 29-31, 2024.

- Kim Le, Davide Rodrigues, Sylvie Delpech, Lavinia Stefan, Céline Cannes, Reactivity of steel container in contact with magnesium phosphate cements, NUWCEM 2022, France-Avignon, May 4-6 2022.

- Céline Cannes, Kim Le, Davide Rodrigues, Sylvie Delpech, Réactivité de l'acier du colis primaire des déchets métalliques radioactifs au contact des ciments phosphomagnésiens, JE 2024, France - Saint-Malo, July 1-5 2024.

REFERENCES

1. Parisot, J.-F.; France. Commissariat à l'énergie atomique. *Nuclear Waste Conditioning*; Editions Le Moniteur, 2009; ISBN 9782281113808.
2. Pourbaix, M.; Burbank, J. Atlas D-Equilibres Electrochimiques. *J Electrochem Soc* **1964**, *111*, 14C, doi:10.1149/1.2426051.
3. Uhlig H., Corrosion and corrosion control, John Wiley and Sons Wiley Interscience, 2008. https://chem.libretexts.org/
4. Gardner, L.J.; Corkhill, C.L.; Walling, S.A.; Vigor, J.E.; Murray, C.A.; Tang, C.C.; Provis, J.L.; Hyatt, N.C. Early Age Hydration and Application of Blended Magnesium Potassium Phosphate Cements for Reduced Corrosion of Reactive Metals. *Cem Concr Res***2021**, *143*, doi:10.1016/j.cemconres.2021.106375.
5. Vollpracht, A.; Lothenbach, B.; Snellings, R.; Haufe, J. The Pore Solution of Blended Cements: A Review. *Mater Struct* **2016**, *49*, 3341–3367, doi:10.1617/s11527-015-0724-1.
6. Poras, G.; Danis, H.; Coumes, C.C.D.; Antonucci, P.; Cannes, C.; Delpech, S.; Perrin, S. Magnesium Potassium Phosphate Cement: A Promising Binder for the Conditioning of Aluminum-Magnesium Alloys Waste. In Proceedings of the WM2023; 2023.
7. Cannes C. et all. Encapsulation of reactive metals in magnesium phosphate cement-based matrices. Deliverable 1.5 – Proceedings of PREDIS May Workshop 2021
8. Perona, R.; Fernández-García, C.; García-Lodeiro, I.; Criado, M.; Bastidas, J.M.; Alonso, M.C. Corrosion Behavior and Immobilization of Pure Aluminum and Al−Mg Alloy LLRW in Magnesium Potassium Phosphate Cements. *Journal of Nuclear Materials***2023**, *582*, 154501, doi:10.1016/j.jnucmat.2023.154501.
9. Fernández-García, C.; Alonso, M.C.; Bastidas, J.M.; García-Lodeiro, I.; Fernández, R. MgO/KH2PO4 and Curing Moisture Content in MPC Matrices to Optimize the Immobilization of Pure Al and Al-Mg Alloys. *Materials***2024**, *17*, 1263, doi:10.3390/ma17061263.
10. Chartier, D.; Sanchez-Canet, J.; Antonucci, P.; Esnouf, S.; Renault, J.P.; Farcy, O.; Lambertin, D.; Parraud, S.; Lamotte, H.; Coumes, C.C.D. Behaviour of Magnesium Phosphate Cement-Based Materials under Gamma and Alpha Irradiation. *Journal of Nuclear Materials* **2020**, *541*, doi:10.1016/j.jnucmat.2020.152411.
11. M. C. Alonso; J. L. García-Calvo; S. Petterson; M. A. Cuñado; M. Vuorio; H. Weber; H. Ueda; H. Naito *AB R-12-02 Development of an Accurate PH Measurement Methodology for the Pore Fluids of Low PH Cementitious Materials*; 2012;
12. Randles, J.E.B. Kinetics of Rapid Electrode Reactions. *Discuss Faraday Soc* **1947**, *1*, 11–19, doi:10.1039/DF9470100011.
13. Stern, M.; Geary, A.L. Electrochemical Polarization I. A Theoretical Analysis of the Shape of Polarization Curves. *J Electrochem Soc* **1957**, *104*, 56–63.
14. ASTM-G102-89 *Standard Practice for Calculation of Corrosion Rates and Related Information from Electrochemical Measurements*; 1999;
15. Caes, S.; Gurning, A.C.; Li, X.; de Souza, V.; Kursten, B. Corrosion of Aluminium in Ordinary Portland Cement Paste: Influence of Matrix Porosity and the Presence of LiNO3 Corrosion Inhibitor. *Materials and Corrosion* **2023**, *74*, 125–137, doi:10.1002/maco.202213296.
16. Choudhary, Lokesh & Macdonald, Digby&Alfantazi, Akram. (2015). Role of Thiosulfate in the Corrosion of Steels: A Review. Corrosion. 71. 150602132136005. 10.5006/1709
17. Sosa, Eliceo & Cabrera-Sierra, R. & Oropeza, Mercedes & Gonzalez, Ignacio. (2002). The influence of different surface conditions in the corrosion process of carbon steel in alkaline sour media. Journal of Applied Electrochemistry. 32. 905-913. 10.1023/A:1020595424251.